Chapter 5

Semi-Online Neural-Q_learning

This chapter contains the main research contribution of this thesis. It proposes the Semi-Online Neural-Q_learning algorithm (SONQL), an RL algorithm designed to learn with continuous states and actions. The purpose of the SONQL algorithm is to learn the state/action mapping of a reactive robot behavior. The chapter concentrates on theoretically analyzing the points taken into account in the design of this approach. The main features of the algorithm are the use of a Neural Network and a database of learning samples which stabilize and accelerate the learning process. The implementation of the algorithm in a reactive behavior is described. Results of the SONQL algorithm will be shown in Chapter 7.

5.1 Reinforcement Learning based behaviors

Reinforcement Learning (RL) is a very suitable technique to learn in unknown environments. Unlike supervised learning methods, RL does not need any database of examples. Instead, it learns from interaction with the environment and according to a scalar value. As has been described in Chapter 4, this scalar value or *reward*, evaluates the environment state and the last taken action with reference to a given task. The final goal of RL is to find an *optimal state/action mapping* which maximizes the sum of future rewards whatever the initial state is. The learning of this optimal mapping or *policy* is also known as the *Reinforcement Learning Problem* (RLP).

The features of RL make this learning theory useful for robotics. There are parts of a robot control system which cannot be implemented without experiments. For example, when implementing a reactive robot behavior, the main strategies can be designed without any real test. However, for the final tuning of the behavior, there will always be parameters which have to be set with real experiments. A dynamics model of the robot and environment could avoid this phase, but it is usually difficult to achieve this model with reliability. RL offers the possibility of learning the behavior in real-time and avoid the tuning of the behaviors with experiments. RL automatically interacts with the environment and finds the best mapping for the proposed task, which in this example would be the robot behavior. The only necessary information which has to be set is the *reinforcement function* which gives the rewards according to the current state and the past action. It can be said that by using RL the robot designer reduces the effort required to implement the whole behavior, to the effort of designing the reinforcement function. This is a great improvement since the reinforcement function is much simpler and does not contain any dynamics. There is another advantage in that an RL algorithm can be continuously learning and, therefore, the state/action mapping will always correspond to the current environment. This is an important feature in changing environments.

RL theory is usually based on *Finite Markov Decision Processes* (FMDP). The dynamics of the environment is formulated as a FMDP and the RL algorithms use the properties of these systems to find a solution to the RLP. *Temporal Difference* (TD) techniques are able to solve the RLP incrementally and without knowing the transition probabilities between the states of the FMDP. In a robotics context, this means that the dynamics existing between the robot and the environment do not have to be known. As far as incremental learning is concerned, TD techniques are able to learn each time a new state is achieved. This property allows the learning to be performed *online*, which in a real system context, like a robot, can be translated to a real-time execution of the learning process. The term "online" is here understood as the property of learning with the data that is currently extracted from the environment and not with historical data.

Of all TD techniques, the best known and most used technique is the *Q_learning* algorithm proposed by Watkins in 1992 [Watkins and Dayan, 1992]. The advantages of this algorithm are its simplicity and the fact that it is an off-policy method. For these reasons, which will be detailed in the next section, Q_learning has been applied to a huge number of applications. The RL algorithm proposed in this dissertation was also based on Q_learning.

The main problem of RL when applied to a real system is the *generalization* problem, treated in Section 4.5. In a real system, the variables (states or actions) are usually continuous. However, RL theory is based on FMDP, which uses discrete variables. Classic RL algorithms must be modified to allow continuous states or actions, see Section 4.6. Another important problem of RL when applied to real systems is the correct observation of the environment state. In a robotic system, it is usual to measure signals with noise or delays. If these signals are related to the state of the environment the learning process will be damaged. In these cases, it would be better to consider the environment as a *Partially Observable MDP*, refer also to Section 4.5.

The approach presented in this thesis attempts to solve only the generalization problem. As commented on above, the approach is based on the Q_learning algorithm and includes a Neural Network (NN) to generalize. NNs are able to approximate very complex value functions, but they are affected by the *interference* problem, as described in Section 4.6.4. To overcome this problem, the presented approach uses a database of *learning samples* which contains a representative set of visited states/action pairs which stabilizes and also accelerates the learning process. The approach has been named *Semi-Online Neural-Q_learning* (SONQL). The next subsections will detail each part of the SONQL algorithm and the phases to be found on its execution.

The combination of Reinforcement Learning with a behavior-based system has already been used in many approaches. In some cases, the RL algorithm was used to adapt the coordination system [Maes and Brooks, 1990, Gachet et al., 1994, Kalmar et al., 1997, Martinson et al., 2002]. Moreover, some researches have used RL to learn the internal structure of the behaviors [Ryan and Pendrith, 1998, Mahadevan and Connell, 1992, Touzet, 1997, Takahashi and Asada, 2000, Shackleton and Gini, 1997] by mapping the perceived states to control actions. The work presented by Mahadevan demonstrated that the breaking down of the robot control policy in a set of behaviors simplified and increased the learning speed. In this thesis, the SONQL algorithm was designed to learn the internal mapping of a reactive behavior. As stated in Chapter 3, the coordinator must be simple and robust. These features cannot be achieved with an RL algorithm since, if the data becomes corrupted, the optimal policy can be unlearnt. Instead, RL can satisfactorily learn a behavior mapping, which simplifies the implementation and tuning of the algorithm. The chapter concludes with the implementation of the SONQL algorithm in a reactive robot behavior.

5.2 Q_learning in robotics

The theoretical aspects of the Q_learning [Watkins and Dayan, 1992] algorithm have been presented in Section 4.4.2. This section analyzes the application of the algorithm in a real system such as a robot. Q_learning is a Temporal Difference algorithm and, like all TD algorithms, the dynamics of the environment do not have to be known. Another important feature of TD algorithms is that the learning process can be performed online. However, the main advantage of Q_learning with respect to other TD algorithms is that it is an *off-policy* algorithm, which means that in order to converge to an optimal state/action mapping, any policy can be followed. The only condition is that all state/action pairs must be regularly visited.

The *policy* in an RL algorithm, indicates the action which has to be executed depending on the current state. A *greedy* policy chooses the best action according to the current state/action mapping; that is, the action which will maximize the sum of future rewards. A *random* policy generates an aleatory action independently of the state. An ϵ*-greedy* policy chooses the greedy action with probability $(1-\epsilon)$, otherwise it generates a random action. The importance of the policy relapses in the *explotation/exploration* dilemma.

Q_learning can theoretically use any policy to converge to the optimal state/action mapping. The most common policy is the ϵ-greedy policy which uses random actions to explore and greedy actions to exploit. The off-policy feature is a very important feature in a robotic domain, since, on occasion, the actions proposed by the learning algorithm can not be carried out. For example, if the algorithm proposes an action which would cause a collision, another behavior with a higher priority will prevent it with the generation of another action. In this case, Q_learning will continue learning using the action which has actually been executed.

Q_learning uses the *action-value* function, Q, in its algorithm. The $Q(s,a)$ function contains the discounted sum of future rewards which will be obtained from the current state s, executing action a and following the greedy policy afterwards. The advantage of using the action-value function resides in the facility of extracting the greedy action from it. For the current state s, the greedy action a_{max} will be the one which maximizes the $Q(s,a)$ values over all the actions a. Consequently, when the Q_learning algorithm converges to the optimal action-value function Q^*, the optimal action will be extracted in the same way. The simplicity of Q_learning is another important advantage in its implementation on a complex system such as a robot.

5.3 Generalization with Neural Networks

When working with continuous states and actions, as is costumary in robotics, the continuous values have to be discretized in a finite set of values. If an accurate control is desired, a small resolution will be used and, therefore, the number of discrete states will be very large. Consequently, the Q function table will also become very large and the Q-learning algorithm will require a long learning time to update all the Q values. This fact makes the implementation of the algorithm in a real-time control architecture impractical and is known as the *generalization* problem. There are several techniques to combat this problem, as overviewed in Section 4.6.

In this thesis, a Neural Network (NN) has been used to solve the generalization problem. The main reason for using an NN was for its excellent ability to approximate any nonlinear function, in comparison with the other function approximators. Also, an NN is easy to compute and the required number of parameters or values is very small. The strategy consists of using the same Q_learning algorithm, but with an NN which approximates the tabular Q function. The number of parameters required by the NN does not depend on the resolution desired for the continuous states and actions. It will depend only on the complexity of the Q function to be approximated. As stated in Section 4.6.4, when generalizing with an NN, the interference problem destabilizes the learning process. This problem was taken into account in the SONQL algorithm and will be treated in Section 5.4.

5.3.1 Neural Networks overview

A Neural Network is a function able to approximate a mathematical function which has a set of inputs and outputs. The input and output variables are real numbers and the approximated functions can be non-linear, according to the features of the NN. Artificial Neural-Networks were inspired by the real neurons found in the human brain, although a simpler model of them is used. The basic theory of NN was widely studied during 1980s and there still are many active research topics. For an overview of NN, refer to [Haykin, 1999].

One model frequently used in the implementation of an artificial neuron is depicted in Figure 5.1. A neuron j located in layer l, has a set of inputs $\{y_1^{l-1}$, y_2^{l-1}, ..., $y_p^{l-1}\}$ and one output y_j^l. The value of this output depends on these inputs, on a set of *weights* $\{w_{j1}^l$, w_{j2}^l, ..., $w_{jp}^l\}$ and on an *activation function* $\varphi^{(l)}$. In the first computation, the induced *local field* v_j^l of the neuron j, is calculated by adding the products of each input y_i^{l-1} by its corresponding weight w_{ji}^l. An extra input y_0^{l-1} is added to v_j^l. This input is called the *bias* term and has a constant value equal to 1. By adjusting the weight w_{j0}^l, the neuron can be activated even if the inputs are equal to 0. The local field v_j^l is then used to calculate the output of the neuron $y_j^l = \varphi^{(l)}(v_j^l)$. The activation function has a very important role in learning efficiency and capability.

As mentioned above, neurons are grouped in different *layers*. The first layer uses as neuron inputs $\{y_0^0$, y_1^0, ..., $y_{in}^0\}$ the input variables of the NN. This set of inputs is also called the *input layer*, although it is not a layer of neurons. The second and consecutive layers use as neuron inputs the neuron

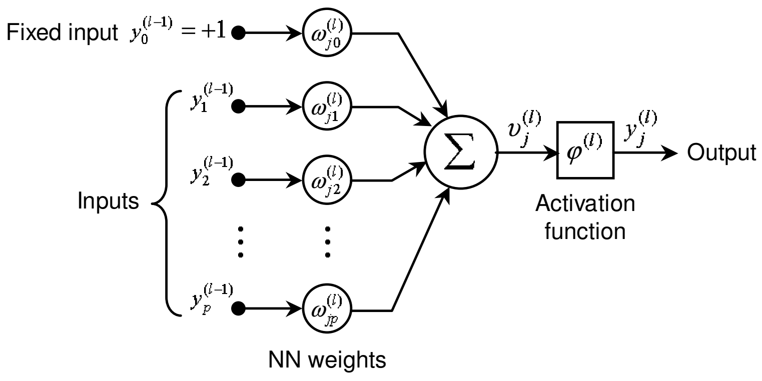

Figure 5.1: Diagram of an artificial neuron j located at layer l.

outputs of the preceding layer. Finally, the last layer of the NN is the *output layer*, in which each neuron generates an output of the network. All the neuron layers preceding the output layer are also called the *hidden layers*, since the neuron output values are not seen from the outside nor are they significant. The learning process in an NN consists of adapting the weights of the network until the output is equal to a desired response. An NN algorithm has the goal of indicating the procedure to modify the values of these weights.

Different network architectures can be found according to the connections among the neurons. *Feed-forward* networks have the same structure as described previously. Neuron inputs always proceed from a preceding layer, and signals are always transmitted forward ending at the output layer. Other kinds of architectures are *recurrent* networks. In this case, a feedback loop connects neuron outputs to the inputs of neurons located in a preceding layer. It is also possible to connect the output of one neuron to its own input, in which case it would be a self-feedback. Recurrent networks have a higher learning capability and performance, although they show a nonlinear dynamical behavior. Besides the signal transmission, NNs are also classified according to the number of layers. *Single-layer* networks have only one layer of neurons, the output layer, and are very suitable for pattern classification. On the other hand, *multilayer* networks have usually one or two hidden layers plus the output layer. Multilayer networks are able to learn complex tasks by progressively extracting more meaningful features from the NN inputs.

5.3.2 Neural Q_learning

In order to approximate the Q function, a feed-forward multilayer neural network has been used. This architecture allows the approximation of any

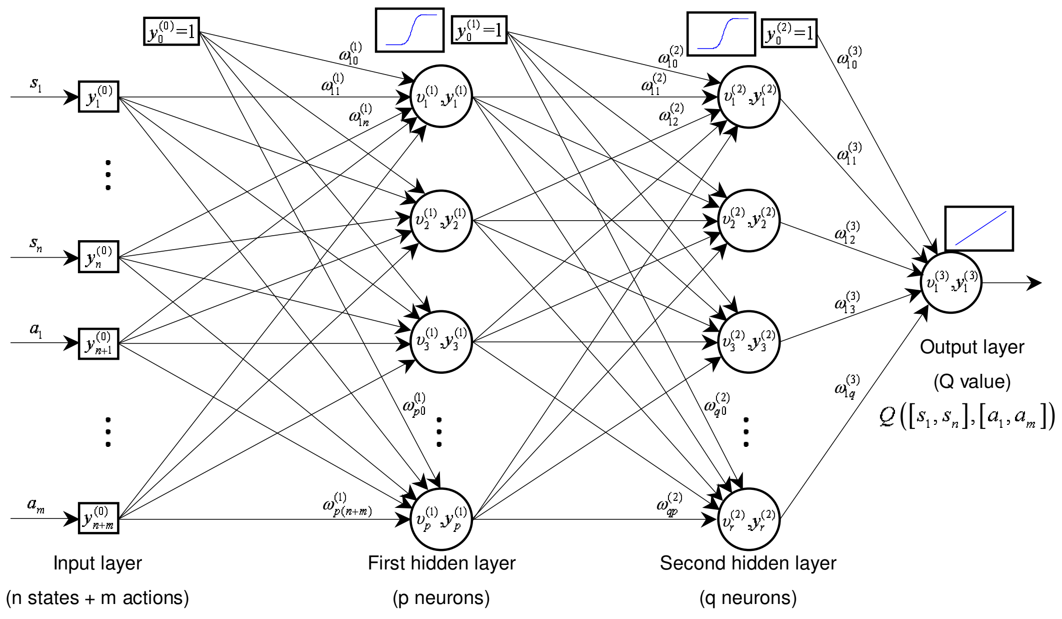

Figure 5.2: Graph of the multilayer NN which approximates the Q_function. In this case, two hidden layers are used. The input layer is composed of the states and the actions. The output layer has only one neuron which contains the Q value for the current input values.

nonlinear function assuming that the number of layers and neuron, and the activation functions are appropriated. The input variables of the NN are the environment states and the actions, which have n and m dimensions respectively. The output of the network has only one dimension and corresponds to the Q value for the current states and actions. The number of hidden layers will depend on the complexity of the Q function. Figure 5.2 shows a schema of the network.

The use of Neural Networks in the Q_learning algorithm is known as Neural-Q_learning (NQL). There are several approaches in which NN can be applied, as commented on Section 4.6.4. In particular, the approximation of the Q function using a feed-forward NN is known as *direct* Q_learning [Baird, 1995]. This is the most straight-forward approach since the whole function is approximated in only one NN. This implementation is affected by the interference problem, which will be treated in the next section. The technique used to learn the Q_function is the *back-propagation* algorithm. This algorithm uses the error between the output neuron and the desired response to adapt the weights of the network.

To compute the desired response of the NN, the update equation of

Q_learning algorithm is used. As detailed in the previous section, the Q value for a given state and action is equal to Equation 5.1. This means that the desired response of the NN has to be equal to Equation 5.1 and the committed error will be used to update the weights of the network.

$$Q(s_t, a_t) = r_{t+1} + \gamma \cdot max_{a_{max}} Q(s_{t+1}, a_{max}) \tag{5.1}$$

As can be seen, the computation of Equation 5.1 requires the use of the same NN to calculate $Q(s_{t+1}, a_{max})$. In order to find the action a_{max}, which maximizes the Q value for state s_{t+1}, a simple strategy is used. The action space is discretized in a set of actions according to the smallest resolution distinguished in the environment . For each action, the Q value is computed and the maximum Q value is used. If the SONQL algorithm is applied in a task in which there is only one continuous action, the computational cost associated with the searching of a_{max} does not represent a problem. However, if more continuous actions are present, the required time can increase appreciably and the feasibility of the algorithm decreases. As will be described in Section 5.7, the SONQL algorithm is used to learn a reactive behavior which can have multiple continuous states and one continuous action for each DOF of the robot. The behavior uses one SONQL algorithm for each DOF and therefore, the computational cost of searching the a_{max} action will not represent any problem.

It is very important to note that two different learning processes are simultaneously in execution and with direct interaction. First of all, the Q_learning algorithm updates the Q values in order to converge to the optimal Q function. On the other hand, the NN algorithm updates its weights to approximate the Q values. While the Q function is not optimal, both processes are updating the weights of the network to fulfill its learning purposes. It is clear that the stability and convergence of the NQL algorithm can be seriously affected by this dual learning. The next section will focus on this issue.

Finally, Equation 5.1 shows that the necessary variables to update the Neural-Q_function are the initial state s_t, the taken action a_t, the received reward r_{t+1} and the new state s_{t+1}. These four variables (the states and actions can be multidimensional) constitute a *learning sample.* This term will be used in the following subsections.

5.3.3 Back-propagation algorithm

The learning algorithm applied to the NQL is the popular back-propagation algorithm, refer to [Haykin, 1999]. This algorithm has two important phases.

In the *forward* phase, an input vector is applied to the input layer and its effect is propagated through the network layer by layer. At the output layer, the error of the network is computed. In the *backward* phase, the error is used in an *error-correction* rule to update the weights of the network starting in the output layer and ending in the first hidden layer. Therefore, the error is propagated backwards.

The correction rule used to update a weight $w_{ji}^{(l)}$ is based on different aspects. A first term is the *local gradient* $\delta_j^{(l)}$ which is influenced by the propagated error and the derivative of the activation function. The derivative is calculated for the induced local field $v_j^{(l)}$ computed in the forward phase. The derivative represents a sensitivity factor which determines the direction of search in the weight space. The second term is the output signal $y_i^{(l-1)}$ transmitted through the weight. The final term is the learning rate α which determines the learning speed. If a small rate is used, the convergence of the NN to the desired function will require many iterations. However, if the rate is too large, the network may become unstable and may not converge. For a more detailed comprehension of back-propagation refer to Algorithm 3. The algorithm has been adapted to the NQL network and uses as input a learning sample k.

The activation function determines the capability of learning nonlinear functions and guarantees the stability of the learning process. The activation function that in the hidden layers is a *sigmoidal* function, in particular the *hyperbolic tangent* function. This function is antisymmetric and accelerates the learning process. The equation of this function can be seen in Algorithm 3 and Figure 5.3 shows its graph. The reason why sigmoidal functions are generally used in neural networks is for its derivative. The maximum of a sigmoidal derivative is reached when the local field is equal to 0. Since the weight change depends on this derivative, its maximum change will be performed when the function signals are in their midrange. According to [Rumelhart et al., 1986] this feature contributes to stability. The activation function of the output neuron is a *linear* function. This permits the Q function to reach any real value, since sigmoidal functions become saturated to a maximum or minimum value.

A final aspect taken into account is the *weight initialization*. This operation is done randomly but the range of values of this random function is very important. For a fast convergence, it is preferred that the activation function operate in the non-saturated medium zone of its graph, see Figure 5.3. To operate in this range, the number of inputs of each neuron and the maximum and minimum values of these inputs has to be known. Therefore, according to these parameters, the maximum and minimum values in which a weight

Algorithm 3: Back-propagation algorithm adapted to NQL.

```
1. Initialize the weights $w_{ji}^{(l)}$ randomly
2. **For** each *learning sample* $k$, composed by:
        $\{s_t(k), a_t(k), s_{t+1}(k), r_{t+1}(k)\}$
  **Repeat:**
    (I) Forward computation
      **For** each neuron $j$ of each layer $l$, **compute:**
        a) the induced local field
            $$v_j^{(l)}(k) = \sum_{i=0}^{n_n(l-1)} w_{ji}^{(l)} y_i^{(l-1)}(k)$$
          where, $n_n(l-1)$ is the number of neurons of layer $l-1$
        b) the output signal $y_j^{(l)}(k)$
            $$y_j^{(l)}(k) = \varphi^{(l)}(v_j^{(l)}(k))$$
          where, $\varphi^{(l)}(x)$ is the activation function of layer $l$, and corresponds to,
          - hyperbolic tangent in hidden layers: $\varphi(x) = 1.7159tanh(0.6667x)$
          - linear function in the output layer: $\varphi(x) = x$
    (II) Error computation
      a) the output of the NQL is found in the last layer $L$ :
            $NQL(s_t(k), a_t(k)) = y_1^{(L)}(k)$
      b) the desired NQL response $d(k)$ is:
            $d(k) = r_{t+1}(k) + \gamma \cdot max_{a_{max}} NQL(s_{t+1}(k), a_{max})$
      c) and the error is:
            $e(k) = d(k) - NQL(s_t(k), a_t(k))$
    (III) Backward computation
      a) compute the local gradient of the output neuron:
            $$\delta_1^{(L)}(k) = e(k)\varphi'_L(v_1^{(L)}(k))$$
        where, $\varphi'_L$ is the derivative of $\varphi$ and it is equal to 1 (as $\varphi(x) = x$)
      b) **For** the rest of the neurons, starting from the last hidden layer,
      **compute** the local gradient:
            $$\delta_j^{(l)}(k) = \varphi'_{l<L}(v_j^{(l)}(k)) \sum_i \delta_i^{(l+1)}(k) w_{ij}^{(l+1)}$$
        where, $\varphi'_{l<L}$ is equal to: $\varphi(x)' = 1.1439(1 - tanh^2(0.6667x))$
      c) **For** all the weights of the NQL, **update** its value according to:
            $$w_{ji}^{(l)} = w_{ji}^{(l)} + \alpha \delta_j^{(l)}(k) y_i^{(l-1)}(k)$$
```

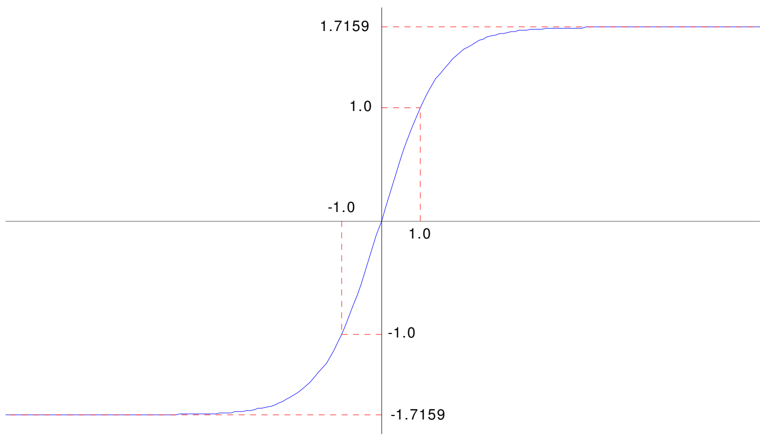

Figure 5.3: Sigmoidal function used as the activation function of the hidden layers. In particular, the function is antisymmetric with the form of a hyperbolic tangent.

can be initialized is calculated. The weight initialization implies that the maximum and minimum values of the input network signals must be known. As these signals are the state and action, which depend on the problem to be solved by reinforcement learning, a normalization, from -1 to 1, must be applied beforehand. Using this normalization, the weight initialization process will not change if the NQL algorithm is applied in different problems.

5.4 Semi-Online Learning

The previous section presented the Neural-Q_learning approach, also known as direct Q-learning. This approach has already been analyzed [Baird, 1995], and demonstrated as being unstable in simple tasks. Therefore, the convergence of Neural-Q_learning is not guaranteed and will depend on the application. This instability has also been verified in a well-known generalization problem, refer to Section 7.2. As will be described, the algorithm was not able to converge in a considerable percentage of the experiments.

The problem Neural Networks have when used to generalize with an RL algorithm is known as the *interference problem*, see Section 4.6.4. Interference in NN occurs when learning in one zone of the input space causes loss of learning in other zones. It is specially prevalent in online applications where the learning process is done according to the states and actions visited rather than with some optimal representation of all the training data [Weaver et al., 1998]. The cause of this problem is that two learning processes are actuating at the same time and each process is based on the other. Q_learning uses the NN to update the Q values and the NN computes the error of the network according to Q_learning the algorithm. This dual learning makes the NQL algorithm very unstable, as has been shown. An important problem is that each time the NN updates the weights, the whole function approximated by the network is slightly modified. If the NQL algorithm updates the network using learning samples, which are all located in the same state/action zone, the non-updated state/action space will be also be affected. The result is the state/action zones which have been visited and learnt are no longer remembered. If the NQL algorithm is updating different state/action zones but with no homogeneity, the interaction between Q_learning and the NN can cause instability.

The solution to the interference problem is the use of a Network which acts locally and assures that learning in one zone does not affect other zones. Approaches with Radial Basis Functions have been proposed to this end [Weaver et al., 1998], however, this implies abandoning the high generalization capability of a multilayer NN with back-propagation. The solution used in this thesis proposes the use of a *database* of *learning samples*. This solution was suggested in [Pyeatt and Howe, 1998], although to the author's best knowledge, there are no proposals which use it. The main goal of the database is to include a representative set of visited learning samples, which is repeatedly used to update the NQL algorithm. The immediate advantage of the database, is the stability of the learning process and its convergence even in difficult problems. Due to the representative set of learning samples, the Q_function is regularly updated with samples of the whole visited state/action space, which is one of the conditions of the original Q_learning algorithm. A consequence of the database is the acceleration of the learning. This second advantage is most important when using the algorithm in a real system. The updating of the NQL is done with all the samples of the database and, therefore, the convergence is achieved with less iterations.

It is important to note that the learning samples contained in the database are samples which have already been visited. Also the current sample is always included in the database. The use of the database changes the concept of online learning which Q_learning has. In this case, the algorithm can be considered as *semi-online*, since the learning process is based on current as well as past samples. For this reason the proposed reinforcement learning algorithm has been named *Semi-Online Neural-Q_learning* algorithm (SONQL).

Each learning sample, as defined before, is composed of the initial state s_t, the action a_t, the new state s_{t+1} and the reward r_{t+1}. During the learning evolution, the learning samples are added to the database. Each new sam-

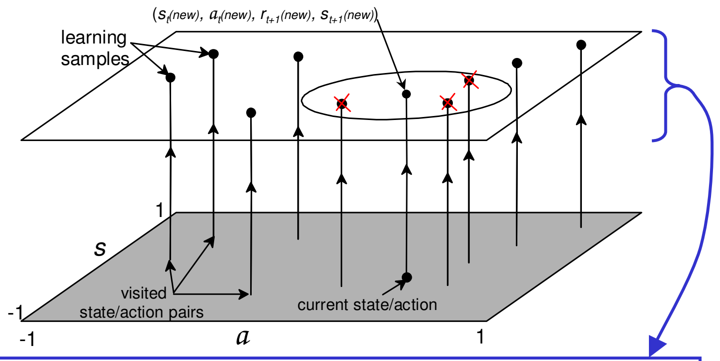
$(s_t(new),\ a_t(new),\ r_{t+1}(new),\ s_{t+1}(new))$
learning samples
1
s
visited state/action pairs
current state/action
-1
-1
a
1

if $\left(\sqrt{\left(s_t(new) - s_t(old)\right)^2 + \left(a_t(new) - a_t(old)\right)^2 + \left(r_{t+1}(new) - r_{t+1}(old)\right)^2} < t\right)$

then: remove the old learning sample $\rightarrow \left\{s_t(old), a_t(old), r_{t+1}(old), s_{t+1}(old)\right\}$

Figure 5.4: Representation of the learning sample database. The state and action have only one dimension. The replacement rule for all the old samples is also shown.

ple replaces older samples previously introduced. The replacement is based on the geometrical distance between vectors (s_t, a_t, r_{t+1}) of the new and old samples. If this distance is less than a *density parameter* t for any old sample, the sample is removed from the database. The size of the database is, therefore, controlled by this parameter which has to be set by the designer. Once the algorithm has explored the reachable state/action space, a homogeneous, and therefore, representative set of learning sample is contained in the database. Figure 5.4 shows a representation of the learning samples database in a simple case in which the state and action are only one-dimensional.

The selection of s_t, a_t and r_{t+1} to determine if an old learning sample has to be removed has several reasons. The use of only s_t and a_t, and not s_{t+1} is due to the assumption that the dynamic of the environment is highly deterministic. Therefore, it is assumed that if two samples have the same s_t and a_t values, but different s_{t+1}, it means that the environment may have changed. It is preferable then to remove the old sample and retain the new sample which should be more representative of the environment. Since the application of the SONQL algorithm is for robot learning, it is assumed that the stochastic transition which may occur is not significative. Finally, the use of r_{t+1} is only to acquire more samples in the space zones in which the reward changes. If s_t and a_t of the old and new samples are very close but the reward is different, it is important to retain both samples. This will allow to the algorithm to concentrate on these samples and learn the cause which make the reward different.

After including the database of learning samples, the difference between a NQL iteration and a SONQL iteration must be distinguished. In each iteration of the SONQL algorithm there will be as many NQL iterations as the number of samples. Moreover, the number of SONQL iterations is equivalent to the number of interactions with the environment. This justifies the learning acceleration, since for each environment interaction, the SONQL algorithm updates the NQL function several times. Finally, the improvements caused by the database have not been theoretically demonstrated, although this section has attempted to justify them. Only empirical results, see Chapter 7, validate the proposal.

5.5 Action Selection

After updating the Q function with the learning samples, the SONQL algorithm must propose an action. As the algorithm is based on Q_learning, which is an off-policy algorithm, any policy can be followed. In practice, the policy followed is the $\epsilon - greedy$ policy, which was described in Section 5.2. With probability $(1 - \epsilon)$, the action will be the one which maximizes the Q_function in the current state s_{t+1}. Otherwise, an aleatory action is generated. Due to the continuous action space in the Neural-Q_function, the maximization is accomplished by evaluating a finite set of actions. The action space is discretized with the smallest resolution that the environment is able to detect. In the case of a robot, the actions would be discretized in a finite set of velocity values considered to have enough resolution for the desired robot performance. As commented in Section 5.3.2, if more than one action is present, the search of the optimal action can require a lot of computation. In that case, the search of the greedy action is necessary to obtain the $Q(s, a_{max})$ value. The search of the greedy action is one of the drawbacks of continuous functions, as pointed out in [Baird and Klopf, 1993]. However, the SONQL algorithm was designed to learn only one DOF of the robot and, therefore, this problem is avoided in the results presented in this thesis. Section 5.7 details the application of the SONQL algorithm.

5.6 Phases of the SONQL Algorithm

In this section, the Semi-Online Neural-Q_learning algorithm is broken down in a set of phases. This break down allows a clearer comprehension of the algorithm. Each phase is used to fulfill a simple task of the algorithm. The algorithm is structured sequentially starting with the observation of the environment state and finishing with the proposal of a new action. The SONQL algorithm is divided into four different phases which are graphically shown in Figure 5.5.

Phase 1. LS Assembly. In the first phase, the current Learning Sample (LS) is assembled. The LS is composed of the state of the system s_t, the action a_t taken from this state, the new state s_{t+1} reached after executing the action, and the reward r_{t+1} received in the new state. The action will usually be the one generated in the fourth phase of this algorithm. However, in some applications an external system can modify the executed action. For instance, in the control architecture proposed in Section 3.2, the action proposed by a higher priority behavior can be selected instead of the one proposed by the SONQL algorithm. Therefore, the real executed action must be observed. The last term to complete the learning sample is the reward r_{t+1}. Although in the original RL problem the reward is perceived from the environment, in this approach it has been included as a part of the algorithm. However, it is computed according to a preprogrammed function which usually uses the state s_{t+1}. This function has to be set by the programmer, and will determine the goal to be achieved.

Phase 2. Database Update. In the second phase, the database is updated with the new learning sample. As has been commented on, old samples similar to the new one will be removed. Therefore, all the samples contained in the database will be compared with the new one.

Phase 3. NQL Update. The third phase consists of updating the weights of the NN according to Algorithm 3. For each sample of the database, an iteration of the NQL algorithm with the back-propagation algorithm is performed.

Phase 4. Action Selection. The fourth and final phase consists of proposing a new action a_{t+1}. The policy followed is the $\epsilon - greedy$, which was described in Section 5.5.

5.7 SONQL-based behaviors

After having analyzed the SONQL algorithm, this section shows the application for which it was designed. The goal of the SONQL algorithm is to learn the state/action mapping of a reactive behavior, as introduced in Section 3.1. An example of a reactive behavior is the *target following* behavior.

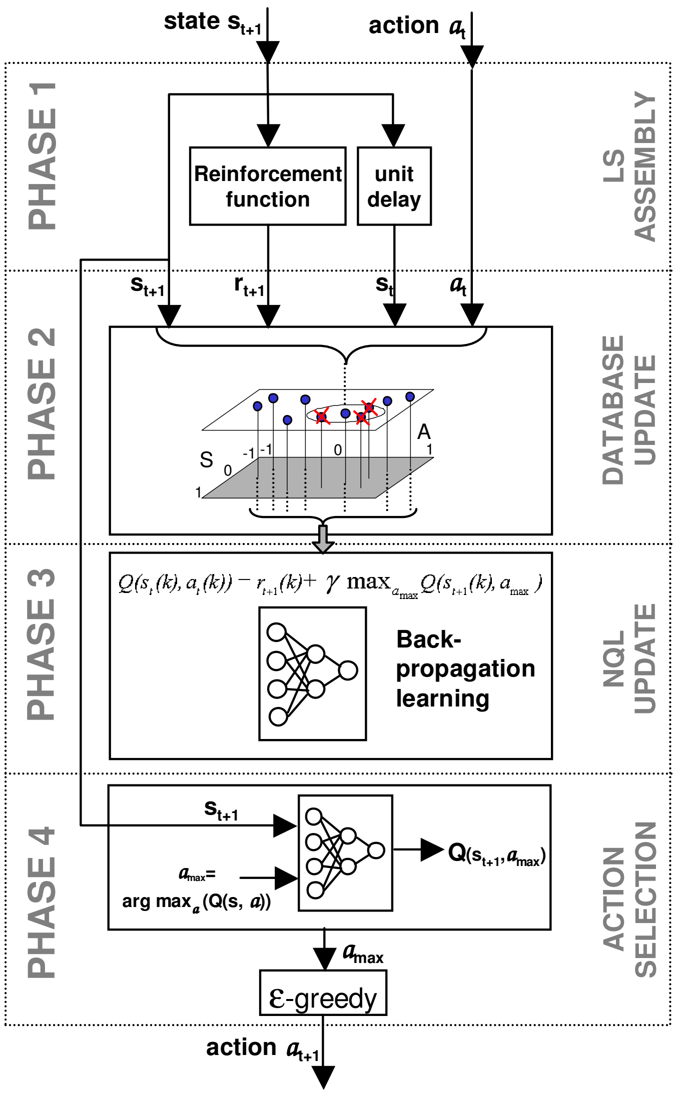

Figure 5.5: Phases of the Semi-Online Neural-Q_learning algorithm.

In this case, the goal of the behavior is to generate the control actions which, according to the position of the target, make the robot follow the target. In this kind of application, the states and actions are usually continuous, which causes the generalization problem. The use of the SONQL algorithm permits the learning of the state/action mapping solving the generalization problem. The SONQL algorithm makes Reinforcement Learning feasible for this application.

The implementation of the reactive behavior with the SONQL algorithm implies the accomplishment of an important condition. The behavior has to generate a control action at the frequency of the high-level controller. This means that the SONQL algorithm cannot stop the periodic execution of the robot control system. To guarantee this constraint, the SONQL algorithm is implemented with two different *execution threads*. The *control* thread has a high priority and is executed at the frequency of the high-level controller. This thread computes phases 1, 2 and 4 of the SONQL algorithm, that is the "LS assembly", the "database update" and the "action selection". These phases do not require a great deal of computation and are used to memorize the new learning sample and to generate a new control action. The second thread is the *learning* thread, which contains phase 3 and requires more computation. This thread has a lower priority and will be executed during all the available time until all the samples of the database have been updated. Therefore, the available computational resources will be used to update the NQL function. Figure 5.6 shows the SOQNL algorithm arranged with these two threads.

As in all Reinforcement Learning problems, the application of the SONQL algorithm in a behavior implies the identification of the environment. Everything external to the algorithm having an influence over the observed state is considered as the environment. The observed state will depend on the current state and the executed control action. This action is generated by the hybrid coordinator which can or cannot use the action proposed by the SONQL algorithm. For this reason, and taking advantage of the *off-policy* feature of Q_learning, this final action is feedback to the SONQL algorithm, see Figure 5.7. Once the final action has been generated, the low-level controller will actuate over the robot which will move accordingly. These systems are considered as the environment of the RL problem. Also, included in the environment, a perception module will be responsible for observing the environment state which will, in turn, be sent to the SONQL algorithm.

It is very important to note that the Q_learning theory is based on the assumption that the environment can be modelled with a FMDP. The most important constraint of this assumption is that the state contains a complete observation of the environment. Therefore, the state must contain all

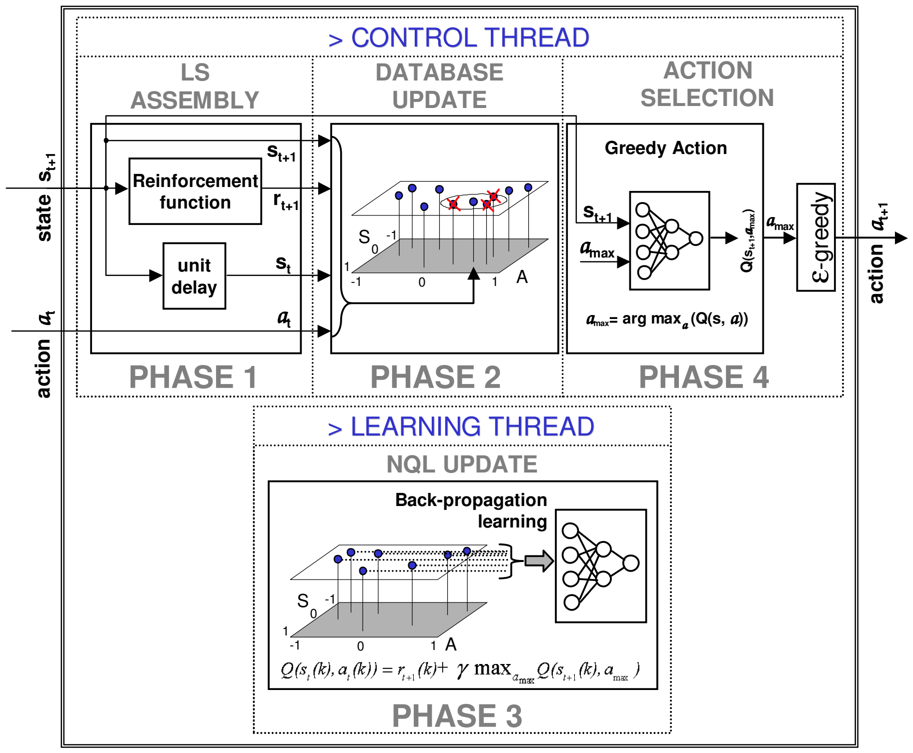

Figure 5.6: Diagram of the SONQL algorithm in its implementation for a robot behavior. The control thread is used to acquire new learning samples and generate the control actions. The learning thread, with less priority, is used to update the NQL function.

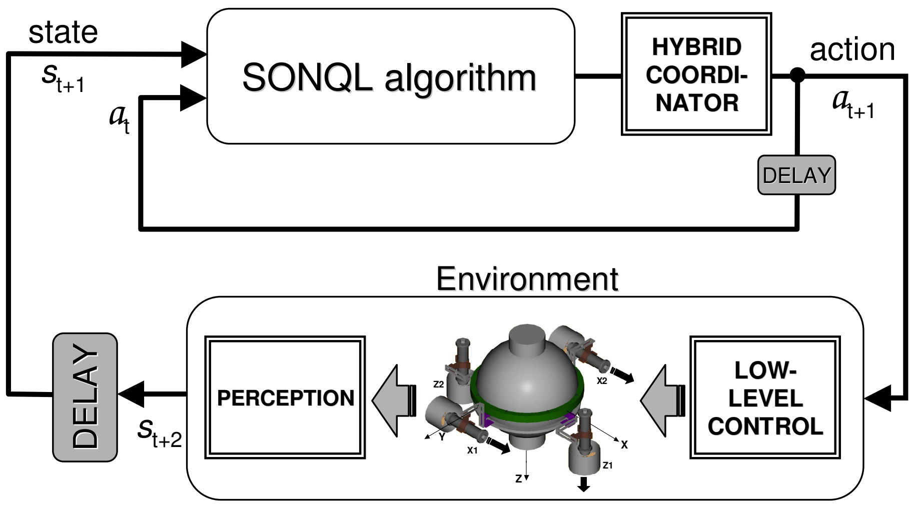

Figure 5.7: Diagram of the SONQL algorithm acting as a behavior, respect to the robot control system.

the variables needed to predict the new state without using past information. An easy mistake when applying RL to a real system is to not provide the complete state, which breaks the theoretical assumptions and makes the learning impossible. It is also very common to not observe the state correctly and this also impedes the learning. The importance of the correct observation of the Markovian state is one of the biggest problems of RL together with the generalization problem. This issue will be covered in the experimental results shown in Chapter 7.

As has been described, the implementation of the reactive behaviors can be accomplished using the SONQL algorithm, which contains the state/action mapping. However, a behavior response, as defined is Section 3.2, is also composed by an *activation level*. The SONQL algorithm does not include this activation level, and has to be manually implemented. For example, in the case of the *target following* behavior, the activation level will be $a_i = 1$ if the target is detected, otherwise it will be $a_i = 0$. Therefore, the implementation of a SONQL-based behavior requires the definition of the reinforcement function and the activation level function.

Another implementation aspect is the uncoupling of the degrees of freedom (DOF) of the robot. For each DOF of the robot, an independent SONQL algorithm is used. This greatly improves the real-time execution of the SONQL algorithm. The searching of the a_{max} action is accomplished by discretizing the action space. If more than one action is present, the num-

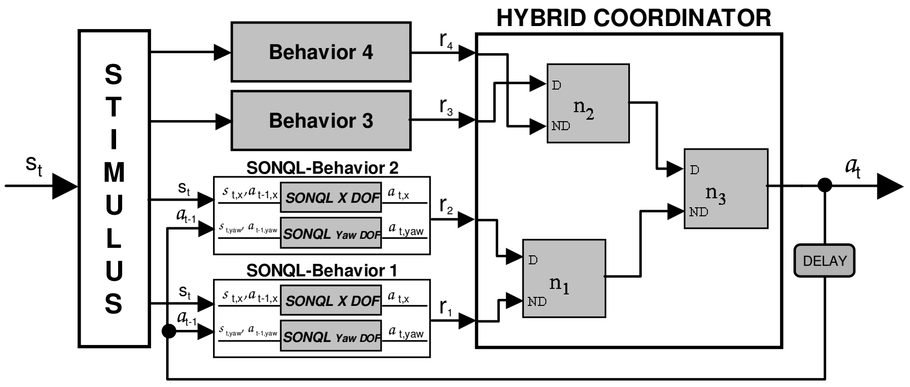

Figure 5.8: Example of the behavior-based control layer with two SONQL-based behaviors.

ber of combinations will be very high and the algorithm will need a number of computations to find the greedy action. It must be noted that, this greedy action has to be found in the fourth phase of the algorithm and for each learning sample learnt in phase two. The use of more than one action with the SONQL algorithm is an important problem to ensure the real-time execution of the algorithm. The adopted solution consists of having a different SONQL for each DOF with each one is independently learnt. This could be a disadvantage. However, the simultaneous learning of two DOFs in practice would make the correct observation of the Markovian state very difficult, as will be shown in Section 7.1. This means that the limitation of the SONQL algorithm with multiple actions is not a basic necessity in most robotics tasks. Figure 5.8 shows an example of the behavior-based control layer in which there are two SONQL-based behaviors and two manually tuned behaviors. Two different learning algorithms have been used for each SONQL behavior.

As already commented on, the state has to contain all the necessary variables to predict the new state. It is very important to simplify the state information as much as possible. For example, the target following behavior will need the position of the target with respect to the robot. If the target is detected through a video camera, it is necessary to reduce the pixel information to a simple value. For each DOF, this value is calculated according to the position of the target in the image or the size of the target. Figure 5.9 shows how the target position has been translated in three variables $\{f_x, f_y, f_z\}$.

Finally, the reinforcement function must be designed in order to point out the goal of the behavior. Although any reward value can be assigned to a state, only a finite set of values are used in the SONQL-based behaviors: $\{-1, 0, 1\}$. Figure 5.9 shows the reinforcement functions $\{r_x, r_y, r_z\}$ for each

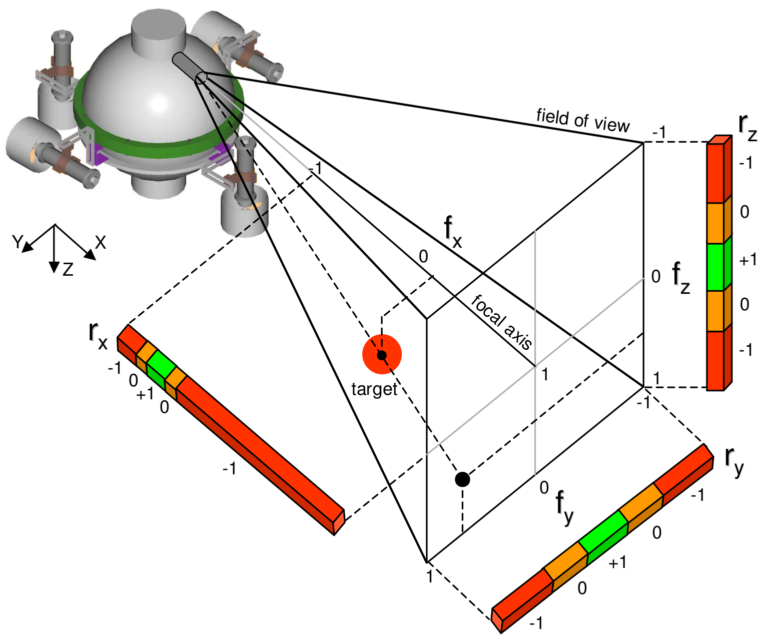

Figure 5.9: State $\{f_x, f_y, f_z\}$ and reward $\{r_x, r_y, r_z\}$ variables in a *target following* behavior.

DOF. The simplicity of the function reduces the necessary knowledge of the designer to implement a new behavior. Section 7 demonstrates the facility and feasibility of this reinforcement function definition.

5.8 Discussion

The proposed SONQL algorithm has been demonstrated to be a feasible approach to learn each DOF of a robot behavior. The experimental results will be analyzed in Chapter 7. However, it is important to summarize the theoretical aspects in which this approach is based. The SONQL is based on Q_learning and uses a Neural Network and a database of learning samples to solve the generalization problem. The use of Q_learning is because its learning procedure is off-policy. Another feature is that it uses the action-value function, Q, from which the optimal policy is easy to extract. The reason a Neural Network was used is for its high generalization capability. However, these two components, Q_learning and NN, contradict some of the convergence proofs explained in Section 4.6. First, the convergence of linear approximators combined with off-policy methods is not guaranteed. Indeed, there are counterexamples which show the divergence. In addition, NN is a non-linear function approximator for which the convergence is also not guaranteed. The large number of successful examples which have been demonstrated in practice are the only reasons to justify the selection of these techniques.

Besides convergence proofs, Neural Networks suffer from the interference problem when they are used as function approximators with RL algorithms as explained in Section 4.6.4. To solve this problem, the SONQL algorithm uses the database of learning samples. The goal of this database is to acquire a representative set of samples,which continually update the NN. The homogeneity which the database provides is able to solve the interference problem. In addition, this database accelerates the learning process since several updates can be performed at each environment iteration.

The main drawback of the SONQL algorithm is the searching of greedy actions. As has been described in Section 5.5, greedy actions are found by discretizing the action space. From a control point of view, this is not a problem if the discretization is fine enough. However, the necessary computation increases if several continuous actions are present. This problem does not appear in the implementation of the SONQL algorithm in a reactive behavior. For each DOF of the robot, an independent SONQL algorithm is used. Since the main goal of this approach was to design an RL algorithm able to learn robot behaviors, this drawback was not considered, although it represents one of the future works of this dissertation.

Finally, the use of the SONQL in a behavior requires the definition of a set of parameters: the NN configuration (number of layers and neurons), the learning rate α, the discount factor γ, the exploration probability ϵ, the database density parameter t, the reinforcement function $r_i(s)$ and the activation level function a_i. Also, the goal to be accomplished by the behavior has to be analyzed, assuring that the state is completely observed. A first conclusion of the SONQL-based behaviors could induce a very complex technique for solving a much simpler problem. However, it has to be noted that most of these parameters will depend on the robot's dynamics and, therefore, they will be equal for other behaviors. These invariant parameters are: the NN configuration (number of layers and neurons), the learning rate, the discount factor, the exploration probability and the database density parameter. Consequently, the implementation of a new behavior will require only the design of the reinforcement function, the activation level function and the analysis of the behavior task. These two functions, as has been shown, are very simple and intuitive.

Chapter 6

URIS' Experimental Set-up

The experimental set-up designed to work with the Autonomous Underwater Vehicle URIS is compounded of a water tank, two sensory systems, a distributed software application and the robot itself. The overall set-up is shown in Figure 6.1. The correct operation of all these systems in real-time computation allows the experimentation and, therefore, the evaluation of the proposed SONQL behaviors and hybrid coordination system. The purpose of this chapter is to report the characteristics of these systems and their interactions. First, the main features of the robot are given. These include the design principles, the actuators and the on board sensors. The two sensory systems, specially designed for these experiments, are then presented. The first of these systems is the target detection and tracking system. The second is the localization system which is used to estimate the three-dimensional position, orientation and velocity of the vehicle inside the water tank. Finally, the software architecture, based on distributed objects, is described.

6.1 Robot Overview

*U*nderwater *R*obotic *I*ntelligent *S*ystem is the meaning of the acronym URIS. This Unmanned Underwater Vehicle (UUV) is the result of a project started in 2000 at the University of Girona. The main purpose of this project was to develop a small-sized underwater robot with which to easily experiment in different research areas like control architectures, dynamics modelling and underwater computer vision. Another goal of the project was to develop an Autonomous Underwater Vehicle (AUV) with the required systems, hardware and software as the word *autonomous* implies. Other principles are flexibility in the tasks to be accomplished and generalization in the developed systems.

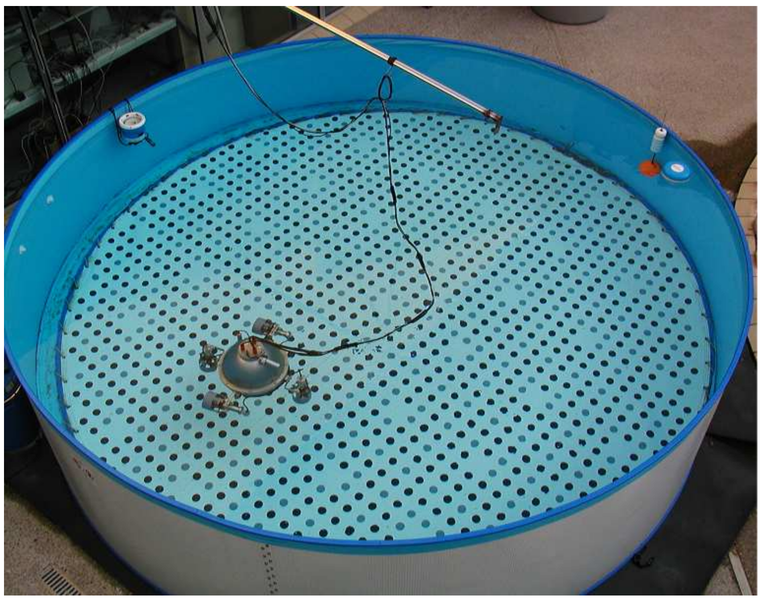

Figure 6.1: URIS' experimental environment.

6.1.1 Design

The design of this vehicle was clearly influenced by its predecessor Garbi UUV [Amat et al., 1996], although some mechanical features were redesigned. The shape of the vehicle is compounded of a spherical hull surrounded by various external elements (the thrusters and camera sensors). The hull is made of stainless steel with a diameter of 350mm, designed to withstand pressures of 3 atmospheres (30 meters depth). On the outside of the sphere there are two video cameras (forward and down looking) and 4 thrusters (2 in X direction and 2 in Z direction). All these components were designed to be water-proof, with all electrical connections made with protected cables and hermetic systems. Figure 6.2 shows a picture of URIS and its body fixed coordinate frame. Referred to this frame, the 6 degrees of freedom (DOFs) in which a UUV can be moved are: *surge*, *sway* and *heave* for the motions in X, Y and Z directions respectively; and *roll*, *pitch* and *yaw* for the rotations about X, Y and Z axes respectively.

URIS weighs 30 Kg., which is approximately equal to the mass of the water displaced and, therefore, the buoyancy of the vehicle is almost neutral. Its gravity center is in the Z axis, at some distance from below the geometrical center. The reason for this is the distribution of the weight inside the sphere. The heavier components are placed at the bottom. This difference between

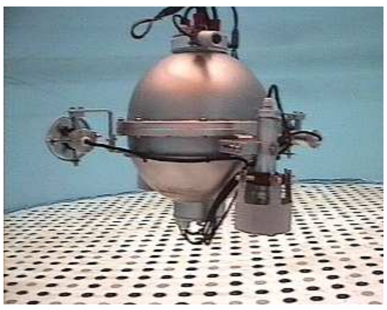
a)

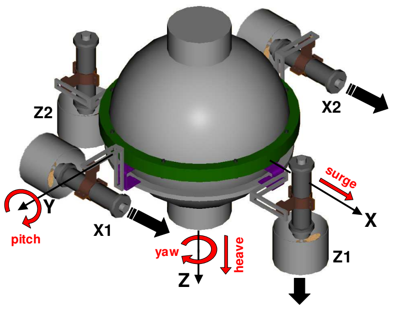

b)

Figure 6.2: URIS' AUV, a) picture b) schema.

the two centers entails a stability in both *pitch* and *roll* DOFs. The further down the gravity center is, the higher the torque which has to be applied in the X or Y axes to incline the robot a certain value in *roll* or *pitch*, respectively.

The movement of the robot is accomplished by its 4 thrusters. Two of them, labelled *X1* and *X2* in Figure 6.2b, exert a force in X axis and a torque in Z axis. The resultant force of both trusters is responsible for the *surge* movement of the vehicle, and the resultant torque is responsible for the *yaw* movement. Analogously, the other two thrusters, Z1 and Z2, exert a force in Z axis and a torque in Y axis. The resultant force is responsible for the *heave* movement of the vehicle, and the resultant torque is responsible for the *pitch* movement. In this case, the *pitch* movement is limited to only a few degrees around the stable position, since the gravity and buoyancy forces cause a high stabilization torque compared to that of the thruster. Therefore, only 4 DOFs can be actuated leaving the *sway* and *roll* movements without control. Like the *pitch* DOF, the *roll* DOF is stabilized by the gravity and buoyancy forces. The *sway* movement is neither controlled nor stabilized by any force, which makes it sensitive to perturbations like water currents or the force exerted by the umbilical cable. Hence, URIS is a nonholonomic vehicle.

The inside of the hull was arranged to contain all the necessary equipment for an autonomous system. First of all, the lower part of the sphere contains various battery packages conceived to power the vehicle for a period of one hour. A second level, above the batteries, contains the drivers of the 4 thrusters. Some electronic boards, mainly sensor interfaces, are also included in this level. In the third level, all the hardware components and electrical connections among all systems is found. The hardware architecture is compounded of two embedded computers. One computer is mainly in charge of the control of the robot and the other is used for image processing and other special sensors. The communication between computers is done through an ethernet network and the communication between these computers and sensors/actuators is done through other interfaces: serial lines, analog and digital inputs and outputs, and video frame grabbers. All these devices, except the thruster drivers, are powered by a DC-DC converter which supplies different voltages. The thruster drivers are directly powered by some battery packages specifically used for that purpose.

Besides the systems located in the robot, URIS' experimental set-up is also compounded of external systems, making some kind of connection indispensable. For this purpose, an underwater umbilical cable is used. Three different types of signals are sent through this cable. First, two power signals are sent to the robot to supply the power for the thrusters and the power for all the electronics independently. The second type of signal is an ethernet connection, connecting the on-board and off board computers. Finally, two video signals from the two on board cameras are also transmitted. Different reasons justify the use of this umbilical cable. First, the use of external batteries increases the operation time of the robot up to the whole journey. The second reason is to help in the understanding of the experiments, allowing a real-time supervision of them through data and video monitoring. The third reason is to allow the computation of a part of the software architecture out board, such as the target tracking (Section 6.2) and the localization system (Section 6.3). The first and second reasons are aids in the development of any new experiment. The third reason allows us to confront some technological problems using external hardware and computational resources.

6.1.2 Actuators

As commented on above, URIS has four actuators to move the vehicle in four DOFs. Each actuator or thruster is equipped with a DC motor, encapsulated in a waterproof hull and connected, through a gear, to an external propeller. Around the propeller, a cylinder is used to improve the efficiency of the water jet. The power of each thruster is 20 Watts carrying out a maximum thrust of 10 Newtons at 1500 rpms. The control of the DC motor is accomplished by a servoamplifier unit. This unit measures the motor speed with a tachodynamo and executes the speed control according to an external set-point. The unit also monitors the values of the motor speed and electric current. Communication between the onboard computer and each motor control unit is done through analog signals.

6.1.3 Sensors

The sensory system is one of the most important parts in an autonomous robot. The correct detection of the environment and the knowledge of the robot state, are very important factors in deciding how to act. URIS has a diverse set of sensors. Some of them are used to measure the state of the robot and others to detect the environment. Hereafter the main characteristics and utility of each sensor are commented upon.

- **Water Leakage Detection**. In order to detect any water leakage, there are several sensors which use the electric conductivity of the water to detect its presence. These sensors are located inside each thruster case as well as inside the lower part of the hull. Any presence of water is immediately sited before valuable systems can be damaged. The interface of the sensors is through digital signals.

- **Thruster monitors**. As commented on in Section 6.1.2, each thruster is controlled by a control unit which monitors the thruster's rotational speed and its electric current. These two analog measures can be used to detect faults. For instance, if the current is much higher or much lower than in normal conditions, it may mean that the helix has been blocked or has been lost. In addition, knowledge of the thruster speeds can be used to calculate the thrust and, using the dynamics model of the vehicle , to estimate the acceleration, velocity and position of the vehicle. Obviously, the inaccuracies of the model, the external perturbations and drift of the estimations would entail to a rough prediction, but combining it with another navigation sensor, a more realistic estimation can be obtained.

- **Inertial Navigation System**. An inertial unit (model MT9 from Xsens) is also placed inside the robot. This small unit contains a 3D accelerometer, a 3D rate-of-turn sensor and a 3D earth-magnetic field sensor. The main use of this sensor is to provide accurate real-time orientation data taken from the rate-of-turn sensor. The accelerometers and the earth-magnetic field sensors provide an absolute orientation reference and are used to completely eliminate the drift from the integration of rate-of-turn data. From this sensor then, the *roll*, *pitch* and *yaw* angles can be obtained. The interface with the sensor is through the serial line.

- **Pressure sensor**. This sensor measures the state of the robot. In this case, the pressure detected by the sensor provides an accurate measurement of the depth of the robot. Due to the electromagnetic noise, the sensor signal needs hardware and software filtering and also data calibration.

- **Forward and Downward looking video cameras**. Unlike previous sensors, the video cameras provide detection of the environment. URIS has two water-proof cameras outside the hull. One of them is a color camera looking along the positive X axis, see Figure 6.2. The use of this camera is to detect targets, as will be shown in Section 6.2. Another use is for teleoperation tasks. The second camera is a black-and-white camera looking along the positive Z axis. The main utility of this camera is the estimation of the position and velocity of the vehicle. For this purpose, two different approaches have been considered. In the first approach, the motion estimation is performed from images of the real underwater bottom using visual mosaicking techniques. This localization system is one of the research lines of the underwater robotics group [Garcia et al., 2001]. The second approach was inspired by the first and was developed to work specifically in the URIS experimental set-up. It is a localization system for structured environments based on an external coded pattern. For further information on both systems refer to Section 6.3.
- **Sonar transducer**. This sensor is used to detect the environment. The sonar transducer (Smart sensor from AIRMAR) calculates the distance to the nearest object located in the sonar beam. The transducer is placed outside the hull looking in the direction in which objects have to be detected. A typical application is to point the beam at the bottom to detect the altitude of the vehicle. The interface of this sensor is through a serial line.

The sensors used in the experiments presented in this dissertation are the water leakage sensors and the two video cameras. The following sections detail the computer vision systems which were developed to extract useful information from the camera images. The forward looking camera was used to detect a moving target in the environment, and the downward looking camera to estimate the state (position and velocity) of the robot inside the water tank.

6.2 Target Tracking

One of the sensory systems developed for the experimental set-up of URIS is the *target detection and tracking* system. This vision-based application

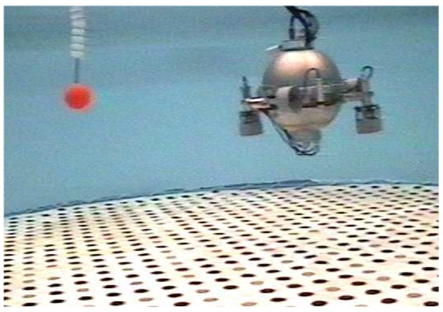

Figure 6.3: URIS in front of the artificial target.

has the goal of detecting an artificial target by means of the forward looking camera. This camera provides a large underwater field of view (about 57^o in width by 43^o in height). This system was designed to provide the control architecture with a measurement of the position of an object to be tracked autonomously. Since the goal of this dissertation is to test control and learning systems, a very simple target was used. The shape selected for the target was a sphere because it has the same shape from whatever angle it is viewed. The color of the target was red to contrast with the blue color of the water tank. These simplifications allowed us to use simple and fast computer vision algorithms to achieve real-time (12.5 Hz) performance. Figure 6.3 shows a picture of the target being observed by URIS.

The procedure of detecting and tracking the target is based on image segmentation. Using this simple approach, the relative position between the target and the robot is found. Also, the detection of the target in subsequent images is used to estimate its relative velocity. The following subsections detail the image segmentation algorithm, the coordinate frame in which the position is expressed and the velocity estimation.

6.2.1 Image Segmentation

The detection of the target is accomplished by color segmentation. This technique is very common in computer vision and consists of classifying each pixel of the image according to its color attributes. The pixels which satisfy the characteristics of the target are classified as part of it. In order to express the color of an object, the *HSL* (Hue, Saturation and Luminance) color space is usually preferred over the standard *RGB* (Red, Green and Blue). Within the HSL color space, the hue and saturation values, which are extracted from the RGB values, define a particular color. Therefore, the color of an object is defined by a range of values in hue and saturation, and the segmented image

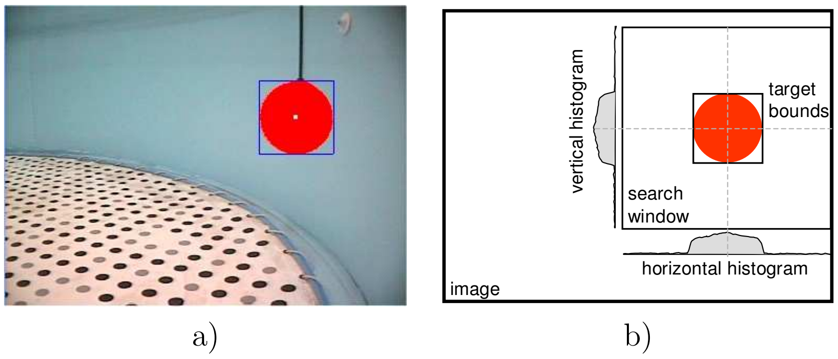

Figure 6.4: Image segmentation, a) real image with the detected target b) scheme used in the segmentation process.

is the one containing the pixels within the hue and saturation ranges.

In this application, the segmentation is carried out in two phases. The first phase consists of finding just a portion of the target within the whole searched image. It is important to ignore pixels which, due to noise or reflections, have a similar color to the target. Therefore, restrictive hue and saturation ranges are applied. The consequence is an image in which only the most saturated portions of the target appear. After the first segmentation, two histograms of the segmented pixels in the horizontal and in the vertical axes of the searched image are calculated. From the two histograms, the maximum values are found. These two coordinates constitute the *starting point* which is considered to belong to the target. In Figure 6.4, the segmentation process in a real image and a scheme of the image, in which the histograms are represented, is shown.

After the computation of the starting point, the second segmentation is carried out. In this case, the segmentation is less severe than the first. What that means is, besides the pixels belonging to the target, other pixels of the image can also be segmented. This segmentation is used to find the portions of the target not detected by the previous one. Using the second segmentation, a region growing process is applied. The growing process is begun at the starting point and will expand the target area until no more segmented pixels are connected between them. At this point, the target has been completely detected, see Figure 6.4a. The position of the target is considered to be the center of the rectangle which contains the target. The size of the target is calculated according to the mean value of the two sides of the rectangle.

The effect of the first segmentation guarantees the correct location of the target even in the presence of noise. On the other hand, the second segmentation guarantees the correct segmentation of portions of the target which may be affected by shadows which reduce the saturation of the color. Finally, instead of searching for the target in the whole image, a smaller window is used, see Figure 6.4b. This window is centered on the position found in the previous image. In case the target is not found inside the window, the whole image is explored.

6.2.2 Target Normalized Position

Once the target has been detected, its relative position with respect to the robot has to be expressed. The coordinate frame which has been used for the camera has the same orientation as the URIS coordinate frame, but is located in the focal point of the camera, see Figure 6.5. Therefore, the transformation between the two frames can be modelled as a pure translation.

The X coordinate of the target is related to the target size detected by the segmentation algorithm. A normalized value between *-1* and *1* is linearly assigned to the range comprised between a maximum and minimum target size respectively. It is important to note that this measure is linear with respect to the size, but non-linear with respect to the distance between the robot and the target measured in X axis. In Figure 6.5 the f_x variable is used to represent the X coordinate of the target.

Similarly, the Y and Z coordinates of the target are related to the horizontal and vertical positions of the target in the image, respectively. However, in this case, the values represented by the f_y and f_z variables do not measure a distance, but an angle. The f_y variable measures the angle from the center of the image to the target around the Z axis. The f_z variable measures the angle from the center of the image to the target around the Y axis. In this case, the angles are also normalized from *-1* to *1* as it can be seen in the Figure 6.5.

As has been described, the coordinates of the target are directly extracted from the position and size found in the segmentation process. This means that the calibration of the camera has not been taken into account. Therefore, the non-linear distortions of the camera will affect the detected position. Moreover, the measures of the f_x variable are non-linear with the distance to the target in X axis. These non-linear effects have consciously not been corrected to increase the complexity with which the SONQL-based behavior will have to deal.

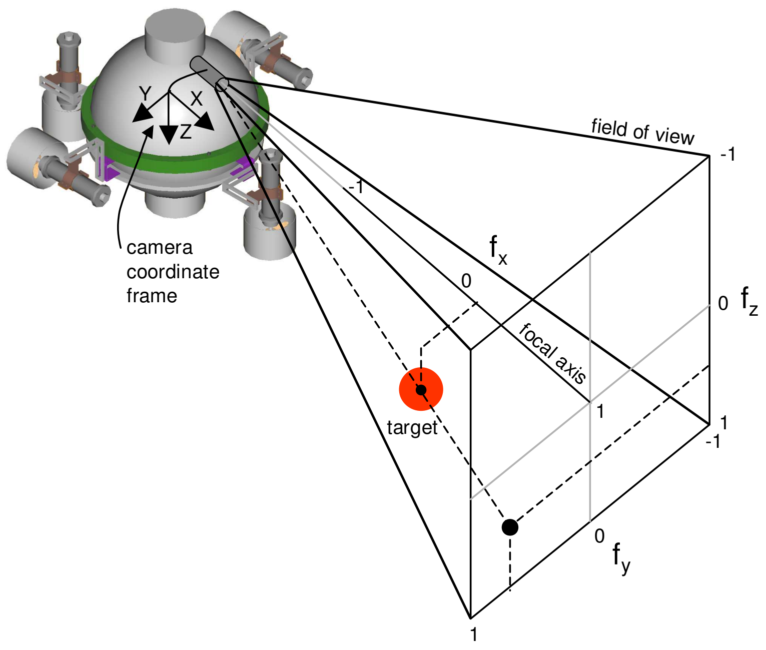

Figure 6.5: Coordinates of the target in respect with URIS.

6.2.3 Velocity Estimation

In order to properly follow the target, the measure of its relative position is not enough. An estimation of its relative velocity is also necessary. To calculate this velocity, the f_x, f_y and f_z variables are differentiated from the sequence of images. In particular, a first order Savitzky-Golay [Savitzky and Golay, 1964] filter, with a first order derivative included, is applied to these signals. The result of this operation is the estimation of $\frac{df_x}{dt}$, $\frac{df_y}{dt}$ and $\frac{df_z}{dt}$. Due to the filtering process, a small delay is added to these signals with respect to the ideal derivatives. However, these delays do not drastically affect the performance of the experiments, as will be shown in Chapter 7. Figure 6.6 shows the movement of the target in Y axis. The target was first moved to the right and then twice to the left. The estimated velocity is also shown.

6.3 Localization System

Localization is the estimation of the vehicle's position and orientation with respect to a global coordinate frame. A localization system is needed when tasks involving positioning have to be carried out. Moreover, an estima-

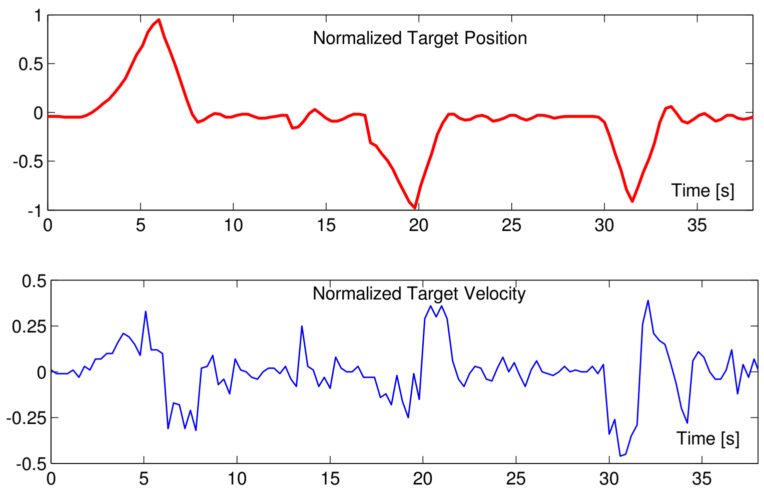

Figure 6.6: Normalized angular position and velocity of the target in Y axis.

tion of the vehicle's velocity is usually required by the low-level controller. The localization of an underwater vehicle is a big challenge. The detection of the vehicle's speed with respect to the water is very inaccurate and not reliable due to water currents. Electromagnetic waves are strongly attenuated when travelling through water, which also dismisses the use of a GPS. Main techniques used for underwater vehicle localization are inertial navigation systems, and acoustic and optical sensors. Among these techniques, visual mosaics have greatly advanced over the last few years offering, besides position, a map of the environment [Negahdaripour et al., 1999, Gracias and Santos-Victor, 2000]. The general idea of visual mosaicking is to estimate the movement of the vehicle by recognizing the movement of some features on the ocean floor. An onboard downward-looking camera is used to perceive these features. Main advantages of mosaicking with respect to inertial and acoustic sensors are lower cost and smaller sensor size. Another advantage is that the environment does not require any preparation, in contrast with some technologies which use a network of acoustic transponders distributed in the environment. However, position estimation based on mosaics can only be used when the vehicle is performing tasks near the ocean floor and requires reasonable visibility in the working area. There are also unresolved problems like motion estimation in presence of shading effects, presence of "marine snow" or non-uniform illumination. Moreover, as the mosaic evolves, a systematic bias is introduced in the motion estimated by the mosaicking algorithm, producing a drift in the localization of the robot [Garcia et al., 2002].

In the experimental set-up used for URIS' AUV, a vision-based localization system was developed. The system was inspired by visual mosaicking techniques [Garcia et al., 2001]. However, simplifications were made in order to have a more accurate and drift free system. Instead of looking at the unstructured ocean floor of a real environment, a coded pattern was used. This pattern has the same size as the water tank and was placed on its bottom. The pattern contains landmarks which can be easily tracked and, by detecting its global position, the localization of the vehicle is accomplished.

The localization system provides an estimation of the three-dimensional position and orientation of URIS referred to in the tank coordinate frame. In addition, an estimation of the vehicle's velocities, including *surge, sway, heave, roll, pitch* and *yaw*, is computed. The algorithm is executed in real-time (12.5 Hz) and is entirely integrated in the controllers of the vehicle.

In the next subsections, detailed information about the localization system is given. First, the projective model of the downward-looking camera is detailed. Then, the design and main features of the coded pattern are described. After describing the main components of the system, the different phases found in the localization algorithm are sequentially explained. Finally, some of the results and experiments concerning the accuracy of the system are presented.

6.3.1 Downward-Looking Camera Model

The camera used by the localization system is an analog B/W camera. It provides a large underwater field of view (about 57^o in width by 43^o in height). We have considered a pinhole camera model, in which a first order radial distortion has been considered. This model is based on the projective geometry and relates a three-dimensional position in the space with a two-dimensional position in the image plane, see Figure 6.7. The equations of the model are the following:

$$\frac{{}^{C}X}{{}^{C}Z} = \frac{(x_p - u_0)(1 + k_1 r^2)}{f k_u} \tag{6.1}$$

$$\frac{{}^{C}Y}{{}^{C}Z} = \frac{(y_p - v_0)(1 + k_1 r^2)}{f k_v} \tag{6.2}$$

$$r = \sqrt{\left(\frac{x_p - u_0}{k_u}\right)^2 + \left(\frac{y_p - v_0}{k_v})\right)^2} \tag{6.3}$$

where, $({}^{C}X, {}^{C}Y, {}^{C}Z)$ are the coordinates of a point in the space with respect to the camera coordinate frame $\{C\}$ and $({}^{I}x_p\ , {}^{I}y_p)$ are the coordinates, measured in pixels, of this point projected in the image plane. And, as to intrinsic

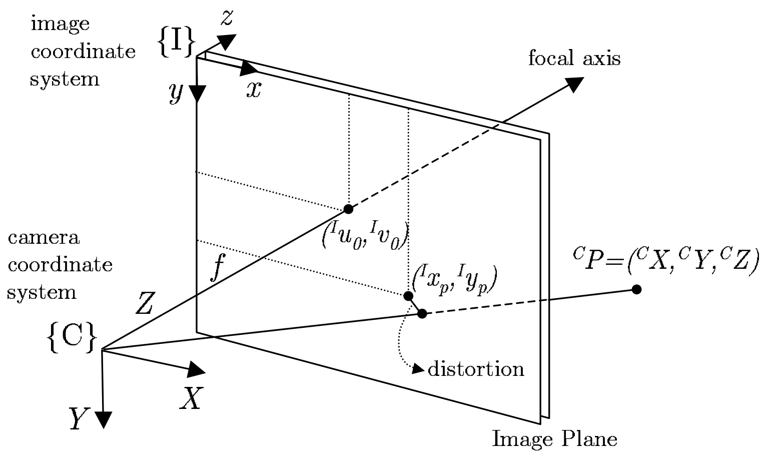

Figure 6.7: Camera projective geometry.

parameters of the camera, $(^Iu_0,^Iv_0)$ are the coordinates of the center of the image, (k_u,k_v) are the scaling factors, f is the focal distance and k_1 is the first order term of the radial distortion. Finally, r is the distance, in length units, between the projection of the point and the center of the image.

The calibration of the intrinsic parameters of the camera was done off-line using several representative images. In each of these images, a set of points were detected and its correspondent global position was found. Applying the Levenberg-Marquardt optimization algorithm [Gill et al., 1981], which is an iterative non-linear fitting method, the intrinsic parameters were estimated. Using these parameters, the radial distortion can be corrected, as can be seen in Figure 6.8. It can be appreciated how radial distortion is smaller for the pixels which are closer to the center of the image $(^Iu_0,^Iv_0)$.

6.3.2 Coded Pattern

The shape of the tank is a cylinder 4.5 meters in diameter and 1.2 meters in height. This environment allows the perfect movement of the vehicle along the horizontal plane and a restricted vertical movement of only 30 centimeters.

The main goal of the pattern is to provide a set of known global positions to estimate, by solving the projective geometry, the position and orientation of the underwater robot. The pattern is based on grey level colors and only round shapes appear on it to simplify the landmark detection, see Figure 6.9. Each one of these rounds or dots will become a global position used in the position estimation. Only three colors appear on the pattern, white as back-

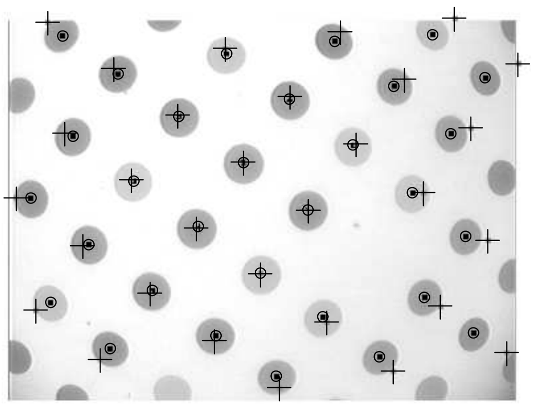

Figure 6.8: Acquired image in which the center of the dots has been marked with a round. After correcting the radial distortion the center of the dots has changed to the one marked with a cross.

ground, and grey or black in the dots. Again, the reduction of the color space was done to simplify the dot detection and to improve the robustness. The dots have been distributed throughout the pattern following the X and Y directions. All lines parallel to the X and Y axis are called the *main lines of the pattern*, see Figure 6.10. This term will be useful in the description of the algorithm used for localization, refer to Section 6.3.3.

The pattern contains some global marks which encode a unique global position. These marks are recognized by the absence of a dot surrounded by 8 dots, see Figures 6.9 and 6.10a. From the 8 dots surrounding the missing dot, 3 are used to find the orientation of the pattern and 5 to encode the global position. The 3 dots marking the orientation appear in all the global marks in the same position and with the same colors. In Figure 6.10a, these 3 dots are marked with the letter "o". In Figure 6.10b it can be seen how, depending on the position of these 3 dots, the direction of the X and Y axis can be detected.

The global position is encoded in the binary color (grey or black) of the 5 remaining dots. Figure 6.10a shows the position of these 5 dots and the methodology in which the global position is encoded. The maximum number of positions is 32. These global marks have been uniformly distributed throughout the pattern. A total number of 37 global marks have been used, repeating 5 codes in opposite positions on the pattern. The zones of the pattern that do not contain a global mark, have been filled with alternately black and grey dots, which help the tracking algorithm, as will be explained in Section 6.3.3.

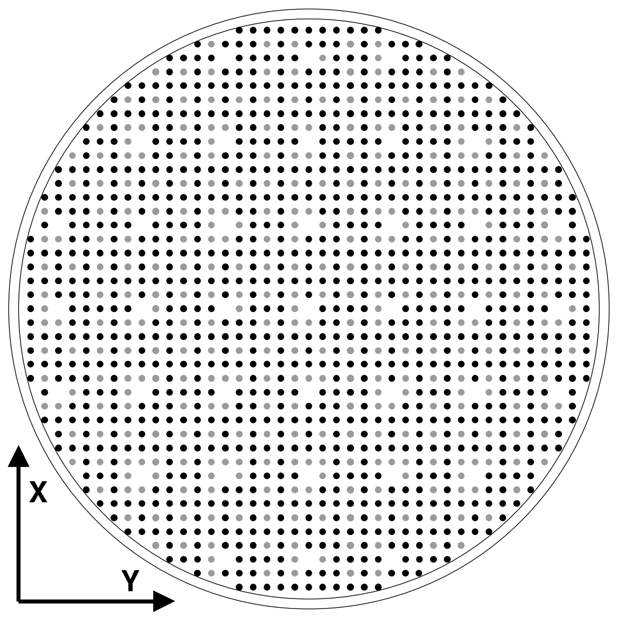

Figure 6.9: Coded pattern which covers the bottom of the water tank. The absence of a dot identifies a global mark.

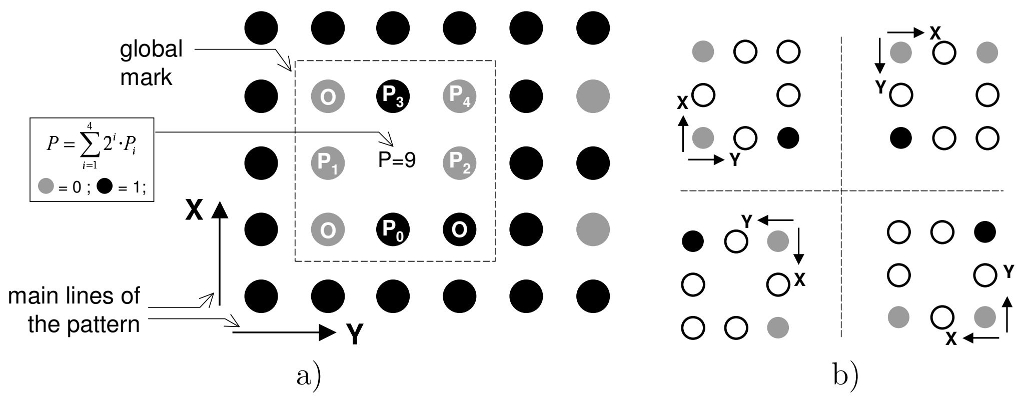

Figure 6.10: Features of the pattern, a) the main lines of the target and details about the absolute marks are shown, b) the three orientation dots of a global mark indicate the direction of the X and Y axis.

In order to decide the distance between two neighboring dots, several aspects were taken into account. A short distance would represent a higher number of dots appearing in the image and, therefore, a more accurate estimation of the vehicle's position. But, if a lot of dots appeared in the image while the vehicle was moving fast, dot tracking would be very hard or even impossible. On the other hand, a long distance between two neighboring dots would produce the opposite effect. Therefore, an intermediate distance was chosen for this particular application. The aspects which influenced the decision were the velocities and oscillations of the vehicle, the camera's field of view and the range of depths in which the vehicle can navigate. The distance between each neighboring dot finally chosen was 10 cm. The range of distances between the center of the robot and the pattern, used in the design are from 50 cm to 80 cm and the minimum number of dots which must be seen is 6, as will be described in the next subsection.

6.3.3 Localization Procedure

The vision-based localization algorithm was designed to work at 12.5 frames per second, half of the video frequency. Each iteration requires a set of sequential tasks starting from image acquisition to velocity estimation. The next subsections describe the phases which constitute the whole procedure.

Pattern Detection

The first phase of the localization algorithm consists of detecting the dots in the pattern. To accomplish this phase, a binarization is first applied to the acquired image, see Figure 6.11a and 6.11b. Due to the non-uniform sensitivity of the camera in its field of view, a correction of the pixel grey level values is performed before binarization. This correction is based on the illumination-reflectance model [Gonzalez and Woods, 1992] and provides a robust binarization of the pattern also under non-uniform lighting conditions.

Once the image is binarized, the algorithm finds the objects in the image. This task is accomplished by an algorithm which scans the entire image and for each pixel that has *white* color, it applies a region growing process. This process expands the region until the boundaries of the objects are found. Some features of the object, like the surface, the center, the boundaries and the aspect ratio, are calculated. Finally, the color of the pixels belonging to the object is changed to *black* and the scanning process is continued until no more *white* pixels are found. Some of the objects which do not fulfill a minimum and maximum surface, or do not have a correct aspect ratio, are

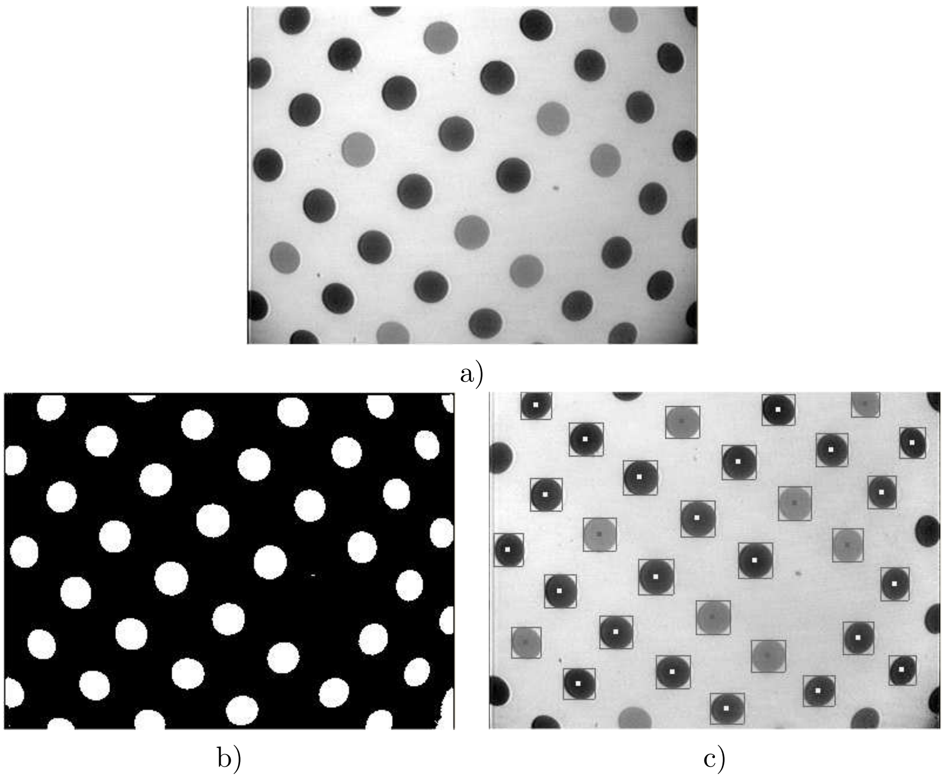

Figure 6.11: Detection of the pattern: a) acquired image, b) binarization, c) detection of the position, size and color of the dots.

dismissed. The other objects are considered to be one of the dots in the pattern.

Finally, for each detected dot and using the original image, the algorithm classifies its grey level, labelling them in three groups: *grey*, *black* or *unknown*. In the case of the label being unknown, the dot will be partially used in following phases, as Section 6.3.3 details. Figure 6.11c shows the original image with some marks on the detected dots. The rectangle containing each dot shows its boundaries. The color of the small point centered in each dot indicates the color which has been detected. If the color is white, the dot has been classified as *black*, if the color is dark grey the dot is *grey*, and if the color is light grey the dot is *unknown*. In the image shown in Figure 6.11c, only *black* and *grey* dots were found.

Dots Neighborhood

The next phase in the localization system consists of finding the neighborhood relation among the detected dots. The goal is to know which dot is next to which other dot. This will allow the calculation of the global position of all of them, starting from the position of only one. The next phase will consider how to find this initial position.

The first step in this phase is to compensate the radial distortion which affects the position of the detected dots in the image plane. Figure 6.8 has already shown the effect of the correction of the radial distortion. Another representation of the same image is shown in Figure 6.12a. In this Figure, the dots before the distortion compensation are marked in black and after the compensation in grey. The new position of the dots in the image is based on the ideal projective geometry. This means that lines in the real world appear as lines in the image. Using this property, and also by looking at relative distances and angles, the two *main lines* of the pattern are found. These two lines can also be seen in the figure. The two *main lines* of the pattern indicate the directions of the X and Y axis, although the correspondence between each main line and each axis it is not known. To detect the main lines, at least 6 dots must appear in the image.

The next step consists of finding the neighborhood of each dot. The algorithm starts from a central dot and goes over the others according to the direction of the main lines. To assign the neighborhood of all the dots, a recursive algorithm was developed which also uses distances and angles between dots. After assigning all the dots, a network joining all neighboring dots can be drawn (see Figure 6.12b).

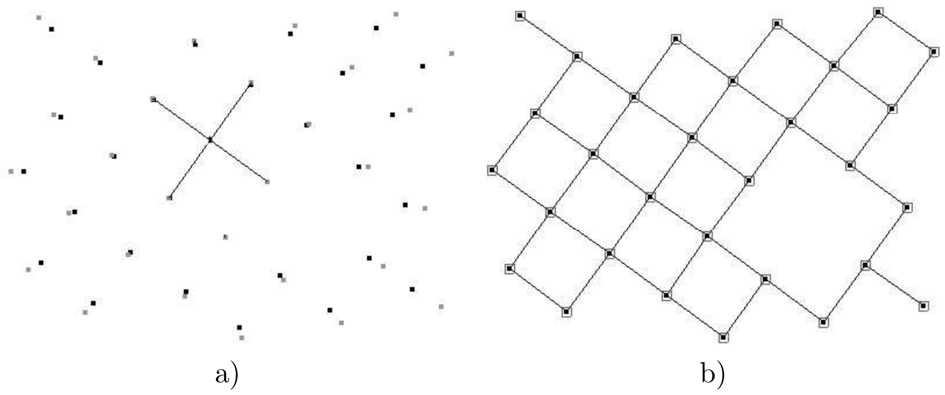

Figure 6.12: Finding the dots neighborhood: a) main lines of the pattern, b) extracted neighborhood.

Dots Global Position

Once the neighborhood of all the dots has been found, the global position of these points is required. Two methodologies are used to identify the global position of a subset of them. After these initial positions are known, the neighborhood network is used to calculate the position of all of these points.

The first methodology is used when a global mark is detected, see Figure 6.12b. The conditions for using a global mark are that a missing dot surrounded by 8 dots appears on the network and the color of these 8 dots is recognizable. In this case, the algorithm checks first the three orientation dots to find how the pattern is oriented. As showed in Figure 6.10b, the algorithm has to check how the pattern is oriented and, therefore, what are the directions of the X and Y axis. From the four possible orientations, only one matches the three colors. After that, the algorithm checks the five dots which encode a memorized global position, refer also to Figure 6.10a. Once the orientation and position of the global mark has been recognized, the algorithm calculates the position of all the detected dots.

The second methodology is used when no global marks appear on the image, or when there are dots of the global mark which have the color label *unknown*. It consists of *tracking* the dots from one image to the next. The dots which appear in a very small zone in two consecutive images are considered to be the same and, therefore, the global position of the dot is transferred. Refer to Figure 6.13 to see a graphical explanation of the tracking process. The high speed of the localization system, compared with the slow dynamics of the underwater vehicle, assures the tracking performance. The algorithm distinguishes between grey and black dots, improving the ro-

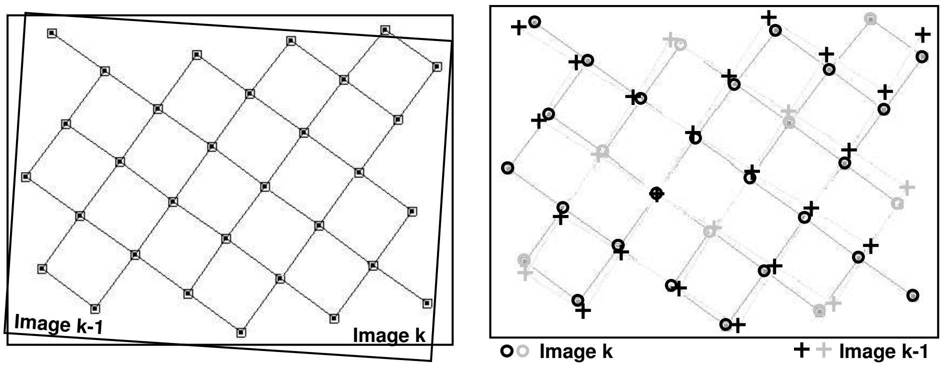

Figure 6.13: Tracking of dots: a) field of view of images k and $k-1$, b) superposition of the dots detected in images k and $k-1$. Dots with the same color which appear very close in two sequential images are considered to be the same dot.

bustness of the tracking. Moreover, since different dots are tracked at the same time, the transferred positions of these dots are compared, using the dot neighborhood, preventing possible mistakes.

Position and Orientation Estimation

Once the global positions of all the detected dots are known, the localization of the robot can be carried out. Equation 6.4 contains the homogeneous matrix which relates the position of one point $({}^CX_i, {}^CY_i, {}^CZ_i)$ with respect to the camera coordinate frame $\{C\}$, with the position of the same point with respect to the water tank coordinate frame $\{T\}$. The parameters of this matrix are the position $({}^TX_C, {}^TY_C, {}^TZ_C)$ and the rotation matrix of the camera with respect to $\{T\}$. The nine parameters of the orientation depend only on the values of *roll* (ϕ), *pitch* (θ) and *yaw* (ψ) angles. For abbreviation, the *cosine* and *sinus* operations have been substituted with "c" and "s" respectively.

$$\begin{pmatrix} {}^TX_i \\ {}^TY_i \\ {}^TZ_i \\ 1 \end{pmatrix} = \begin{pmatrix} c\psi c\theta & -s\psi c\phi + c\psi s\theta s\phi & s\psi s\phi + c\psi s\theta c\phi & {}^TX_C \\ s\psi c\theta & c\psi c\phi + s\psi s\theta s\phi & -c\psi s\phi + s\psi s\theta c\phi & {}^TY_C \\ -s\theta & c\theta s\phi & c\theta c\phi & {}^TZ_C \\ 0 & 0 & 0 & 1 \end{pmatrix} \begin{pmatrix} {}^CX_i \\ {}^CY_i \\ {}^CZ_i \\ 1 \end{pmatrix} \tag{6.4}$$

For each dot i, the position $({}^TX_i, {}^TY_i, {}^TZ_i)$ is known, as well as the ratios:

$$\frac{{}^CX_i}{{}^CZ_i} = V_{ix} \text{ and } \frac{{}^CY_i}{{}^CZ_i} = V_{iy} \tag{6.5}$$

which are extracted from Equations 6.1 and 6.2, and have been named V_{ix} and V_{iy}. The estimation of the state of the robot is accomplished in two phases. In the first phase, ${}^TZ_C$, *roll* (ϕ) and *pitch* (θ) are estimated using the non-linear fitting method proposed by Levenberg-Marquardt [Gill et al., 1981]. This recursive method estimates the parameters which best fit in a non-linear equation from which a set of samples are known.

Given two dots i and j, the square of their distance is the same when computed with respect to $\{C\}$ or to $\{T\}$, see Equation 6.6. From this equation, ${}^CX_i$ and ${}^CY_i$ can be substituted applying Equation 6.5. After the substitution, Equation 6.7 is obtained, in which D_{ij} is the square of the distance between the two dots and is calculated with the right part of Equation 6.6.

$$\begin{aligned}({}^CX_i - {}^CX_j)^2 + ({}^CY_i - {}^CY_j)^2 + ({}^CZ_i - {}^CZ_j)^2 = \\ ({}^TX_i - {}^TX_j)^2 + ({}^TY_i - {}^TY_j)^2 + ({}^TZ_i - {}^TZ_j)^2\end{aligned} \tag{6.6}$$

$$(({}^CZ_iV_{ix} - {}^CZ_jV_{jx})^2 + ({}^CZ_iV_{iy} - {}^CZ_jV_{jy})^2 + ({}^CZ_i - {}^CZ_j)^2 = D_{ij} \tag{6.7}$$

By rearranging the terms of Equation 6.7, Equation 6.8 can be written. This equation is the one to be optimized by the Levenberg-Marquardt algorithm. The unknowns of the equation are ${}^CZ_i$ and ${}^CZ_j$. These values can be calculated using Equations 6.9 and 6.10, which have been extracted from Equation 6.4. The unknowns of Equations 6.9 and 6.10 are ${}^TZ_C$, *roll* (ϕ) and *pitch* (θ). Therefore, from each pair of detected dots, one Equation 6.8 can be written depending only on the three unknowns ${}^TZ_C$, *roll* (ϕ) and *pitch* (θ). The algorithm finds the values for these three unknowns which best fit with a certain number of equations. In order to compute a solution, the minimum number of equations must be the number of unknowns. Therefore, three equations, from three different dots, are required in order to have an estimation. Evidently, the higher the number of dots, the more accurate the estimations are.

$$\begin{aligned}{}^CZ_i^2(V_{ix}^2 + V_{iy}^2 + 1) + {}^CZ_j^2(V_{jx}^2 + V_{jy}^2 + 1) \\ -2\,{}^CZ_i\,{}^CZ_j(V_{ix}V_{jx} + V_{iy}V_{jy} + 1) = D_{ij}\end{aligned} \tag{6.8}$$

$$^{C}Z_i = \frac{^{T}Z_i - {^{T}Z_C}}{-s\theta V_{ix} + c\theta s\phi V_{iy} + c\theta c\phi} \tag{6.9}$$

$$^{C}Z_j = \frac{^{T}Z_j - {^{T}Z_C}}{-s\theta V_{jx} + c\theta s\phi V_{jy} + c\theta c\phi} \tag{6.10}$$

The second phase consists of estimating the $^{T}X_C$ and $^{T}Y_C$ positions and the *yaw* (ψ) angle. In this case, a linear least square technique is applied. This technique uses a set of linear equations to estimate a set of unknowns. The general form of the linear system can be seen in Equation 6.11. The $y(t)$ term is a vector which contains the independent terms of the linear equation. The $H(x(t),t)$ matrix contains the known values which multiply the unknown parameters contained in θ. The solution of the linear system can be easily computed applying Equation 6.12.

$$y(t) = H(x(t),t)\theta \tag{6.11}$$

$$\theta = (H^T H)^{-1} H^T y \tag{6.12}$$

The equations which contain the three unknowns ($^{T}X_C$, $^{T}Y_C$ and ψ) are included in Equation 6.4, and can be rewritten as Equations 6.13 and 6.14. Both equations can be applied to each dot i. The equations are non linear due to the *cosine*($c\psi$) and *sinus*($s\psi$) of the *yaw* angle. However, instead of considering the *yaw* as one unknown, each operation ($c\psi$ and $s\psi$) has been treated as an independent unknown. Equations 6.13 and 6.14 can be rewritten to Equations 6.15 and 6.16, which have the same structure as Equation 6.11. The number of files n of the terms $y(t)$ and $H(x(t),t)$ is the double of the number of detected dots, since for each dot there are two available equations. To solve the linear system, Equation 6.12 is applied obtaining the four unknowns, $c\psi, s\psi,^{T} X_C$ and $^{T}Y_C$. The *yaw* (ψ) angle is calculated applying the *atan2* operation.

$$\begin{aligned} ^{T}X_i = (c\psi c\theta)\,^{C}X_i + \\ (-s\psi c\phi + c\psi s\theta s\phi)\,^{C}Y_i + \\ (s\psi s\phi + c\psi s\theta c\phi)\,^{C}Z_i + {^{T}X_C} \end{aligned} \tag{6.13}$$

$$\begin{aligned} ^{T}Y_i = (s\psi c\theta)\,^{C}X_i + \\ (c\psi c\phi + s\psi s\theta s\phi)\,^{C}Y_i + \\ (-c\psi s\phi + s\psi s\theta c\phi)\,^{C}Z_i + {^{T}Y_C} \end{aligned} \tag{6.14}$$

$$\begin{pmatrix} {}^{T}X_1 \\ {}^{T}Y_1 \\ ... \\ ... \\ {}^{T}X_i \\ {}^{T}Y_i \\ ... \\ ... \\ {}^{T}X_n \\ {}^{T}Y_n \end{pmatrix} = H \begin{pmatrix} c\psi \\ s\psi \\ {}^{T}X_C \\ {}^{T}Y_C \end{pmatrix} \tag{6.15}$$

$$H = \begin{pmatrix} c\theta\,{}^{C}X_1 + (s\theta s\phi)\,{}^{C}Y_1 + (s\theta c\phi)\,{}^{C}Z_1 & -c\phi\,{}^{C}Y_1 + s\phi\,{}^{C}Z_1 & 1 & 0 \\ c\phi\,{}^{C}Y_1 - s\phi\,{}^{C}Z_1 & c\theta\,{}^{C}X_1 + (s\theta s\phi)\,{}^{C}Y_1 + (s\theta c\phi)\,{}^{C}Z_1 & 0 & 1 \\ ... & ... & ... & ... \\ ... & ... & ... & ... \\ c\theta\,{}^{C}X_i + (s\theta s\phi)\,{}^{C}Y_i + (s\theta c\phi)\,{}^{C}Z_i & -c\phi\,{}^{C}Y_i + s\phi\,{}^{C}Z_i & 1 & 0 \\ c\phi\,{}^{C}Y_i - s\phi\,{}^{C}Z_i & c\theta\,{}^{C}X_i + (s\theta s\phi)\,{}^{C}Y_i + (s\theta c\phi)\,{}^{C}Z_i & 0 & 1 \\ ... & ... & ... & ... \\ ... & ... & ... & ... \\ c\theta\,{}^{C}X_n + (s\theta s\phi)\,{}^{C}Y_n + (s\theta c\phi)\,{}^{C}Z_n & -c\phi\,{}^{C}Y_n + s\phi\,{}^{C}Z_n & 1 & 0 \\ c\phi\,{}^{C}Y_n - s\phi\,{}^{C}Z_n & c\theta\,{}^{C}X_n + (s\theta s\phi)\,{}^{C}Y_n + (s\theta c\phi)\,{}^{C}Z_j & 0 & 1 \end{pmatrix} \tag{6.16}$$

Once the three-dimensional position and orientation of the camera has been found, a simple translation is applied to find the position of the center of the robot. Figure 6.14 shows a representation of the robot position in the water tank. Also, the detected dots are marked on the pattern.

Filtering and Velocity Estimation

In the estimation of the position and the orientation, there is an inherent error. The main sources of this error are the simplifications, the quality of the systems and the uncertainty of some physical parameters. Refer to the next section for more detailed information about the accuracy of the system. Due to this error, small uncertainties about the vehicle position and orientation exist and cause some oscillations even if the robot is static. To eliminate these oscillations, a first order Savitzky-Golay [Savitzky and Golay, 1964] filter has been applied. This online filter uses a set of past non-filtered values to estimate the current filtered position or orientation.

Finally, the velocity of the robot with respect to the onboard coordinate frame $\{R\}$ is also estimated. A first order Savitzky-Golay filter with a first order derivative included is applied to the position and orientation values. This filter is also applied online and uses a window of past non-filtered samples. The output of the filtering process is directly the filtered velocity.

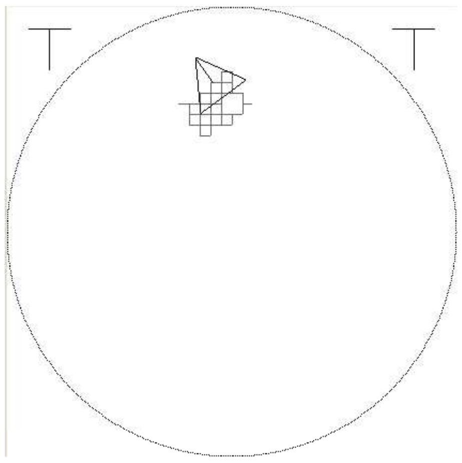

Figure 6.14: Estimated position and orientation of the robot in the water tank. The triangle indicates the *X, Y* and *Yaw* state of the robot. *Roll* and *Pitch* angles are indicated by two vertical lines at the top left and right corners respectively. Finally, the dots seen by the robot are also drawn.

After calculating the velocities with the Savitzky-Golay filter, a transformation from $\{T\}$ to $\{R\}$ coordinate frames is applied. Therefore, the position and orientation are referred to the water tank coordinate frame $\{T\}$, while the velocities are referred to the onboard coordinate frame $\{R\}$.

As usual when filtering a signal, an inherent delay will be added to the velocity or position. However, it has been verified that this small delay does not affect the low-level controller of the vehicle, as will be shown in Section 6.4.2. Figure 6.15 shows the estimated three-dimensional position and orientation with and without filtering, and also the velocities for the same trajectory.

6.3.4 Results and Accuracy of the System

The localization system offers a very accurate estimation of the position, orientation and velocity. The system is fully integrated on the vehicle's controller, providing measures at a frequency of 12.5 times per second. Because of the high accuracy of the system, other measures like the heading from a compass sensor or the depth from a pressure sensor are not needed. In addition, the localization system can be used to calibrate sensors, to validate other localization systems or to identify the dynamics of the vehicle. An example of a trajectory measured by the localization system can be seen in Figure 6.16.

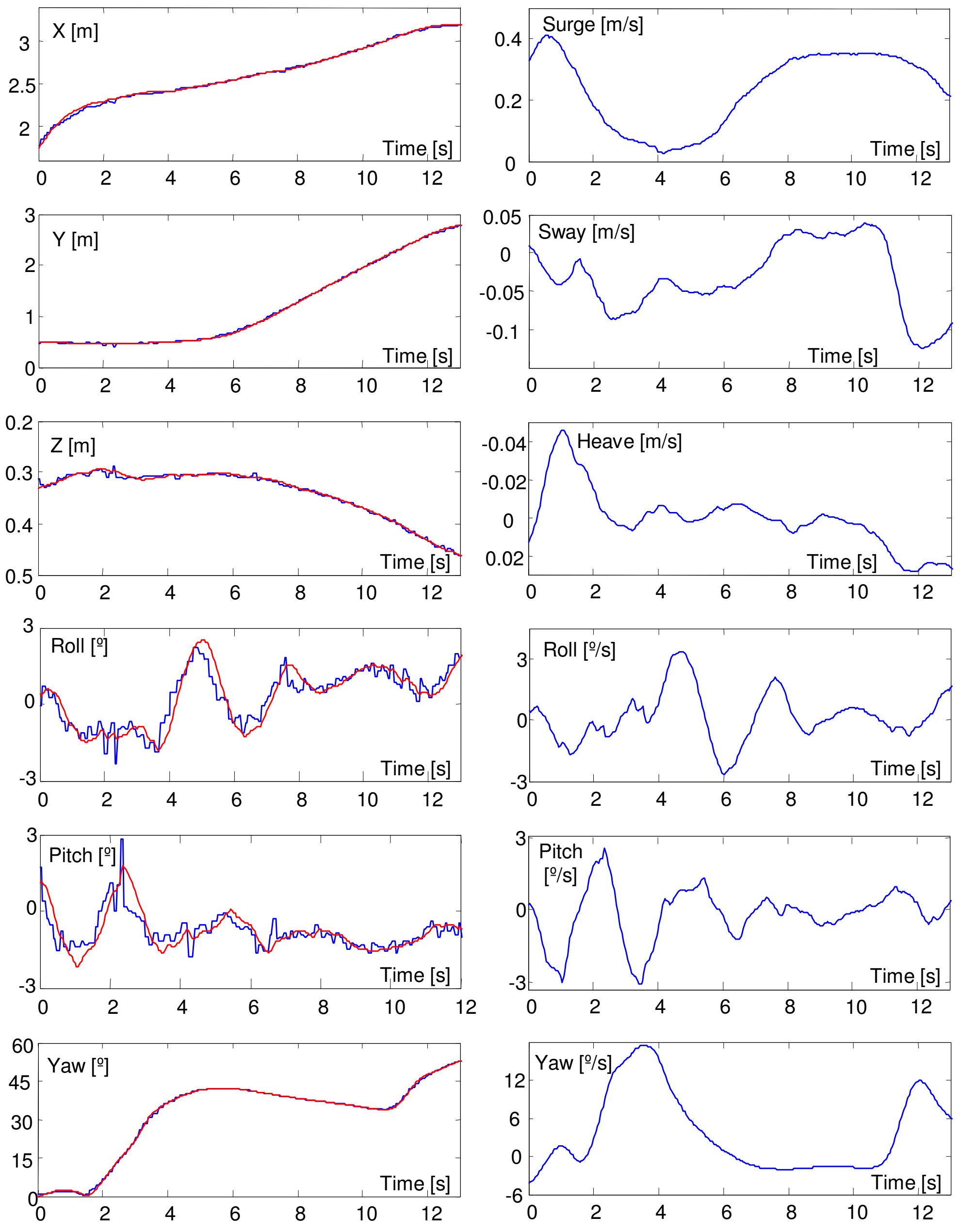

Figure 6.15: The left column shows the position and orientation before and after filtering during a trajectory. The right column shows the velocity for the 6 DOFs with respect to the on board coordinate frame $\{R\}$.

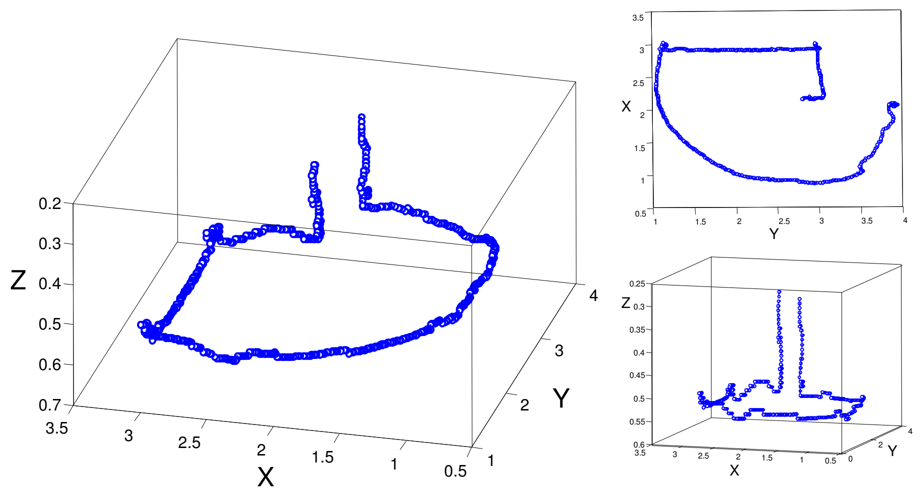

Figure 6.16: Three-dimensional trajectory measured by the localization system. Three views are shown.

In order to determine the accuracy of the system, the errors affecting the estimations have been studied. Main sources of error are the imperfections of the pattern, the simplification on the camera model, the intrinsic parameters of the camera, the accuracy in detecting the centers of the dots and the error of least-square and Levenberg-Marquardt algorithms on its estimations. It has been assumed that the localization system behaves as an aleatory process in which the mean of the estimates coincides with the real position of the robot. It is important to note that the system estimates the position knowing the global position of the dots seen by the camera. In normal conditions, the tracking of dots and the detection of global marks never fails, which means that there is no drift in the estimates. By normal conditions we mean, when the water and bottom of the pool are clean, and there is indirect light from the sun.

To find out the standard deviation of the estimates, the robot was placed in 5 different locations. In each location, the robot was completely static and a set of 2000 samples was taken. By normalizing the mean of each set to zero and grouping all the samples, a histogram can be plotted, see Fig. 6.17. From this data set, the standard deviation was calculated obtaining these values: 0.006[m] in X and Y, 0.003[m] in Z, 0.2[°] in *roll*, 0.5[°] in *pitch* and 0.2[°] in *yaw*.

The accuracy of the velocity estimations is also very high. These measurements are used by the low level controller of the vehicle which controls the *surge*, *heave*, *pitch* and *yaw* velocities.

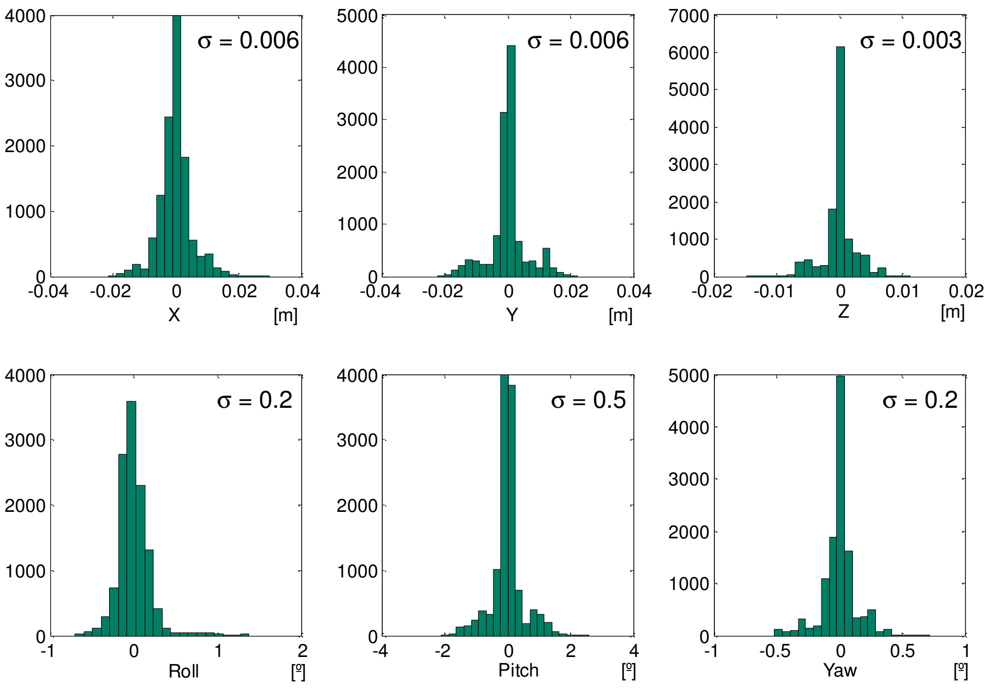

Figure 6.17: Histogram of the estimated position and orientation.

The only drawback of the system is the pattern detection when direct light from the sun causes shadows to appear in the image. In this case, the algorithm fails in detecting the dots. Any software improvement to make a more robust system in presence of shadows would increase the computational time and the time cycle of the algorithm would be too slow. However, the algorithm is able to detect these situations and the vehicle is stopped.

6.4 Software Architecture

In this section, the software architecture used to control URIS AUV is detailed. As will be described, a software framework was developed as a tool to easily implement the architecture needed to carry out a mission. After the description of this framework, the particular architecture used in the experiments of this thesis is detailed.

6.4.1 Distributed Object Oriented Framework

When working with physical systems such as an underwater robot, a real-time Operating System (OS) is usually required. The main advantage is better control of the CPU work. In a real-time OS, the scheduling of the processes to be executed by the CPU is done according to preemptive priorities. More priority processes will be first executed and will also advance processes which are already in execution. Using a correct priority policy it is possible to guarantee the frequency in which the control architecture has to be executed, which is very important to assure the controllability of the robot.

A software framework, based on a real-time operating system was specially designed for URIS AUV. In particular, QNX OS was used. This framework is intended to assist the architecture designers to build the software architecture required to carry out a particular mission with URIS AUV. The framework proposes the use of a set of distributed objects which represent the architecture. Each object represents a component of the robot (sensors or actuators), or a component of the control system (low-level or high-level controllers). An Interface Definition Language (IDL) is used to define the services which the object supports. From the information contained in the IDL, the object skeleton is automatically generated. Each object has usually two threads of execution. One of them, the *periodic thread*, is executed at a fixed sample time and is used to perform internal calculations. The other thread, the *requests thread*, is used to answer requests from clients.

The priority of each object thread is set independently and, depending on that, the objects will be executed. If a sample time is not accomplished, a notification is produced. These notifications are used to redesign the architecture in order to accomplish the desired times.

The software framework allows the execution of the objects in different computers without any additional work for the architecture designer. A server name is used in order to find the location of all the objects. Evidently, objects that are referred to as physical devices, such as sensors or actuators, have to be executed in the computer which has the interfaces for them. Communication between objects is performed in different ways depending on whether they are executed sharing the same logical space and if they are executed in the same computer. However, these variations are hidden by the framework, which only shows a single communication system to the architecture designer.

Although this software framework was developed to work under a real-time operating system, the execution of objects under other conventional OS is also supported. The main reason for that is the lack of software drivers of some devices for the QNX OS.

6.4.2 Architecture Description

The software architecture used in the experiments presented in this thesis can be represented as a set of components or objects which interact among them. The objects which appear in the architecture can be grouped in three categories: actuators, sensors and controllers. A scheme of all the objects, with the connections between them, can be seen in Figure 6.18. The actuators' category contains the four *actuators* objects. The sensor category contains the *water detection*, *target tracking* and *localization* objects and, the controllers category contains the *low-level*, *high-level* and the two *SONQL behaviors*. It is important to remark on the difference between *low* and *high* level controllers. The low-level controller is in charge of directly actuating on the actuators of the robot to follow the movement set-points which the high-level controller generates. On the other hand, the high-level controller is responsible for the mission accomplishment and generates the set-points which the low-level controller has to reach.

All these objects are mainly executed in the on board embedded computer, but two external computers have also been used. The *on board computer* contains the actuators, controllers and sensory objects. As can be seen, not all the sensors presented in Section 6.1.3 have been used. One of the external computers, which has been called the *vision computer*, contains the two vision-based sensory systems, which are the target tracking (Section 6.2) and the localization system (Section 6.3). The other external computer, which has been called the *supervision computer*, is only used as

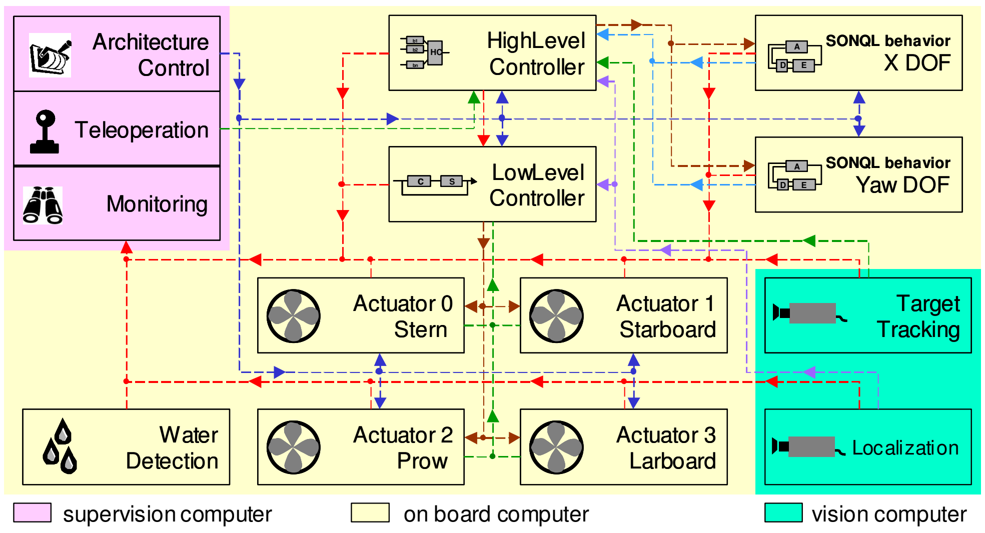

Figure 6.18: Objects which appear in the software architecture used in the experiments. The connections between the objects show the direction in which the information is transferred. The execution of the objects is performed in the on board computer or in the two external computers as indicated.

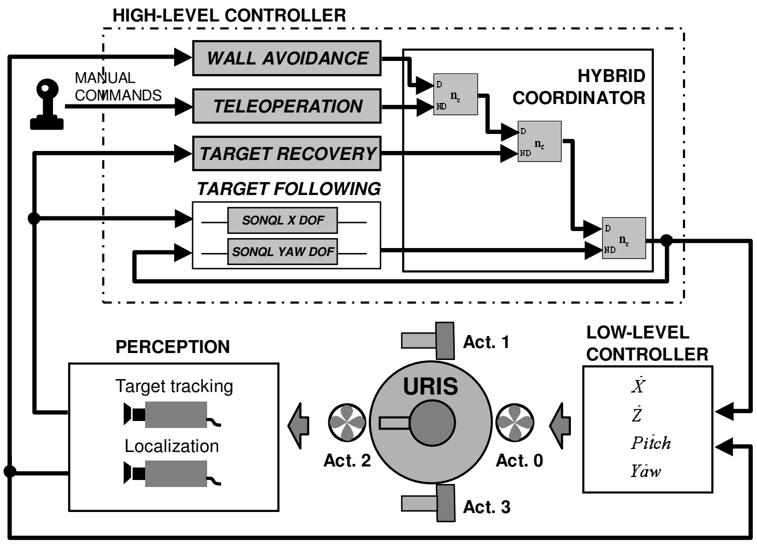

Figure 6.19: Components of the control system architecture used in the target following task.

a client of the previous objects. Its main goal is to control the operation of the objects and to monitor them. It is also used to send commands for robot teleoperation.

Another representation of the same architecture can be seen in Figure 6.19. In this case, the objects or components are seen from the point of view of the control system. In this representation, the sensing components, high-level controller, low-level controller and actuators are more clearly differentiated.

Hereafter, a more detailed description of each object is given. First, the objects belonging to the *onboard* embedded computer are reviewed. This computer is responsible for the control of the robot and runs the QNX real-time operating system.

- **Actuators**. The four thrusters of the robot are controlled through these four objects. These objects have only one thread for the requests from the clients. There is no internal calculation to perform. The services which these objects accept are used to modify the set-point velocity of the motor, enable/disable the thruster, and to read the real velocity and electric current of the motor.

- **Water Leakage Detection**. This object is used to measure the five water leakage sensors contained in the vehicle. The object has only one thread to attend to the requests from the clients. The only service which this object supports is to give the state of the five water sensors.

- **Low-Level Controller**. This object is in charge of the computation of the low-level controller of the vehicle. Its goal is to send control actions to the actuators to follow the set-points given by the high-level controller. Unlike the previous objects, a *periodic thread* is used to regularly recalculate and send these control actions. In particular, a sample time of 0.1 seconds is used. The DOFs to be controlled are four: *surge*, *heave*, *pitch* and *yaw*. The control system implemented for each DOF is a simple PID controller. The state which is controlled is the velocity of each DOF. The feedback measure of this velocity is obtained from the *localization* object. The four PID controllers are executed in parallel at each iteration and the control actions are superposed and sent to the actuators. In Figure 6.20 the performance of the *surge* and *yaw* controllers is shown.

  The low-level controller offers different services. The most important service is to receive the set-points. Three set-points are requested: the surge, the heave and the yaw velocities. The pitch velocity is not

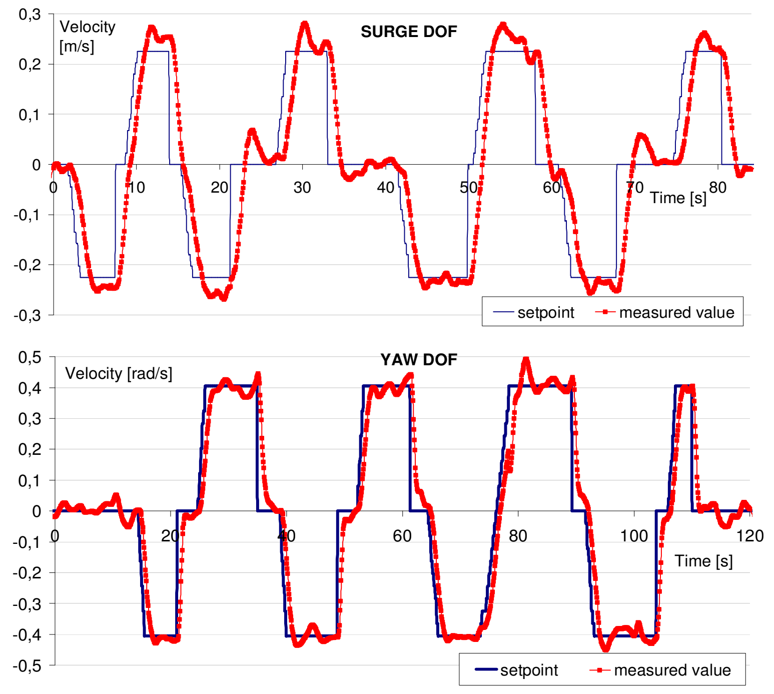

Figure 6.20: Performance of the surge and yaw velocity-based controllers.

requested as it is always considered to be zero. Other services are also available which are mainly used for the tuning of the controllers. By calling these services, the parameters of the controllers can be modified online, and internal variables can be checked. There is also a general service to enable/disable the controller.

- **High-Level Controller**. This object is the one which contains the behavior-based control architecture and, therefore, the part which is evaluated in this thesis. It contains the set of behaviors and the hybrid coordination system which has been designed to accomplish a particular task.

  Each behavior requests information from other objects, such as the target tracking object or the localization object, in order to generate its response. After the behaviors have been executed, the coordinator computes the final response and sends it to the low-level controller.

  As with the low-level controller, a *periodic thread* is used, but in this case with a sample time of 0.3 seconds. The services offered by this object allow us to enable/disable the controller and each behavior. Another service is in charge of receiving the response which a teleoperation behavior will have. Using this service, an external user can command the robot.

- **SONQL-based Behaviors**. Although the behaviors are executed in the high-level controller, two auxiliary objects are used to implement the SONQL-based behaviors. Each one is used to learn a different DOF of the behavior. These objects contain the learning algorithm proposed in this thesis. The structure of the algorithm is divided in two threads. The *periodic thread* is in charge of updating the NN weights with the *learning samples database*, refer to section 5.7. The rest of the SONQL algorithm is executed every time a request is received.

  Each time the high-level controller has to calculate the response of a SONQL-based behavior, it sends to one of the SONQL-based behaviors the current and past states of the environment and the last taken action. For example, in the case of the X DOF of a target following behavior, it sends the current and past positions and velocities in X axis of the target, and the last taken action in *surge*. The SONQL-based behavior receives the states and action through the *requests thread.* This thread has a higher priority than the *periodic thread* and, therefore, the execution of the last one is stopped. Using the received state, the reinforcement is calculated completing a new *learning sample.* This sample is added to the *learning sample database.* Finally, an action is calculated and is returned to the high-level controller. The *requests thread* is finished, and the *periodic thread* starts again to update the NN weights but with the recently added *learning sample.*

  The services which these objects offer are basically to receive new *learning samples* and to configure all the parameters of the SONQL algorithm. It is also possible to reset the NN weights and all the variables.

The objects which will next be reviewed belong to the *vision computer.* This computer is one of the external computers and is run by the Windows operating system. The reason why a non real-time operating system has been used is because the frame grabbers, which are used to acquire images, do not provide software drivers for QNX OS. This computer was not located inside the robot because, at the time of the experiments, the embedded vision computer was not available.

- **Target Detection and Tracking**. This object implements the vision algorithm to detect and track an artificial target located in the water tank, as has been described in Section 6.2. The algorithm is executed in the *periodic thread.* In this case, the sample time of the thread is 0.08

seconds (12.5 Hz), which is double the sample time in which a video camera acquires a complete image. This means that the algorithm is applied once every images. The *requests thread* is used to send the last calculated position and velocity of the target.

- **Localization**. Similar to the previous object, the localization object implements the algorithm which estimates the position, orientation and velocity of the robot inside the water tank, refer to Section 6.3. The localization algorithm is also executed in the *periodic thread* at a sample time of 0.08 seconds. The *requests thread* is used to send the last calculated position and velocity of the robot.

The last components of the software architecture are the object clients which are contained in the *supervision computer*. The main uses of these clients are to control and monitor the architecture.

- **Architecture Control**. This component is used to enable and disable some of the objects of the architecture. Concretely, these objects are those belonging to the actuator and controller categories, refer to Figure 6.18.

- **Teleoperation**. As has been commented above, the high-level controller contains a teleoperation behavior which is commanded from the exterior. The teleoperation component then has the goal of getting the control command from a human and sending it to the high-level controller. This human-machine interface is accomplished by a joystick.

- **Monitoring**. Finally a monitoring component is in charge of consulting the state of all the objects through their services. This component will aid in the comprehension of the experiments.

Chapter 7

Experimental Results

This chapter presents the experimental results of this thesis. The chapter is organized in two parts. The first part describes the application of the behavior-based control layer to fulfill a robot task. This task consisted of following a target with the underwater robot URIS using the experimental set-up described in Chapter 6. The main goal of these experiments was to test the feasibility of the hybrid coordination system as well as the SONQL based behaviors. To accomplish this, a set of behaviors were designed, from which one was learnt with the SONQL algorithm while the other behaviors were manually implemented. A detailed description of the whole control system will be given and the results presented. The results will first focus on the SONQL algorithm, showing the learning of the X DOF, the Yaw DOF and some tests concerning the convergence of the algorithm. The hybrid coordination system will then be tested with the manual and learnt behaviors. The second part of this chapter shows the results of the SONQL algorithm in an RL benchmark. In this case, the task was used to test the generalization capability of the algorithm. The problem is called the ”mountain-car” task and was executed in simulation. The suitability of the SONQL algorithm for solving the generalization problem will be stated.

7.1 Target-following task

The task consisted of following a target with the underwater robot URIS. Three basic aspects were considered. The first was to avoid obstacles in order to ensure the safety of the vehicle. In this case, the wall of the pool was the only obstacle. The second aspect was to ensure the presence of the target within the camera's field of view. The third aspect was to follow the target at a certain distance. Each one of these aspects was translated to a robot behavior, hence, the behaviors were: the "wall avoidance" behavior, the "target recovery" behavior and the "target following" behavior. It is important to note the simplicity which behavior-based controllers offer. It is much simpler to design each behavior independently rather than developing a single control strategy to handle all of the considerations.

An additional behavior was included, the "teleoperation" behavior, which allowed the robot to move according to the commands given by a human. This behavior did not influence the outcome of the target following task, but was used to test the performance of the system, for example, by moving the vehicle away from the target.

Due to the shallow water in the tank in which the experiments were performed, only the motions on the horizontal plane were considered. Therefore, to accomplish the target following task, only the *surge* and *yaw* control actions were generated by the behaviors. The other two controllable DOFs (*heave* and *pitch*) were not used. In the case of the heave movement, the low-level controller maintained the robot at an intermediate depth. Regarding the pitch orientation, a zero degree set-point (normal position) was used.

Following the behavior-based control layer proposed in Chapter 3, each behavior b_i generated a response r_i, which was composed of an activation level a_i and a control action v_i. Since the heave movement was not present, the control action vector was $v_i = (v_{i,x}, 0, v_{i,yaw})$. The range used for the actions was $v_{i,j} = [-1, 1]$, corresponding to the maximum backward and forward velocity set-points in surge and yaw.

After defining the behaviors present in this task, the next step was to set their priorities. To determine these priorities, the importance of each behavior goal was ranked. This is the hierarchy used:

1. *"Wall Avoidance" behavior.* This was the highest priority behavior in order to ensure the safety of the robot even if the task was not accomplished.

2. *"Teleoperation" behavior.* This was given a higher priority than the next two behaviors in order to be able to drive the robot away from the target when desired.

3. *"Target Recovery" behavior.* This was given a higher priority than the target following behavior so as to be able to find the target when it was not detected.

4. *"Target Following" behavior.* This was the lowest priority behavior since it should only control the robot when the other behavior goals had been accomplished.

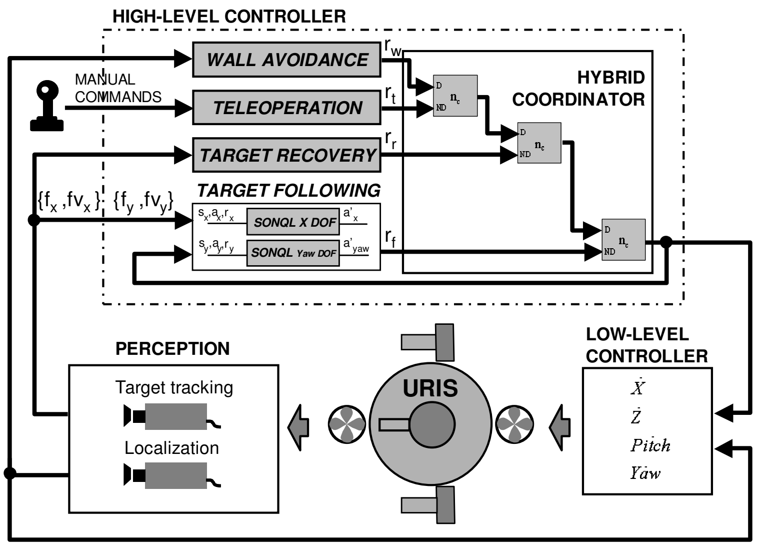

Figure 7.1: Implementation of the target following task with the proposed behavior-based control layer.

The establishment of the priorities allowed the composition of the behavior-based control layer. Figure 7.1 shows the implementation of the four behaviors using three hybrid coordination nodes. Finally, the last step was the definition of the internal state/action mapping and the activation level function for each behavior. The "target following" behavior was implemented with the SONQL algorithm. Its implementation and learning results will be described in the next section. As far as the other behaviors go, the main features were:

"Wall Avoidance" behavior This behavior was manually implemented. It used the absolute position of the robot as input, see Figure 7.1. The robot position was used to calculate the minimum distance to the circular wall of the water tank called d_w, see Figure 7.2. The behavior response r_w was computed according to this distance. The idea was to activate the behavior linearly with close proximity to the wall. To accomplish this, two threshold distances were set, $t_{w,min}$ and $t_{w,max}$, where $t_{w,min} < t_{w,max}$. If $d_w > t_{w,max}$, this meant the robot was too far from the wall and the behavior was not active ($a_w = 0$). On the other hand, when $d_w < t_{w,min}$, the robot was too close to the wall. Therefore, the activation was set at $a_w = 1$ and the coordinator actuated competitively in order to restore the safety of the robot. Finally, if $t_{w,min} < d_w < t_{w,max}$, this meant the robot was close to the wall

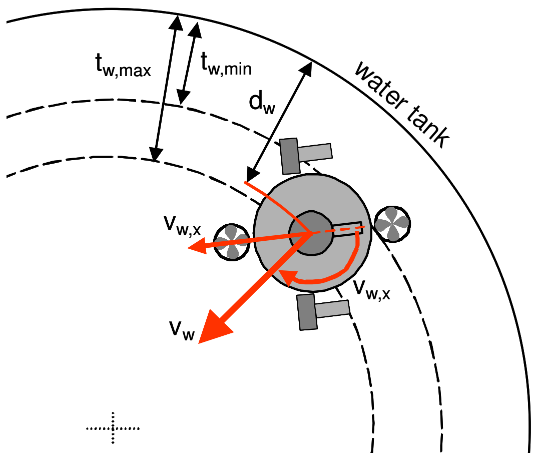

Figure 7.2: Schema of the "wall avoidance" behavior. The control action and the zones where the behavior is active are shown.

but not in a dangerous position and the activation was linearly calculated between 0 and 1. The control action v_w was only calculated when the activation was larger than 0. In that case, in order to drive the robot away from the wall, the control action was set to point towards the center of the circumference. According to the vehicle's yaw angle, this two-dimensional control action was split in the surge and yaw movements. The implementation of the "wall avoidance" behavior was designed experimentally with the thresholds and other parameters also obtained experimentally.

"Teleoperation" behavior The "teleoperation behavior" had to reflect the commands given by a joystick module. The teleoperation response r_t was composed of the activation level a_t and the control action vector v_i. The activation level of this behavior was 1 when the joystick was activated to send commands, otherwise it was set to 0. Moreover, the control actions were taken directly from the joystick. The surge movement $v_{j,x}$ corresponded to the forward/backward joystick command and the yaw movement $v_{j,yaw}$ corresponded to the left/right command.

"Target Recovery" behavior This behavior was also manually implemented but was much simpler than the "wall avoidance" behavior. The input of this behavior was the target position in respect to the robot, see Figure 7.1. This behavior was active $a_r = 1$ only when the target was not detected. In that case, it generated a constant rotational movement $v_{r,yaw} = \pm 0.8$ which spun the robot in the direction in which the target had last been detected.

To conclude, the hybrid coordinator was implemented with a quadratic parameter $k = 2$. This parameter assured the prevalence of higher priority behaviors, and was also experimentally set.

7.1.1 SONQL behavior

The "target following" behavior was learnt using two SONQL algorithms, one for each DOF. The goal of this algorithm was to learn the state/action mapping of this behavior. This mapping determined the movements the robot had to perform in order to locate itself at a certain distance from the target and pointing directly at it. In order to generate the robot response r_f, the activation level was $a_f = 1$ whenever the target was detected and $a_f = 0$ otherwise. Moreover, the control action v_f was generated by the SONQL algorithms. In particular, the SONQL algorithm of the X DOF generated the $v_{f,x}$ control action and the algorithm of the Yaw DOF generated the $v_{f,yaw}$. The next paragraphs will describe the state variables, the reinforcement function and the parameters of the SONQL algorithm used in each DOF.

Environment State

A reinforcement learning algorithm requires the observation of the complete environment state. If this observation is not complete or the signals are too corrupted with noise or delays, the convergence will not be possible. The state of the environment must therefore contain all the required measurements relating the target to the robot. The first measurement was the relative position between the target and the robot: f_x in X DOF and f_y in Yaw DOF. The procedure to compute these continuous values was described in Section 6.2. A second necessary measurement was the relative velocity between the target and the robot. For instance, let's consider the case when the target is in front of the robot but there is a relative angular velocity between them. If the algorithm decides to execute the action $v_{f,yaw} = 0$, in the next step, the target will not be directly in front of the robot. On the contrary, if the relative velocity between them is zero and the executed action is again zero, in the next step, the target will still be located in front of the robot. Hence, we have two situations in which the target was located in the same place and the executed action was also the same, yet the system was brought to a different state. Since the environment is considered to be deterministic, this pointed out that the relative velocity was also required to differentiate both states. These measurement were: fv_x for the X DOF and fv_y for the Yaw DOF.

Finally, if the target and the robot are both rotating at a velocity which makes the relative position and relative velocity equal to zero, a new measurement would be required to differentiate this state from the state in which everything is stopped and the target is directly in front of the robot. In this case, the absolute velocity of the robot or the absolute velocity of the target would also be required. This new measurement would be necessary to learn the behavior in case the target was moving. However, this case was not tested due to the complexity it would have represented in the exploration of a three-dimensional space. Instead, the behavior was learnt using a static target.

Besides the number of variables which composed the environment state, the quality of these variables was also very important. The target tracking system was designed to accurately estimate the relative positions and velocities. Indeed, the estimation of the relative velocity was especially difficult, as in the filtering process in which a delay was unavoidably added to the signal. Initially, this delay did not allow the system to learn, since the estimated velocities did not match the real movement. The filtering had to be accurately improved in order to remove part of this delay. Finally, it must be remembered that the state variables have been extracted from a vision-based system in which the non-linear distortions were not corrected. Moreover, the f_x measure is non-linear with respect to the relative distance to the target. All these non-linear effects, which were consciously not corrected, should not pose a problem for the learning algorithm since a Markovian environment does not imply linearity.

In summary, the state for the X DOF of the SONQL algorithm was composed of f_x and fv_x; and the YAW DOF of the SONQL algorithm was composed of f_y and fv_y. Figure 7.1 shows these measurements as inputs for the "target following" behavior and Figure 7.3 shows a two-dimensional representation of the f_x and f_y axes.

Reinforcement Function

The reinforcement function is the only information a designer must introduce in order to determine the goal of the behavior. The reinforcement function must be a deterministic function which relates the state and action spaces to a reward value. In the case of the "target following" behavior, the reinforcement function took only the target position as input. Therefore, according to these variables, f_x in the X DOF and f_y in the Yaw DOF, a reward value was given. Only three reward values were used: -1, 0 and 1, simplifying the

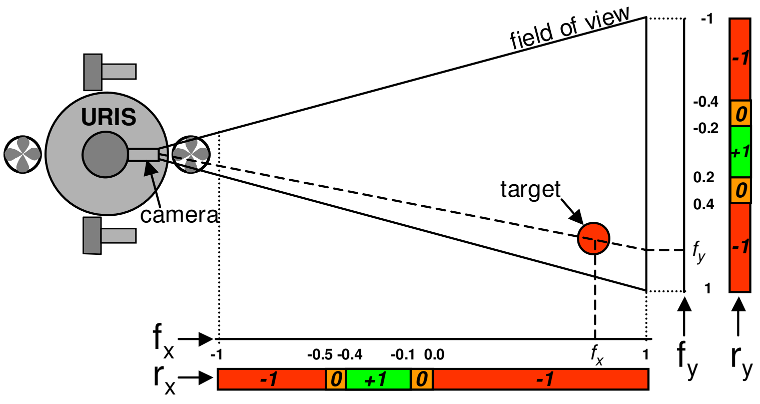

Figure 7.3: Relative positions f_x and f_y and the reinforcement values r_x and r_y, for the "target following" behavior.

implementation of this function. Figure 7.3 shows the reward values according to the target relative position. Basically, in order to maintain the target in front of the robot, the positive rewards $r = 1$ were given when the position of the target was around $f_y = 0$ and at a certain distance from the robot in X axis, around $f_x = -0.25$. The other reward values were progressively given if the target was farther. The r_x variable was used for the X DOF and the r_y variable for the Yaw DOF. As can be observed, the reward functions change the values at some thresholds, which were found experimentally.

SONQL parameters

After defining the states, actions and reinforcement function, the final step to learn the "target following" behavior with the SONQL algorithm consisted of setting the parameters of the algorithm. The same parameter values were used for both DOFs. The values of the parameter and some considerations are described, as follows:

NN configuration. The Neural Network had 3 continuous variables as inputs: $\{f_x, fv_x, v_{f,x}\}$ for the X DOF and $\{f_y, fv_y, v_{f,yaw}\}$ for the Yaw DOF. The output was the estimated $Q(s, a)$ value. Only one hidden layer was used with 6 neurons. This configuration was found experimentally and used for both DOFs. Different configurations were also tested, although this one provided the best compromise between generalization capability and convergence time. The more neurons, the higher the generalization capability, but also, the higher number of learning iterations needed to converge.

Learning rate α. A diverse set of values were tested. The final learning rate was set to $\alpha = 0.1$, which demonstrated a fast and stable learning process.

Discount factor γ. The discount factor was set to $\gamma = 0.9$. Since the learning of a robot behavior is a continuous task without a final state, a discount factor smaller than 1 was required. In the case of using $\gamma = 1.0$, the Q function values would increase or decrease, depending on the state/action zone, until they reach $-\infty$ or ∞. This value was chosen experimentally without exploring many values.

Exploration probability ϵ. The learning was performed with a $\epsilon - greedy$ policy. The exploration probability was $\epsilon = 0.3$. A smaller exploration probability increased the time required to converge, and a higher probability caused the robot to act too randomly. The value was also set experimentally.

Database Density Parameter t. The density parameter was set to $t = 0.5$. However, this parameter does not provide intuitive information about the number of learning samples. It indicates the minimum distance between two learning samples. This distance is calculated according to the vectors (s, a, r) of each sample, which, in this case was a four-dimensional vector since the state has two dimensions. In practice, the number of learning samples resulted in being less than 30, although it depended on the state/action space exploration. Several parameters were tested, concluding that with a larger value (less samples) the convergence was not always achieved due to the interference problem. Similar results were obtained for both DOFs.

7.1.2 Learning Results

An exhaustive set of experiments were carried out in order to test the SONQL algorithm. In these experiments, optimal parameters were found and a fast and effective learning of the robot behavior was achieved.

X DOF

The experiments in the X DOF were carried out by placing the target in front of the robot and starting the learning algorithm. The target was placed next to the wall of the water tank and the robot was placed in front of it at the center of the circular tank. This positioning gave the robot the maximum space in which to explore the state. In addition, as the target was placed

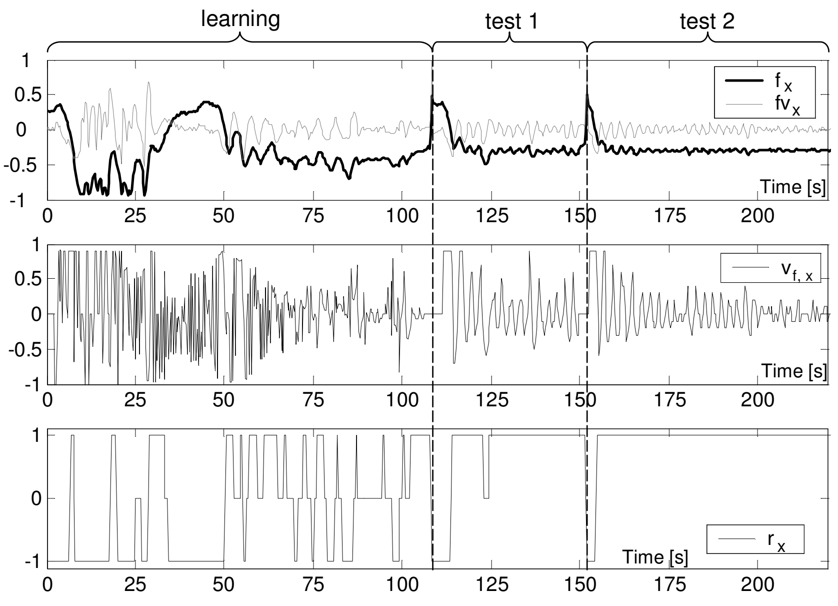

Figure 7.4: Real-time learning evolution and behavior testing in the X DOF. In the same experiment, the behavior was first learnt and then tested. In the learning phase, the state/action space exploration can be appreciated. The testing consisted of moving the robot away from the target first, and then allowing the behavior to reach it again. The evolution of the states, actions and rewards is shown.

close to the wall of the tank, the vehicle was stopped by the "wall avoidance" behavior when it came too close to the wall, preventing a collision with the target.

The learning of the X DOF took about 110 seconds, which represents about 370 learning iterations (sample time = 0.3 seconds). Figure 7.4 shows a typical real-time learning evolution. It can be seen how the robot explored the state in the learning phase. Immediately after the learning phase the behavior was tested by applying, with the "teleoperation" behavior, an action which moved the vehicle away from the target. It can be seen how the target was again reached and the maximum rewards achieved.

The policy learnt after this learning can be seen in Figure 7.5. The optimal action $v_{f,x}$ according to the state $\{f_x, fv_x\}$ can be appreciated. For example for $f_x = 1$ and $fv_x = 0$, which means that the target is at the farthest distance and the velocity is zero, the optimal action is $v_{f,x} = 1$, that is, "go forward". This is a trivial case, however, but the policy also shows situations in which intermediate action values are given.

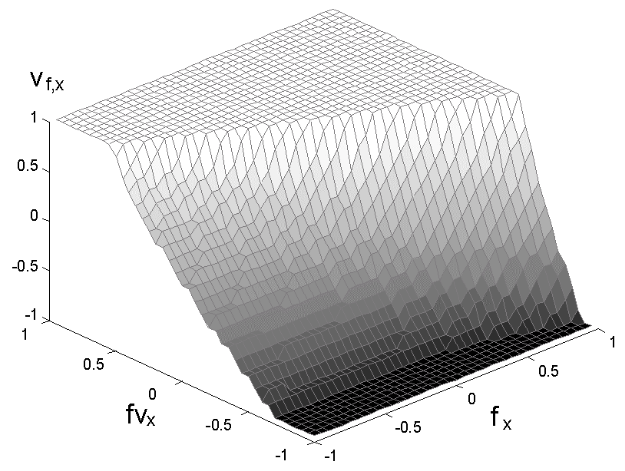

Figure 7.5: State/action policy learnt for the X DOF.

The Q-function learnt in one of the experiments can also be seen. Figure 7.6 shows the maximum Q value for each state $s = (f_x, fv_x)$ which is also the state value $V(s)$. It can be appreciated that the maximum values are in the target positions (f_x) where the reinforcement function was maximum. However, according to the velocity variable, fv_x, the value of zones with the same position f_x change. This is due to the prediction provided by the state value function. If the target is located at the position where the reward is maximum but the velocity causes it to move away, the value of this state is lower than the states in which the future rewards will also be maximum. Finally, it must be noted that the function approximated by the NN is not only the one shown in this figure. Another dimension, corresponding to the continuous action $v_{f,x}$, is also contained in the function. This demonstrates the high function approximation capability of NN.

YAW DOF

Similar experiments were performed for the Yaw DOF. The target was located in front of the robot when the SONQL was started. During the exploration of the space, the robot frequently lost the target but the "target recovery" behavior became active and the target was detected again.

The learning of the Yaw DOF took about 60 seconds, which represents about 200 learning iterations (sample time = 0.3 seconds). The learning of this DOF was faster than the learning of the X DOF since the state/action space to be explored was smaller. Figure 7.7 shows a typical real-time learning evolution. As happened with the X DOF, learning and testing phases

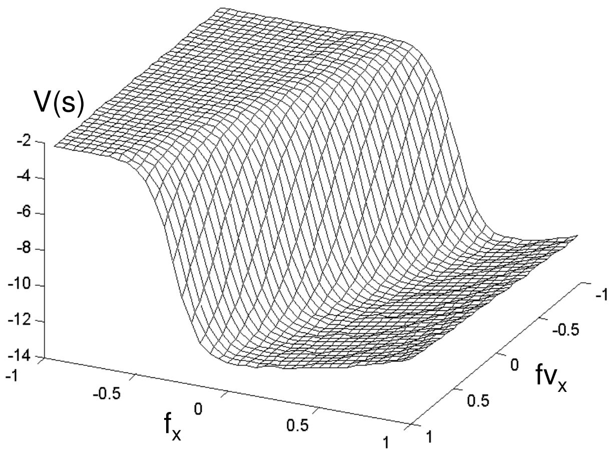

Figure 7.6: State value function, $V(s)$, after the learning for the X DOF.

were consecutively performed. During the testing phase, the "teleoperation" behavior was used to interfere with the "target following", causing the robot to loose the target. It can be seen how the target was always reached again and the maximum rewards were achieved.

The policy and state value functions for the Yaw DOF can be seen in Figure 7.8 and Figure 7.9 respectively. The policy relates the optimal action $v_{f,yaw}$ according to the environment state $\{f_y, fv_y\}$. As far as the state value function $V(s)$ is concerned, it can be clearly appreciated how the maximum values are in the target positions near the center ($f_y = 0$).

Convergence Test

The SONQL algorithm demonstrated that it converges to the optimal policy in a relatively small time, as commented above. The only condition to assure the convergence was to guarantee the reliability of the observed state. This means that perturbations like the influence of the umbilical cable had to be avoided. Figure 7.10 shows six consecutive learning attempts of the Yaw DOF. This figure also shows that the averaged reward increased, demonstrating that the behavior was being learnt. It can be seen that the algorithm started exploring the state in order to find the maximum reward. Once the whole state had been explored, the algorithm exploited the learnt Q_function and obtained the maximum reward.

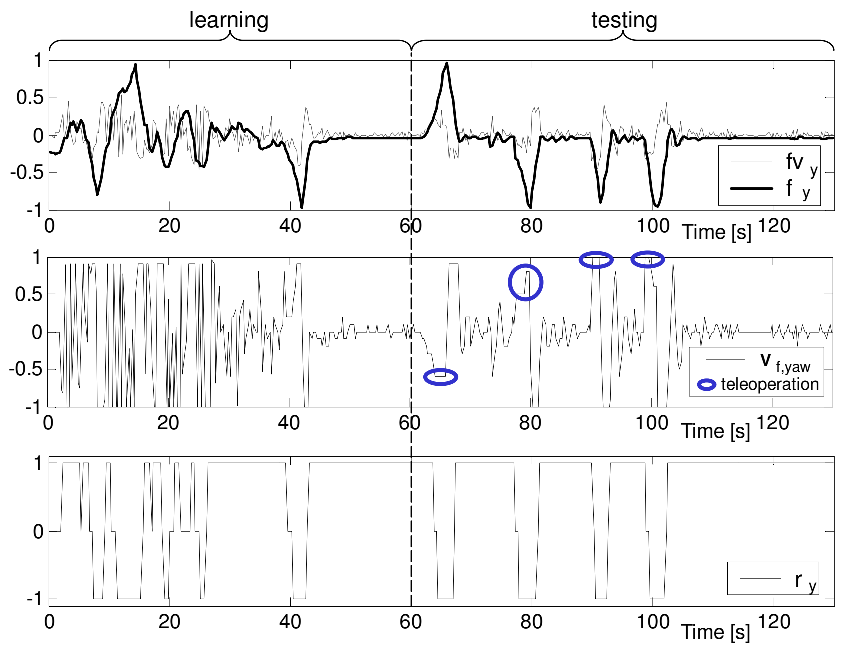

Figure 7.7: Real-time learning evolution and behavior testing of the Yaw DOF. In the same experiment, the behavior was learnt first and then tested. The testing consisted of moving the robot away from the target with the "tele-operation" behavior and allowing the "target following" behavior to reach it again. The evolution of the states, rewards and actions is shown.

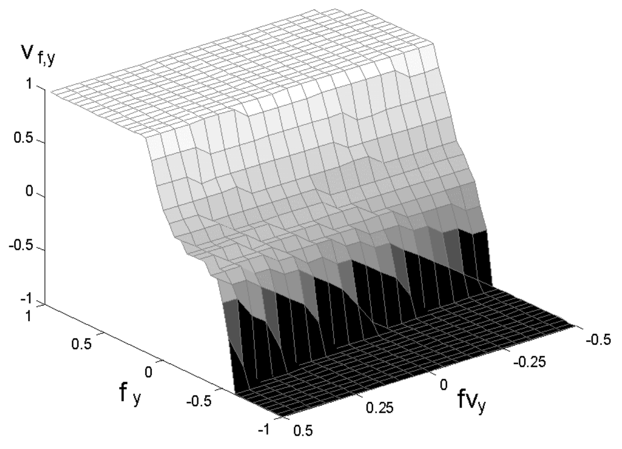

Figure 7.8: State/action policy learnt for the Yaw DOF.

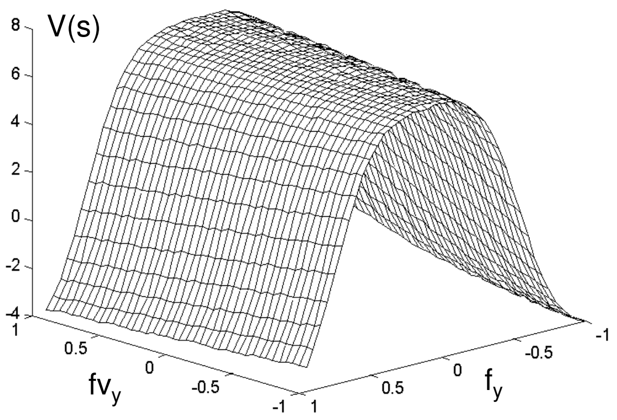

Figure 7.9: State value function $V(s)$, after the learning of the Yaw DOF.

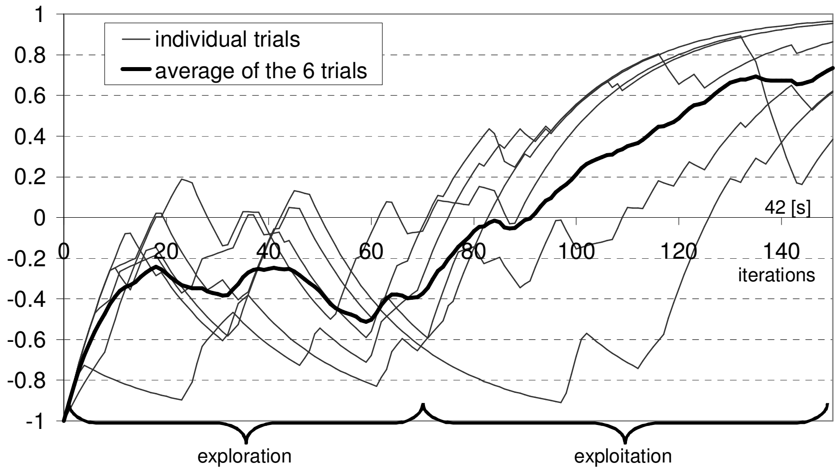

Figure 7.10: Behavior convergence for different attempts. The results of six different learning trials in the Yaw DOF are shown. Each graph represents the mean of the last 20 rewards. This representation is useful to verify that the algorithm is receiving the maximum rewards. The minimum and maximum values correspond to the minimum ($r_y = -1$) and maximum rewards ($r_y = 1$). Also, the average of the six experiments can be seen, pointing out that the accumulated rewards increased while the behavior was learnt.

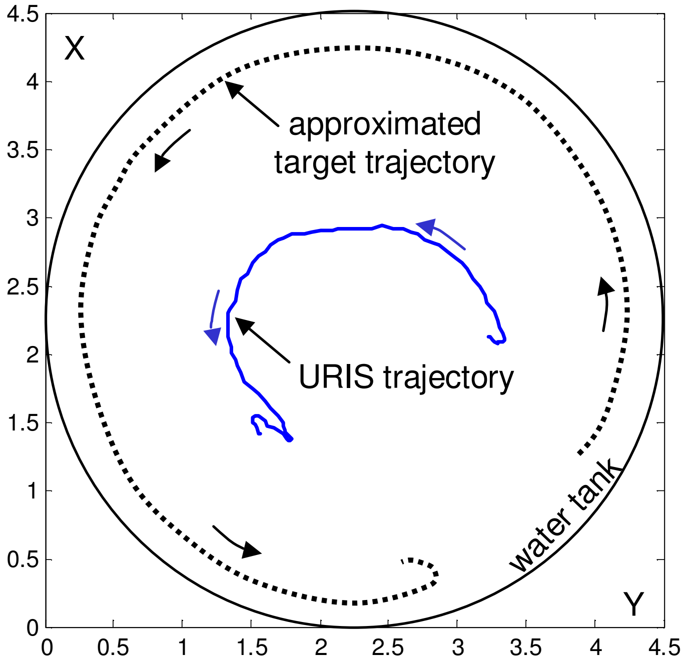

Figure 7.11: Trajectory of URIS while following the target in the water tank.

7.1.3 Task achievement

This section shows the performance of the behavior-based control layer in two situations. The first situation shows the accomplishment of the target following task, see Figure 7.11. In this figure, it can be seen how the robot followed the target at a certain distance. The target was moved manually around the water tank and, therefore, the robot trajectory was also a circumference. Note that the position of the target is approximate since there is no system to measure it. The behavior responses for this experiment are shown in Figure 7.12. It can be seen that at the beginning of the trajectory the target was not detected since the "target recovery" behavior was active. This behavior generated a constant yaw movement until the target was detected (see the Yaw DOF graph). Then, the "target following" behavior became active and generated several surge and yaw movements generating the circular trajectory (see X and Yaw graphs). Finally, the target was moved very fast, causing the activation of the "target recovery" behavior again.

The second situation of interest is the coordination of the "wall avoidance" and "target following" behaviors, see Figure 7.13. In this case, the target was used to push the robot backwards to the wall of the tank. The signals in this figure show how the "wall avoidance" behavior became active and stopped the

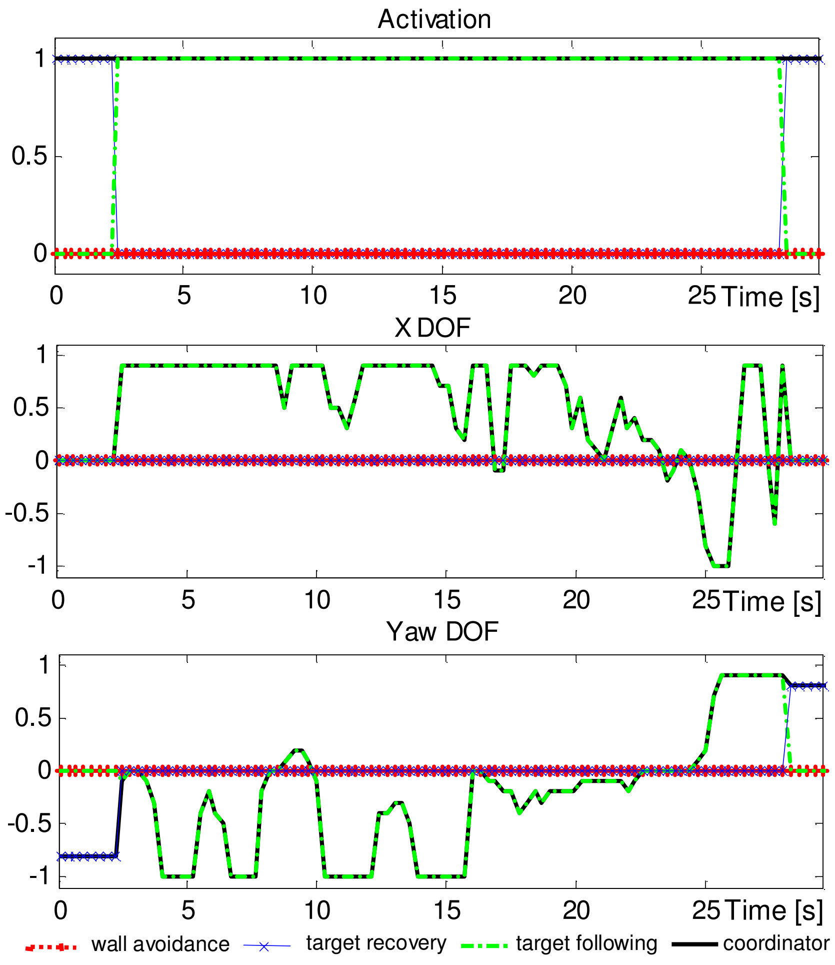

Figure 7.12: Activation levels and control actions for the "wall avoidance", "target recovery" and "target following" behaviors. The response of the coordinator is also shown. These signals correspond to the trajectory shown in Figure 7.11.

control action of the "target following" behavior. The coordinated response in the surge movement (see the X DOF graph) was nearly zero, although the "target following" behavior was generating a backward movement. The result was that the vehicle stopped between the target and the wall of the tank, thus producing the desired effect of the hybrid coordinator.

7.1.4 Conclusions and Discussion

After the presentation of the real experiments with URIS, some conclusions can be extracted:

- The behavior-based control layer and, in particular, the hybrid coordinator system is a suitable methodology to solve a robot task. The task must be previously analyzed and a set of behaviors with their priorities must be designed. The proposal is simple and actuates with robustness and good performance. The parameter k, used by the coordinator nodes, is not a parameter to tune and does not greatly affect the final performance. It simply determines the degree to which dominant behaviors will subsume the non-dominant ones.

- The design and implementation of some behaviors is sometimes very simple, like the "target recovery" behavior. However, other behaviors, like the "target following" behavior, require a deeper analysis. For this kind of behavior it is interesting to use the SONQL algorithm.

- The SONQL algorithm simplifies the designing of robot behaviors. The definition of the reinforcement function and the analysis of the observed state are the most important tasks. The parameters of the algorithm can first be taken from other behaviors and then refined if necessary. The SONQL will learn the optimal mapping between the state and the action, whatever the relation is.

- Another advantage of the SONQL algorithm is that it is an off-policy algorithm. This feature allows the interaction of the other behaviors while performing the learning. This is especially important in behavioral architectures where more than one behavior is simultaneously enabled.

- An RL learning algorithm should not be considered as a classic controller. The problem solved by RL is the maximization of the sum of future rewards. Therefore, an optimal mapping is the one which solves this problem. The optimal control action, according to control theory,

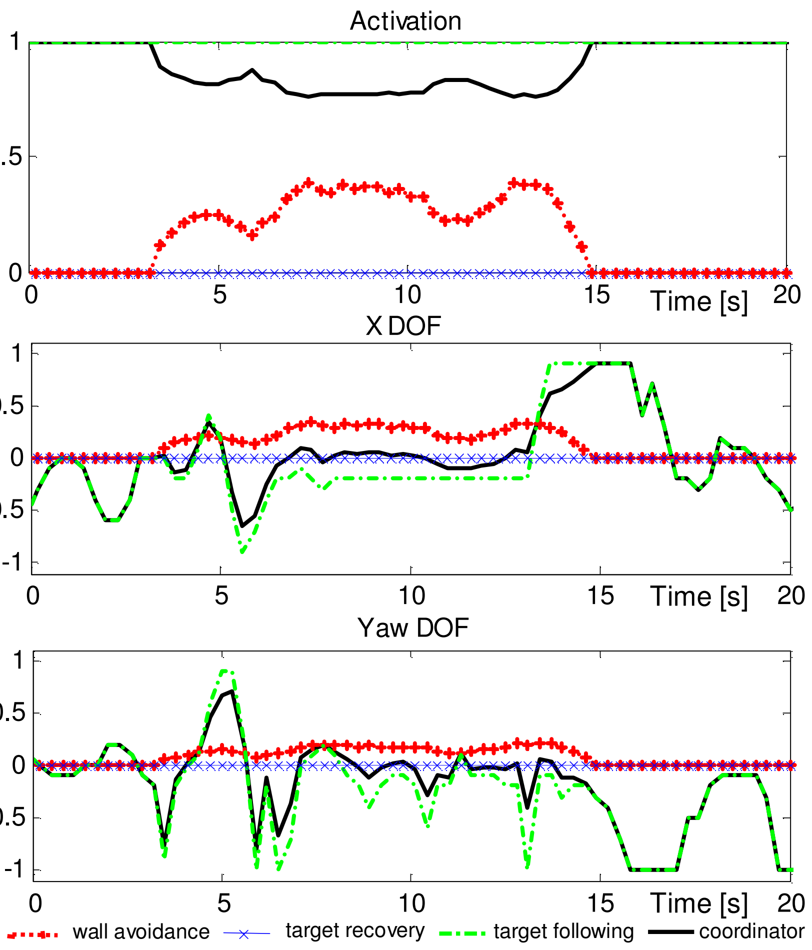

Figure 7.13: Performance of the hybrid coordination system. It can be seen how the "wall avoidance" behavior stopped the movement of the "target following" behavior. This experiment was achieved by bring the target closer to the robot, making the robot go backwards until the wall was found.

can only be achieved if the terms defining this optimality are considered in the design of the reinforcement function.

- One of the most important drawbacks is the accuracy required in the observation of the environment state. If the state is not fully observed, or has noise or delays, the learning cannot be accomplished. When selecting the components of the state, it is important to choose the variables which can be measured with more accuracy. Also, the measurement of the state will depend on the sample time of the algorithm. If the sample time is very small (fast execution), the state measurement must have a higher precision. The use of eligibility traces (see Section 4.4.3) could probably minimize this problem. Algorithms using eligibility traces update the values of a set of past states and this causes an average effect less sensitive to the poor accuracy of the state measurement. However, the implementation of eligibility in dealing with the generalization problem is much more complicated.

- Finally, an implementation issue concerning the action used in the learning process must be commented on. In the RL update rule, action a_t is the one proposed at time t and contributes to the achievement of state s_{t+1}. Surprisingly, when this action was used, the learning had many problems in converging. After analyzing the state transitions and the executed actions, it was found that there was a more logical state transition when considering action a_{t-1} for the change from s_t to s_{t+1}. By applying action a_{t-1}, the learning became much more stable due to the fast execution of the SONQL algorithm. As commented in Section 6.4.2, the high level controller is executed every 0.3 seconds, while the low-level controller id executed at 0.1 seconds. The low-level controller did not have enough time to achieve the set-points, and the actions were not effective until the next iteration. Again, this problem could also be solved with eligibility traces.

7.2 SONQL in the "Mountain-Car" task

This section presents the application of the SONQL algorithm to the "mountain-car" benchmark. This problem is widely accepted by the RL research community as a convenient benchmark to test the convergence and generalization capabilities of an RL algorithm. Although the convergence of the SONQL algorithm cannot be formally probed, it is assumed that if it is able to converge on this complex task, it will also be able to converge in simpler tasks, such as the reactive robot behavior at hand. The "mountain-car" benchmark is not a continuous task like a robot behavior, but an episodic task. Moreover, contrary to a robot behavior, the environment is completely observable without or noise. Hence, this task is highly suitable to test the generalization capability of the SONQL only.

This section first describes the "mountain-car" task. Then, in order to have a performance baseline, the Q_learning algorithm is applied to the problem. After showing the performance of the Q_learning, the SONQL algorithm is applied. The results of the algorithm using different configurations will be analyzed. Finally, a comparison of the SONQL performance with respect to other RL algorithms is done.

7.2.1 The "Mountain-Car" task definition

The "mountain-car" task [Moore, 1991, Singh and Sutton, 1996] was designed to evaluate the generalization capability of RL algorithms. In this problem, a car has to reach the top of a hill. However, the car is not powerful enough to drive straight to the goal. Instead, it must first reverse up the opposite slope in order to accelerate, acquiring enough momentum to reach the goal. The states of the environment are two continuous variables, the position p and the velocity v of the car. The bounds of these variables are $-1.2 \leq p \leq 0.5$; and $-0.07 \leq v \leq 0.07$. Action a is a discrete variable with three values $\{-1, 0, +1\}$, which correspond to reverse thrust, no thrust and forward thrust respectively. The mountain geography is described by the equation: $altitude = sin(3p)$. Figure 7.14 shows the "mountain-car" scenario. The dynamics of the environment, which determines the state evolution, is defined by these two equations:

$$v_{t+1} = bound[v_t + 0.001\, a_t - 0.0025\, cos(3\, p_t)] \tag{7.1}$$

$$p_{t+1} = bound[p_t + v_{t+1}] \tag{7.2}$$

in which the *bound* operation maintains each variable within its allowed range. If p_{t+1} is smaller than its lower bound, then v_{t+1} is reset to zero. On the other hand, if p_{t+1} achieves its higher bound, the episode finishes since the task is accomplished. The reward is -1 everywhere except at the top of the hill, where it is 1. New episodes start at random positions and velocities and run until the goal has been reached or a maximum of 200 iterations have elapsed. The optimal state/action mapping to solve the "mountain-car" task is not trivial since, depending on the position and the velocity, a forward or reverse action must be applied.

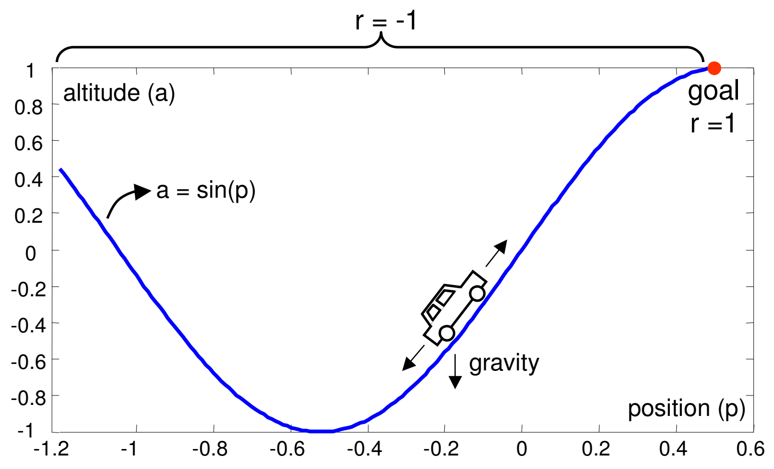

Figure 7.14: The "mountain-car" task domain.

7.2.2 Results with the Q_learning algorithm

To provide a performance baseline, the classic Q_learning algorithm was applied. The state space was finely discretized, using 180 states for the position and 150 for the velocity. The action space contained only three values, -1, 0 and 1. Therefore, the size of the Q table was 81000 positions. The exploration strategy was an $\epsilon - greedy$ policy with ϵ set at 30%. The discount factor was $\gamma = 0.95$ and the learning rate $\alpha = 0.5$, which were found experimentally. The Q table was randomly generated at the beginning of each experiment. In each experiment, a learning phase and an evaluation phase were repeatedly executed. In the learning phase, a certain number of iterations were executed, starting new episodes when it was necessary.

In the evaluation phase, 500 episodes were executed. The policy followed in this phase was the *greedy* policy, since only exploitation was desired. In order to numerically quantify the *effectiveness* of the learning, the average time spent in each episode is used. This time is measured as the number of iterations needed by the current policy to achieve the goal. After running 100 experiments with Q_learning, the average episode length in number of iterations once the optimal policy had been learnt was 50 iterations with 1.3 standard deviation. The number of learning iterations to learn this optimal policy was approximately 10^7. Figure 7.15 shows the effectiveness evolution of the Q_learning algorithm after different learning iterations.

It is interesting to compare this mark with other state/action policies. If a forward action ($a = 1$) is always applied, the average episode length is 86. If a random action is used, the average is 110, see Figure 7.15. These

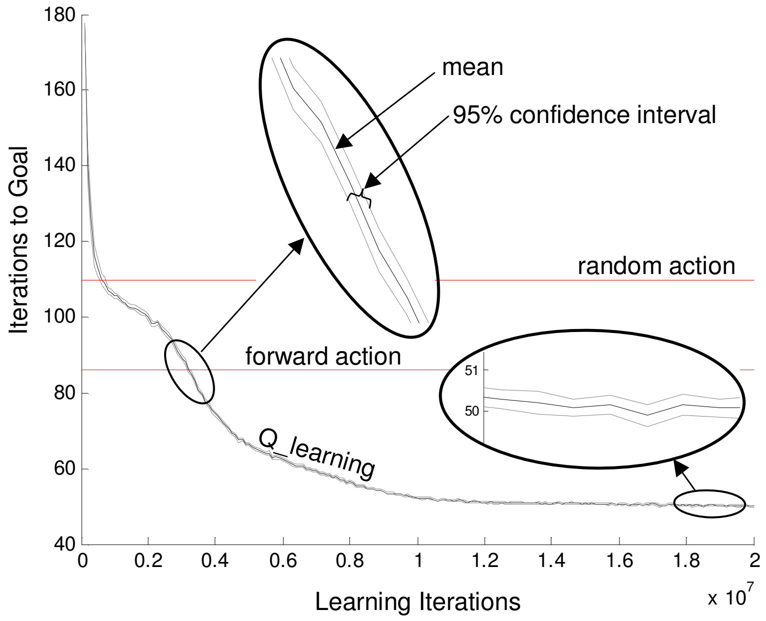

Figure 7.15: Effectiveness of the Q_learning algorithm with respect to the learning iterations. During the first iterations the efficiency was very low, requiring many iterations to reach the goal. The graph was obtained by averaging 100 trials. In each trial, the effectiveness was calculated by averaging the number of iterations to goal in 500 episodes. After converging, the effectiveness was maximum, requiring only 50 iterations to accomplish the goal. The 95% confidence intervals are also shown. Finally, the effectiveness levels of random and forward policies can be observed.

averages depend highly on the fact that the maximum number of iterations in an episode is 200, since in many episodes these policies do not fulfill the goal.

The optimal policy learnt by Q_learning is shown in Figure 7.16. This mapping relates the state of the environment (car position and velocity) with the discrete actions, $a = \{-1, 0, 1\}$. In this figure four different mappings are presented which correspond to the same trial but at different learning iterations. It can be observed how the optimal policy becomes more defined as a function of the learning iterations. It is important to note the non-linear relation between the mapping and the optimal action. The disadvantage of a discrete state space is that each state/action pair must be updated several times until a homogeneous policy is obtained. This causes a high number of learning iterations.

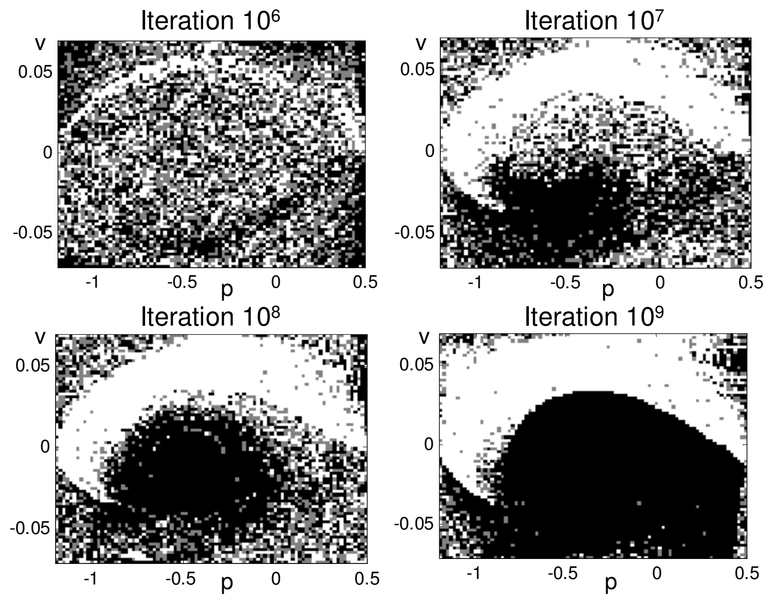

Figure 7.16: State/action policy after several number of learning iterations for the Q_learning algorithm. The actions are represented in different colors: white for forward thrust, gray for no-thrust, and black for reverse thrust.

Similar to the experiments with the URIS robot, the Q function can also be represented. In Figure 7.17, the maximum $Q(s, a)$ value for each state value is represented which is also the $V(s)$ function. For a clearer visualization, the $V(s)$ axis has been inverted. Hence, the states with a higher state-value are the ones which correspond to the lower parts of the three-dimensional surface. It can be observed how the shape of the state-value function evolves according to the learning iterations. Also, it is interesting to compare the evolution of the $V(s)$ function with respect to the evolution of the optimal policy. The $V(s)$ function evolves much faster to its definitive shape, while the policy is learnt slowly.

7.2.3 Results with the SONQL algorithm

The SONQL was also applied to the "mountain-car" task. Since the state space had been finely discretized with the Q_learning algorithm, it was assumed that with only three actions, the minimum number of iterations to fulfill the goal is 50. The SONQL algorithm cannot improve this mark as it is based on the Q_learning algorithm. However, it is expected that it can reduce the number of iterations required to learn the optimal policy.

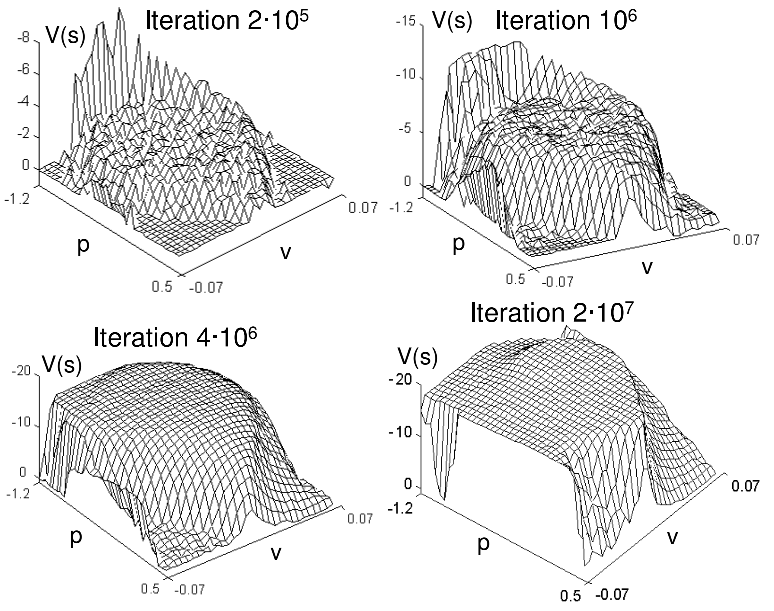

Figure 7.17: State value function $V(s)$ after different learning iterations for the Q_learning algorithm.

An extensive number of experiments were executed with the SONQL algorithm in order to find the best configuration. The NN had three layers with 15 neurons in the two hidden layers. Only three actions were used, as with the Q_learning experiments. The optimal learning rate and discount factor were $\alpha = 0.0001$ and $\gamma = 0.95$. And the ϵ parameter was set at 30%. Note the difference between the optimal learning rate of the SONQL algorithm and the Q_learning algorithm. The Q_learning has a higher rate but only one value of the discrete function is updated. On the other hand, the SONQL algorithm has a much smaller learning rate but each NN update affects the whole continuous space. The density parameter of the database was set to $t = 0.09$, which entailed approximately 470 learning samples at the end of each trial.

As with the Q_learning algorithm, each trial had a learning phase and an evaluation phase. In the evaluation phase 500 episodes were tested. For each experiment with a SONQL configuration, a total number of 100 trials were run. The average episode length in number of iterations for the parameters detailed above was 53 with 2.1 standard deviation. The number of learning iterations were only 20000, approximately. This result demonstrates that the SONQL algorithm is able to converge much faster than the Q_learning algorithm (from 10^7 to 20000 learning iterations), although it is not able to

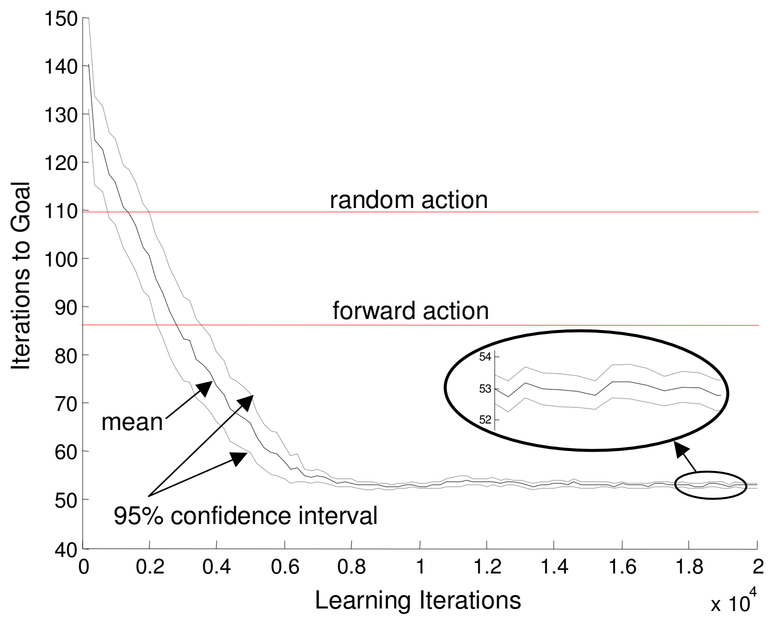

Figure 7.18: Effectiveness of the SONQL algorithm with respect to the learning iterations. The graph is the average of 100 trials. The 95% confidence intervals are also shown.

learn exactly the same optimal policy. The policy learnt by the Q_learning algorithm was able to solve the "mountain-car" task in 50 iterations, while the SONQL required 53 iterations. This difference is very small and, therefore, the feasibility of the SONQL algorithm in solving the generalization is affirmed. The convergence of the algorithm also proved to be very high and in all the experiments the optimal policy was learnt.

Figure 7.18 shows the performance evolution with respect to the number of learning iterations. After 20000 learning iterations, the number of iterations required to accomplish the goal are 53. It is also observed how the SONQL algorithm maintains effectiveness until the end of the experiment without diverging. Figure 7.19 shows another representation of the same experiment. In this case, the graph is drawn with respect to the total number of NN updates, considering each sample of the database as a learning iteration. The number of iterations is higher than before since, for each SONQL iteration, all the samples of the database are learnt. However, the number of NN updates are also significantly fewer than with the Q_learning algorithm, which is also represented. The total number of NN updates was approximately $8 \cdot 10^6$ iterations.

The optimal policy learnt by the SONQL algorithm is shown in Fig-

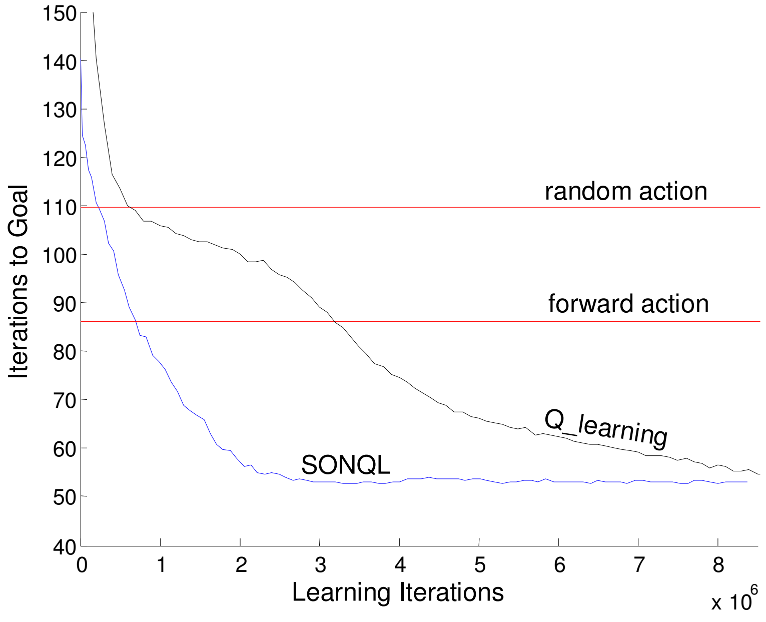

Figure 7.19: Effectiveness of the SONQL algorithm with respect to the number of NN updates.

ure 7.20. As previously done with the Q_learning algorithm, four different mappings are presented, which correspond to different learning iterations. It can be observed how the optimal policy becomes more defined as the learning is performed. It is interesting to compare the policies learnt by the two algorithms, see Figure 7.16 and Figure 7.20. In the policy learnt by the SONQL, the optimal actions are more clearly defined, although both have similar shapes. The state zones of the Q_learning policy which are less defined, indicate that they were not visited enough and, consequently, a higher divergence between the Q_learning and SONQL policies can be found.

The Q function at different learning iterations is represented in Figure 7.21. As in previous representations, the maximum value for each state is shown, which is the state-value function $V(s)$. It can be observed how the shape of the function evolves according to the learning iterations. The $V(s)$ axis has been inverted for a clearer visualization. It is interesting to compare the shape of the $V(s)$ function learnt by the SONQL algorithm with the one of the Q_learning algorithm, see Figure 7.17. The function learnt by the SONQL is much smoother, although the shape is similar. The ranges of the two functions are not exactly the same. The maximum and minimum values of the SONQL function are higher, which is caused by the interference of the NN when updating the samples. However, the values of different actions at

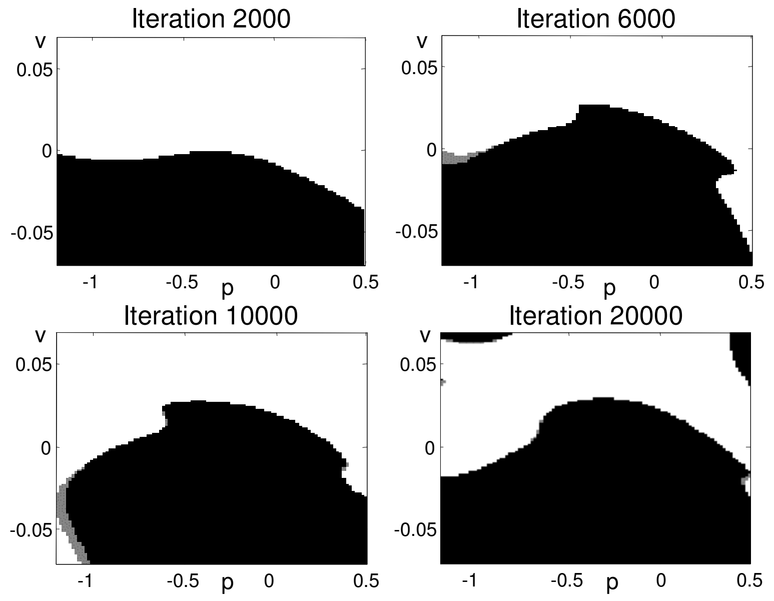

Figure 7.20: State/action policy after different learning iterations for the SONQL algorithm. The actions are represented in different colors: white for forward thrust, gray for no-thrust, and black for reverse thrust.

the same states maintain the same relation which finally defines the policy. The $V(s)$ function learnt by the SONQL algorithm after 20000 iterations is shown in Figure 7.22. In this figure two different views of the approximated state-value function can be observed.

The influence of the database was analyzed using the same SONQL configuration and changing the database size. Instead of referring to the density parameter t, the number of samples stored in the database will be used. The total number of NN updates was fixed at $8 \cdot 10^6$ iterations approximately, and in each experiment 100 trials were simulated. The first experiment consisted of learning with only the current learning sample, that is, without using the database. Figure 7.23 shows the obtained result. It can be appreciated that the algorithm is not able to learn an optimal mapping. The effectiveness occurs in 110 iterations, which is the same effectiveness as with a random policy. The confidence interval is very large, since each of the 100 trials had a very different result. The first conclusion is that, although the NN is able to approximate the optimal Q-function, the interference problem does not allow the stability of the learning process. The database is therefore necessary to ensure the convergence.

Three more experiments were executed in which the number of learn-

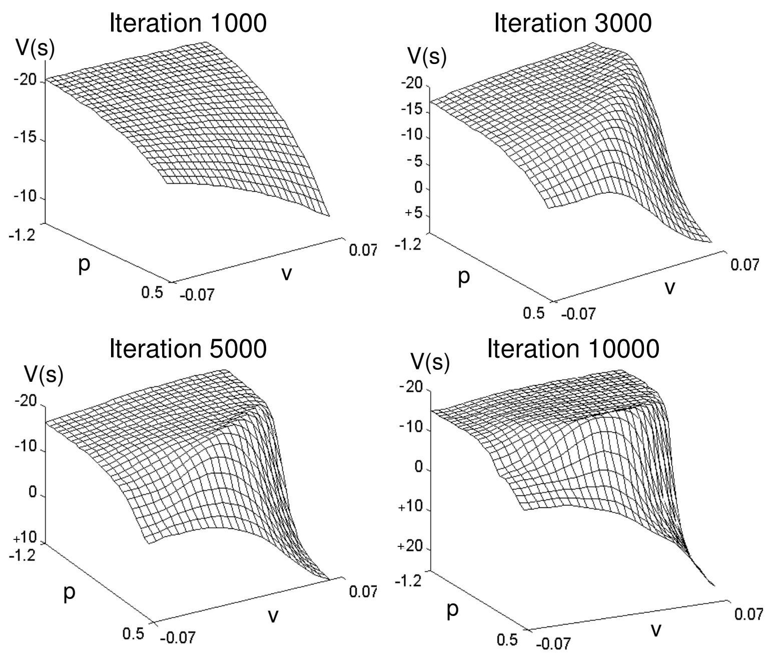

Figure 7.21: State value function $V(s)$ after several learning iterations for the SONQL algorithm.

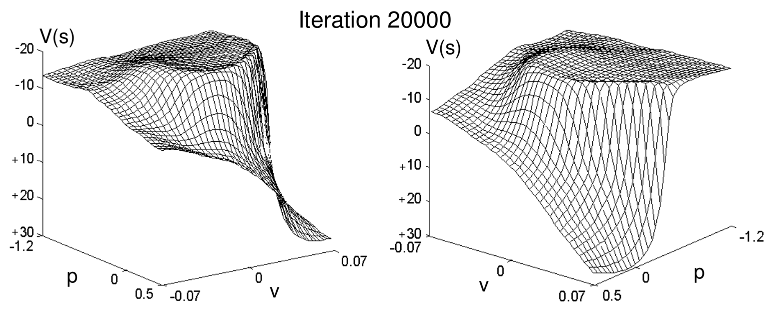

Figure 7.22: Two views of the state value function $V(s)$ after 20000 learning iterations with the SONQL algorithm.

ing samples were 280, 150 and 85 samples. In Figure 7.24, the effectiveness of these experiments, together with the previous ones, are shown. The graphs represent the number of NN updates. It can be observed that all the SONQL algorithms finished at the same number of iterations ($8 \cdot 10^6$). The convergence time is not drastically different, although the experiments with a smaller database converged sooner. However, the experiments with a larger database obtained a better effectiveness. The averages of the "D=470", "D=280", "D=150" and "D=85" experiments are 53, 54, 56 and 58 respectively. Figure 7.25 shows the same graphs but with respect to the number of learning iterations of the SONQL algorithm. The number of iterations is smaller since the number of NN updates is equal and the database is larger. A second conclusion can be extracted from these results; with a larger database, a better learning is achieved. A large database implies a large set of learning samples uniformly distributed throughout the visited space. This representative set of samples improves the learning capacity of the direct Q_learning. Finally, besides the improvement of the effectiveness, a larger database also implies a higher computation of the SONQL algorithm for the same number of iterations, which must be taken into account in a real-time application.

The results obtained in this section empirically demonstrate the benefit of using the SONQL algorithm, and especially the learning samples database, for solving the generalization problem.

7.2.4 Discussion

The comparison between the SONQL algorithm and the Q_learning algorithm must only be considered as an evaluation of the SONQL policy with respect to the optimal one, which was supposed to be the one learnt by Q_learning. The Q_learning exhibited a long convergence time since it was affected by the generalization problem. It is interesting to compare the performance of the SONQL algorithm with respect to other RL algorithms that have also dealt with the "moutain-car" task. The results of some of them are next commented. These algorithms have been classified according to the generalization methodology.

Decision Trees A decision tree used to generalize the Q_learning algorithm was proposed by Vollbrecht [Vollbrecht, 1999]. The effectiveness of this algorithm was 58 iterations to goal, and the convergence time was 20000 learning episodes. The number of learning iterations was not detailed. Another interesting work can be found in [Munos and Moore, 2002]. In this work, a detailed study of the value function and policy function was presented, although the effectiveness was not mentioned.

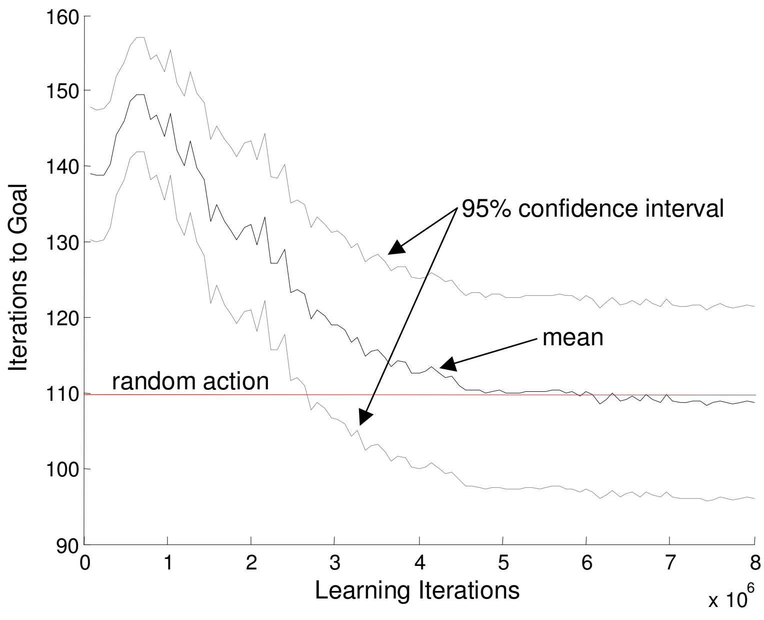

Figure 7.23: Effectiveness of the SONQL algorithm with respect to the learning iterations without using the database. In this case, the number of learning iterations is the same as the number of NN updates.

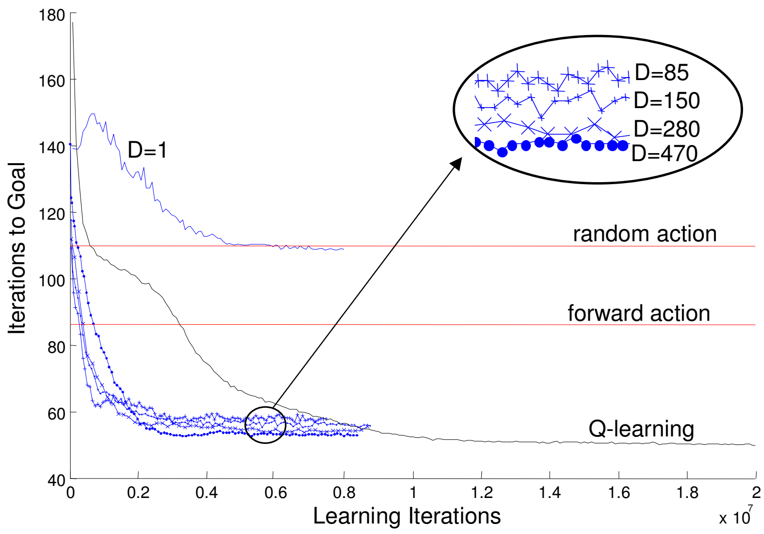

Figure 7.24: Effectiveness of the SONQL algorithm with respect to the number of NN updates. The performance of the database is shown with five different sizes (D=1,85,150,280 and 470).

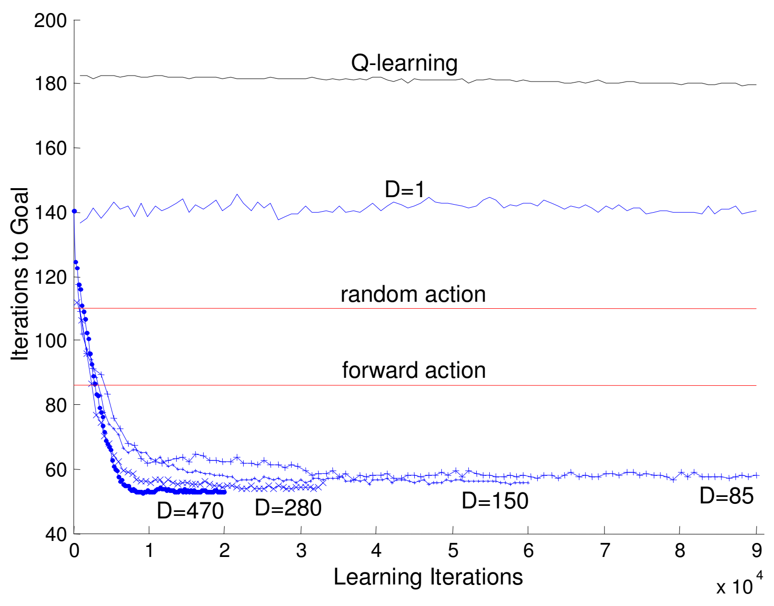

Figure 7.25: Effectiveness of the SONQL algorithm with respect to the learning iterations. The performance of the database is shown with five different sizes (D=1,85,150,280 and 470).

CMAC The use of the CMAC function approximator in the "mountain-car" task is also common. The most known application was done by Sutton [Sutton, 1996], who centered his work in the value function. He also analyzed the use of eligibility traces. CMAC was implemented with 10 tilings, having 9x9 tiles each. However, the effectiveness was not mentioned. Another implementation can be found in [Kretchmar and Anderson, 1997], in which they applied a CMAC function with 11 tilings and 3x3 tiles. The effectiveness was 68 iterations to goal and the convergence time was 1500 episodes. In the same work, the use of a radial basis function approximator was also reported. The results showed a better effectiveness with the same convergence time, the number of iterations to goal was 56.

Memory-based In [Smart, 2002], a memory-based method using locally weighted regression was evaluated with the "mountain-car" task. The effectiveness of the algorithm was 70 iterations to goal and the convergence time was not clearly stated.

Neural Networks To the authors best knowledge there are no successful examples that apply Neural Networks to the "mountain-car" task. In

[Boyan and Moore, 1995], the divergence of Neural Networks in this problem was stated using a 2 layer network with 80 hidden neurons and using back-propagation updating. This result is the same obtained with the SONQL algorithm when the database was not used. Therefore, the SONQL algorithm, making use of the database, can be considered as one successful case in which a NN was able to solve the generalization problem proposed in the "mountain-car" task.

The results of these algorithms does not improve the mark obtained with the SONQL algorithm. Any of them was able to reach an effectiveness of 53 iterations to goal. As far as the number of learning iterations, it was not clearly stated in these works and, therefore, it cannot be directly compared. However, from the comments about this feature, it is extracted that the SONQL algorithm requires less iterations to converge. They talk about the number of episodes to learn, which even if it is multiplied by the final effectiveness, gives a higher number of iterations. Another important aspect is the computational cost. Although it cannot be quantitatively compared, the SONQL algorithm may require more computation than these algorithms, due to the high number of learning samples to update at each SONQL iteration. Therefore, the conclusion of this comparison is, the SONQL has a higher generalization capability and a short convergence time, but these features must be balanced with respect to the available computational power and real-time requirements.

Finally, after presenting the results of the SONQL algorithm in the "mountain-car" benchmark, it can be concluded that:

- The SONQL algorithm was able to solve the generalization problem found in the "mountain-car" task. The generalization capability of the NN allowed the approximation of the Q-function. The database of learning samples was also a requirement to guarantee the convergence in 100% of the cases.

- The number of learning samples clearly influenced the performance of the SONQL algorithm. The higher the number of samples, the higher the performance. However, a high number of samples also implies a high computational cost, which must be taken into account in a real-time application.

- The effectiveness of the SONQL algorithm was not as good as the effectiveness of the Q_learning algorithm. However, a drastic reduction of the number of iterations needed to converge was demonstrated by the SONQL algorithm. Even the number of NN updates was significantly smaller than the number of iterations needed for the convergence of the Q_learning algorithm.

- The results of the SONQL algorithm with respect to other RL algorithms has shown a higher effectiveness and a smaller convergence time.
- It has been demonstrated that the SONQL algorithm is a suitable approach for reinforcement learning problems in which a generalization and fast learning are required.

Chapter 8

Conclusions

This chapter concludes the work presented throughout this dissertation. It first summarizes the thesis by reviewing the contents described in each chapter. It then points out the research contributions extracted from the proposals and the experiments. In addition, all aspects which have not been accomplished as well as some interesting future research issues are commented on in the future work section. Then, the research framework in which this thesis was achieved is described. Finally, the publications related to this work are listed.

8.1 Summary

In order to develop an autonomous robot, a control architecture must be included in the robot control system. The control architecture has the goal of accomplishing a mission which can be divided into a set of sequential tasks. Chapter 2 presented Behavior-based control architectures as a methodology to implement this kind of controllers. Its high interaction with the environment, as well as its fast execution and reactivity, are the keys to its success in controlling autonomous robots. This chapter also compared some classic approaches by testing their performance in a simulated task with an Autonomous Underwater Vehicle. The main attention was given to the coordination methodology. Competitive coordinators assured the robustness of the controller, whereas cooperative coordinators determined the performance of the final robot trajectory. Chapter 3 proposed the structure of a control architecture for an autonomous robot. Two main layers are found in this schema; the deliberative layer which divides the robot mission into a set of tasks, and the behavior-based layer which is in charge of accomplishing these tasks. This chapter and the thesis centered only on the behavior-based layer. A behavior coordination approach was proposed. The main feature is its hybrid coordination of behaviors, between competitive and cooperative approaches. The approach was tested with the simulated task as well.

The second part of the thesis centered on the implementation of the robot behaviors. It proposed the use of a learning algorithm to learn the internal mapping between the environment state and the robot actions. Chapter 4 presented Reinforcement Learning as a suitable learning theory for robot learning. Its online applicability and the non-requirement of any previous information about the environment are the most important advantages. In addition, the Q_learning algorithm was presented, which is specially adequate for its capability in off-policy learning. The most important drawback is the generalization problem. Reinforcement Learning algorithms are based on discrete representations of the state and action spaces. When these algorithms are applied to continuous variables, as most robotics applications require, the discretization of the variables causes an enormous number of states and a long learning time. The generalization makes the application of Reinforcement Learning in robotics impractical. However, several techniques were presented which attempt to solve this problem. Chapter 5 proposed a Reinforcement Learning algorithm designed to be applied to robotics. The goal of the SONQL algorithm is to learn robot behaviors. It is based on the Q_learning algorithm and solves the generalization problem by using a Neural Network and a database of the most representative learning samples.

The thesis has shown some experiments with the Autonomous Underwater Vehicle URIS. Chapter 6 detailed the experimental set-up specifically designed for these experiments. A description of the vehicle was done first, followed by the presentation of two sensory systems. The target detection and tracking system was in charge of detecting an artificial target by using computer vision. Its purpose was to provide the detection of the environment state for the SONQL algorithm. The second sensorial system was the localization system, which also uses computer vision to estimate the position and velocity of the vehicle. The system was responsible for the fine controllability of the robot. Finally, Chapter 7 showed some results of the SONQL algorithm. The feasibility of the approach was demonstrated by learning a target following behavior in real-time computation. The hybrid coordination system demonstrated to be a suitable methodology, by coordinating the SONQL-based behavior and other manually implemented behaviors. The SONQL algorithm was also tested in a simulated benchmark. This task demonstrated empirically the feasibility of this algorithm in a complex generalization problem.

8.2 Contributions

This thesis has accomplished the proposed goal which is the development of a robot control architecture for an AUV able to achieve simple tasks and exhibit real-time learning capabilities. In the development of this goal, some research contributions were achieved. Hereafter these contributions are listed:

Online learning of robot behaviors . The most important contribution has been the online learning of robot behaviors. The use of Reinforcement Learning in robotics is very common nowadays. However, there are not many approaches which perform an online learning. It is, therefore, an important contribution to demonstrate the feasibility of the SONQL in a real-time task, specially in a complex domain such as underwater robotics. The algorithm proved able to learn the state/action mapping of one DOF in less than 400 iterations, which was less than two minutes. Although the best parameters were used and the experiments were designed in detail, these results point out the important role learning algorithms will have in future robotics applications.

SONQL as a continuous state RL algorithm . The second contribution is also related to the SONQL algorithm. This algorithm demonstrated a high generalization capability in the "mountain-car" benchmark. The combination of the Neural Network and the learning samples database resulted in an algorithm able to face the generalization problem. The Neural Network offered a high function approximation capability, and the database guaranteed its stability by avoiding the interference problem. To the best of the author's knowledge, similar approaches have not been found in the literature and, therefore, the SONQL represents a contribution in the Reinforcement Learning field. However, it must be noted that, although the action space is continuous in the Neural Network, the search of greedy actions requires a discretization of this space. Therefore, the SONQL must be considered only as an algorithm to solve the generalization problem in the state space.

Methodologies for Generalizing . The generalization problem in Reinforcement Learning was treated in detail. The most important methodologies currently being applied were described. This study was not considered as an exhaustive survey but a general overview of the most used techniques.

Development of a behavior-based control system . Another contribution was the development of the behavior-based control layer, and in particular, the hybrid coordination methodology. The main features of the coordination system are its simplicity and robustness which assure the safety of the vehicle. In addition, the cooperation between behaviors improves the final robot trajectory. The behavior-based control layer demonstrated as being an efficient tool in the implementation of a set of behaviors and the obtained results were highly satisfactorily.

Behavior-based control architectures . Four classic Behavior-based control architectures were presented, tested and compared. These architectures represent the most important principles in this field. Therefore, this study offers an exemplified introduction to Behavior-based Robotics. The testing of the architectures in a simulated environment also led to the identification of the dynamics model of GARBI and URIS underwater robots.

Development of a localization system . A localization system for underwater robots in structured environments was proposed. The system is able to estimate the position and orientation in three degrees of freedom and also the velocity. The localization is based on a coded pattern and a computer vision system. The high accuracy of the estimations and the real-time execution of the algorithm are the main features. The localization system has been one of the most important factors for the success of the presented experiments.

8.3 Future Work

The development of a research project always provokes the discovery of new problems as well as new interesting research topics. Future work of the sort contained in this thesis has elements of both kinds. Five different points were considered to be the most logical lines to continue this research. The order in which they are presented corresponds to its hypothetic chronological execution, and also to its specification level.

Exploration/Exploitation policy . The policy which was followed while the SONQL was learning is the $\epsilon-greedy$ policy. The advantage of this is the exploration of new state/action pairs which could have a higher Q value. The effectiveness of random actions in exploring is, at the same time, a problem when working with real systems. Random actions cause very abrupt changes of the robot's movement, which puts at risk the safety and controllability of the robot. A future improvement could be the design of a exploration/exploitation policy which is more appropriate for robotics. This policy could make use of the learning sample database which already contains the non-explored space. However, the convergence of the algorithm and its necessary time should be studied and compared with the $\epsilon - greedy$ policy.

Further SONQL testing . The experimental results have shown the learning of the "target tracking" behavior. This behavior was chosen for the ease in detecting an artificial target with a computer vision system. It would be interesting to add a new state dimension to allow the learning of moving targets. It would also be interesting to test the feasibility of the SONQL with other behaviors. A "trajectory following" behavior, for instance, has a difficult solution for non-holonomic vehicles. The solution adopted by the SONQL algorithm would certainly be interesting. Another important test would be the execution of the algorithms in a natural environment, which usually has much more perturbations, and would also allow the learning of the heave DOF.

Action space generalization . As was treated throughout this dissertation, the SONQL algorithm cannot work effectively if several continuous actions are present. In the learning of the robot behaviors, only one continuous action was used since each DOF was independently learnt. However, the extension of the algorithm to more than one continuous action cannot be easily accomplished. The main reason for that resides in the difficulty in finding the maximum value of the Q_learning function when it is implemented with a Neural Network. This problem, which is also found in other generalization techniques, also constitutes a future work.

Other RL issues . Besides the generalization problem, the correct observation of the Markovian state is also a very important point in robotics. Partially Observable Markov Decision Processes were presented in Chapter 4 to deal with environments in which the state is corrupted. The use of a POMDP algorithm should be considered in future research since the difficulty in having a correct observation is very high. Also the use of eligibility traces has been pointed in the experimental results for their higher suitability in Non-Markovian environments. In addition, some other research issues about Reinforcement Learning were pointed out. Policy methods and hierarchical learning are two interesting topics which have recently received a lot of attention and are very suitable to robotics.

Deliberative layer This thesis has concentrated on the behavior-based layer of a complete control architecture only. It is logical to note as a future work the development of the upper layer, which is the deliberative layer. This layer would allow the execution of real missions instead of simple tasks. The deliberative layer would configure a set of behaviors by setting the priorities among them to execute a particular task. After the fulfillment of this task, a new one would be started. This would be repeated until the mission was completed. However, in order to test the deliberative layer, an assorted set of sensors and behaviors must first be fully working. This future work also involves a new research line since behavior-based robotics is not a suitable approach for mission planning.

8.4 Research Framework

The results and conclusions presented in this thesis are based on a set of experiments. During the period in which this thesis was completed, several robot platforms were used. This section summarizes the research facilities and evolution of this thesis. The most relevant research publications will be referred and can be checked in the next section.

The first experiments consisted of testing some Behavior-based Robotics control architectures. At that time, the robot GARBI was available for teleoperation tasks but it was still not ready to test a control architecture. As has been described throughout this dissertation, in order to perform a test with a control architecture, the subordinate components, such as sensors, actuators and the low-level controller, must be properly working. Therefore, the experimentation was performed with a simulated dynamics model of GARBI and a simulated underwater environment. This led to the identification of the dynamics model of this vehicle [CAMS'01a]. Moreover, further work on dynamics identification was conducted since then [IIA'01,MED'02,GCUV'03b]. This realistic model allowed the execution of a simulated task and the comparison of different control architectures [MCMC'00,QAR'00]. This work was carried out during a research stage at the University of Wales College, Newport, under the supervision of Prof. Geoff Roberts. Also, the hybrid coordinator methodology [IROS'01a,IIA'00] was designed using this simulator.

The second part of this thesis discussed the use of a Reinforcement Learning algorithm to learn the internal structure of a behavior. The first steps in this field were carried out with simulation and published in [IROS'01a]. At that time, as a result of a research stay at the University of Hawaii, under the supervision of Prof. Junku Yuh, the learning algorithms were applied to two different robots. The first one was a commercial mobile robot (Magellan

Pro mobile robot). The advantages of using this platform first, instead of an AUV, were certainly great. The ease in controlling the vehicle and the environment allowed the execution of a high number of experiments [IIA'03]. The utility of these experiments was the detection of the interference problem in the Neural Network. This problem was solved by designing a first version of the SONQL algorithm which was tested with a second robot. In this case, an underwater robot called ODIN, developed in the University of Hawaii. The experiments with ODIN [IFAC'02,OCEANS'01] demonstrated the feasibility of Reinforcement Learning with an autonomous underwater robot.

The experiments were then improved and reproduced with the underwater robot URIS [IROS'02], which are the experiments presented in this thesis. In this case, several sensory systems were specifically developed. Among them, the accurate localization system permitted a fine control of the robot [ICRA'03a,GCUV'03a]. The experiments with URIS are the most complete, although they could not have been achieved without the previous experience. Finally, the generalization capability of the SONQL with the "mountain-car" task was evidently performed in simulation [IROS'03].

8.5 Related Publications

Reinforcement Learning and Robotics

[IROS'03] Marc Carreras, Pere Ridao and Andres El-Fakdi, "Semi-Online Neural-Q-_learning for Real-time Robot Learning", IEEE-RSJ International Conference on Intelligent Robots and Systems, Las Vegas, USA, October 27 - 31, 2003.

[IROS'02] Marc Carreras, Pere Ridao, Joan Batlle and Tudor Nicosevici, "Efficient Learning of Reactive Robot Behaviors with a Neural-Q_Learning Approach", IEEE/RSJ International Conference on Intelligent Robots and Systems, Lausanne, Switzerland, September 30 - October 4, 2002.

[IFAC'02] Marc Carreras, Junku Yuh and Joan Batlle, "High-level Control of Autonomous Robots using a Behavior-based Scheme and Reinforcement Learning", 15th IFAC World Congress on Automatic Control, Barcelona, Spain, July 21-26, 2002.

[IIA'03] Marc Carreras, Junku Yuh, Pere Ridao and Joan Batlle, "A Neural-Q_learning Approach for Online Robot Behavior Learning". (research

work performed in 2001 at the Autonomous Systems Laboratory, University of Hawaii). Research report IIA 03-06-RR. Institute of Informatics and Applications. University of Girona. May 2003.

[OCEANS'01] Marc Carreras, Junku Yuh and Joan Batlle. "An hybrid methodology for RL-based behavior coordination in a target following mission with an AUV". OCEANS 2001 MTS/IEEE Conference. Honolulu, Hawaii, USA, 5-8 November, 2001.

[IROS'01a] Marc Carreras, Joan Batlle and Pere Ridao. "Hybrid Coordination of Reinforcement Learning-based Behaviors for AUV Control". IROS 2001, International Conference on Intelligent Robots and Systems. Maui, Hawaii, USA, October, 2001.

Behavior-based control architectures

[MCMC'00] Marc Carreras, Joan Batlle, Pere Ridao and Geoff Roberts. "An overview on behaviour-based methods for AUV control". MCMC'2000, 5th IFAC Conference on Manoeuvring and Control of Marine Crafts. Aalborg, Denmark. 23-25 August, 2000.

[QAR'00] Marc Carreras, Joan Batlle and Pere Ridao. "Reactive control of an AUV using Motor Schemas". QAR'2000, International conference on Quality control, Automation and Robotics. Cluj Napoca, Rumania. 19-20 May, 2000.

[IIA'00] Marc Carreras. "An Overview of Behaviour-based Robotics with simulated implementations on an Underwater Vehicle". Research report IIA 00-14-RR. Institute of Informatics and Applications. University of Girona. October 2000.

Vision-based Localization System for an AUV

[ICRA'03a] Marc Carreras, Pere Ridao, Rafael Garcia and Tudor Nicosevici, "Vision-based Localization of an Underwater Robot in a Structured Environment", IEEE International Conference on Robotics and Automation ICRA'03, Taipei, Taiwan, 2003.

[GCUV'03a] Marc Carreras, Pere Ridao, Joan Batlle and Xavier Cufí, "AUV navigation in a structured environment using computer vision", 1st IFAC Workshop on Guidance and Control of Underwater Vehicles GCUV '03, Wales, UK, April 9-11, 2003.

UUV Dynamics Identification

[GCUV'03b] Marc Carreras, Antonio Tiano, Andres El-Fakdi, Antonio Zirilli and Pere Ridao, “On the identification of non linear models of unmanned underwater vehicles” (part II), 1st IFAC Workshop on Guidance and Control of Underwater Vehicles GCUV '03, Wales, UK, April 9-11, 2003.

[MED'02] Antonio Tiano, Marc Carreras, Pere Ridao and Antonio Zirilli, “On the identification of non linear models of unmanned underwater vehicles” (part I), 10th Mediterranean Conference on Control and Automation, Lisbon, Portugal, July 9-12, 2002.

[CAMS'01a] Pere Ridao, Joan Batlle and Marc Carreras. “Model identification of a low-speed UUV with on-board sensors”. IFAC conference CAMS'2001, Control Applications in Marine Systems. Glasgow, Scotland, U.K., 18-20 July, 2001.

[IIA'01] Pere Ridao, Joan Batlle and Marc Carreras. “Dynamics Model of an Underwater Robotic Vehicle”. Research report IIiA 01-05-RR. Institute of Informatics and Applications. University of Girona. April 2001.

Related work in underwater robotics

[ICRA'03b] Rafael Garcia, Xavier Cufí, Marc Carreras and Pere Ridao, “Correction of Shading Effects in Vision-Based UUV Localization”, IEEE International Conference on Robotics and Automation ICRA'03, Taipei, Taiwan, 2003.

[CEP'02] Pere Ridao, Joan Batlle and Marc Carreras, "O^2CA^2, a new object oriented control architecture for autonomy: the reactive layer”, Control Engineering Practice, Volume 10, Issue 8, Pages 857-873, August 2002.

[ICRA'01] Pere Ridao, Joan Batlle, Josep Amat and Marc Carreras. “A distributed environment for virtual and/or real experiments for underwater robots”. ICRA'01, 2001 IEEE International Conference on Robotics and Automation, Seoul, Korea, 21-26 May, 2001.

[CAMS'01b] Pere Ridao, Marc Carreras, Joan Batlle and Josep Amat. “O^2CA^2: A new hybrid control architecture for a low cost AUV”. IFAC conference CAMS'2001, Control Applications in Marine Systems. Glasgow, Scotland, U.K., 18-20 July, 2001.

[IROS'01b] Rafael Garcia, Xevi Cufí and Marc Carreras. “Estimating the motion of an Underwater Robot from a Monocular Image Sequence”.

IROS 2001 International Conference on Intelligent Robots and Systems. Maui, Hawaii, USA, October, 2001.

[MED'01] Joan Batlle, Pere Ridao and Marc Carreras. "An Underwater Autonomous Agent. From Simulation To Experimentation". 9th Mediterranean Conference on Control and Automation. Dubrovnik, Croatia, 27-29, 2001.

Bibliography

[Agre and Chapman, 1987] Agre, P. and Chapman, D. (1987). Pengi: an implementation of a theory of activity. In *Proceeding of the Sixth Annual Meeting of the American Association for Artificial Intelligence*, pages 268–272, Seattle, Washington.

[Albus, 1971] Albus, J. S. (1971). A theory of cerebellar function. *Mathematical Biosciences*, 10:25–61.

[Albus, 1981] Albus, J. S. (1981). *Brain, behavior and robotics.* Byte Books, Peterborough, NH.

[Albus, 1991] Albus, J. S. (1991). Outline for a theory of intelligence. *IEEE Transactions on Systems, Man, and Cybernetics*, 21(3):473–509.

[Amat et al., 1996] Amat, J., Batlle, J., Casals, A., and Forest, J. (1996). GARBI: a low cost ROV, constrains and solutions. In *6ème Seminaire IARP en robotique sous-marine*, pages 1–22, Toulon-La Seyne, France.

[Arbib, 1981] Arbib, M. A. (1981). Perceptual structures and distributed motor control. In *Handbook of physiology-The nervous system II: Motor Control*, chapter 33, pages 1449–1480. Oxford University Press, Oxford, UK.

[Arkin, 1986] Arkin, R. C. (1986). Path planning for a vision-based autonomous robot. In *Proceedings of the SPIE Conference on Mobile Robots*, pages 240–249, Cambridge, MA.

[Arkin, 1987] Arkin, R. C. (1987). Motor schema based navigation for a mobile robot: an approach to programming by behaviour. In *Proceedings of the IEEE Int. Conference on Robotics and Automation*, pages 264–271, Raleigh, NC.

[Arkin, 1989] Arkin, R. C. (1989). Motor schema-based mobile robot navigation. *International Journal of Robotics Research, August 1989*, 8(4):92–112.

[Arkin, 1992] Arkin, R. C. (1992). Behaviour-based robot navigation for extended domains. *Adaptive Behaviour, Fall 1992*, 1(2):201–225.

[Arkin, 1993] Arkin, R. C. (1993). Modeling neural function at the schema level: Implications and results for robotic control. In *Biological neural networks in invertebrate neuroethology and robotics*, page 17. Boston: Academic Press.

[Arkin, 1998] Arkin, R. C. (1998). *Behavior-based Robotics.* MIT Press.

[Atkenson et al., 1997] Atkenson, C., Moore, A., and Schaal, S. (1997). Locally weighted learning. *Artificial Intelligence Review*, 11:11–73.

[Bagnell and Schneider, 2001] Bagnell, J. and Schneider, J. (2001). Autonomous helicopter control using reinforcement learning policy search methods. In *Proceedings of the IEEE International Conference on Robotics and Automation*, Korea.

[Baird, 1995] Baird, K. (1995). Residual algorithms: Reinforcement learning with function approximation. In *Machine Learning: Twelfth International Conference*, San Francisco, USA.

[Baird and Klopf, 1993] Baird, L. and Klopf, A. (1993). Reinforcement Learning with High-Dimensional, Continuous Action. Technical Report WL-TR-93-1147, Wright Laboratory.

[Bakker et al., 2002] Bakker, B., Linaker, F., and Schmidhuber, J. (2002). Reinforcement learning in partially observable mobile robot domains using unsupervised event extraction. In *IEEE/RSJ International Conference on Intelligent Robots and Systems*, Lausanne, Switzerland.

[Balch and Arkin, 1993] Balch, T. and Arkin, R. (1993). Avoiding the past: A simple but effective strategy for reactive navigation. In Werner, Robert; O'Conner, L., editor, *Proceedings of the 1993 IEEE International Conference on Robotics and Automation: Volume 1*, pages 678–685, Atlanta, GE. IEEE Computer Society Press.

[Barto and Mahadevan, 2003] Barto, A. and Mahadevan, S. (2003). Recent advances in hierarchical reinforcement learning. *Discrete-Event Systems journal*, in press.

[Barto et al., 1983] Barto, A., Sutton, R., and Anderson, C. (1983). Neuronlike elements that can solve difficult learning control problems. *IEEE Transactions on Systems, Man and Cybernetics*, 13:835–846.

[Baxter and Barlett, 2000] Baxter, J. and Barlett, P. (2000). Reinforcement learning in POMDPs via direct gradient ascent. In *Proceedings of the Seventeenth International Conference on Machine Learning*.

[Bellman, 1957] Bellman, R. (1957). *Dynamic Programming.* Princenton University Press.

[Bertsekas and Tsitsiklis, 1996] Bertsekas, D. and Tsitsiklis, J. N. (1996). *Neuro-Dynamic Programming.* Athena Scientific, Belmont, MA.

[Boyan and Moore, 1995] Boyan, J. and Moore, A. (1995). Generalization in reinforcement learning: Safely approximating the value function. In *NIPS-7*, San Mateo, CA, USA.

[Brooks, 1986] Brooks, R. A. (1986). A robust layered control system for a mobile robot. *IEEE Journal of Robotics and Automation*, RA-2(1):14–23.

[Brooks, 1989] Brooks, R. A. (1989). A robot that walks; emergent behaviours from a carefully evolved network. *Neural Computation, 1989*, 1(2):253–262.

[Brooks, 1990] Brooks, R. A. (1990). The behavior language: User's guide. Technical Report AIM-1227, Massachusetts Institute of Technology.

[Brooks, 1991a] Brooks, R. A. (1991a). Intelligence without reason. In Mylopoulos, J. and Reiter, R., editors, *Proceedings of the 12th International Joint Conference on Artificial Intelligence (IJCAI-91)*, pages 569–595, Sydney, Australia. Morgan Kaufmann publishers Inc.: San Mateo, CA, USA.

[Brooks, 1991b] Brooks, R. A. (1991b). New approaches to robotics. *Science*, 235:1227–1232.

[Buck et al., 2002] Buck, S., Beetz, M., and Schmitt, T. (2002). Approximating the value function for continuous space reinforcement learning in robot control. In *IEEE/RSJ International Conference on Intelligent Robots and Systems*, Lausanne, Switzerland.

[Cassandra et al., 1994] Cassandra, A., Kaelbling, L., and Littman, M. (1994). Acting optimally in partially observable stochastic domains. In *Proceedings of the Twelfth National Conference on Artificial Intelligence*, Seattle, WA.

[Chapman and Kaelbling, 1991] Chapman, D. and Kaelbling, L. (1991). Input generalization in delayed reinforcement learning: an algorithm and preformance comparisons. In *Proceedings of the Twelfth International Joint Conference on Artificial Intelligence*, pages 726–731, San Mateo, CA.

[Chatila and Laumond, 1985] Chatila, R. and Laumond, J. (1985). Position referencing and consistent world modelling for mobile robots. In *IEEE International Conference on Robotics and Automation*, pages 138–170.

[Connell, 1990] Connell, J. H. (1990). *Minimalist Mobile Robots.* Academic Press, Perspectives in Artificial Intelligence Series San Diego, 1990, 175 pages. Introduction by Rodney Brooks.

[Crites and Barto, 1996] Crites, R. and Barto, A. (1996). Improving elevator performance using reinforcement learning. In *NIPS-8*, Cambridge, MA. MIT Press.

[Dayan, 1992] Dayan, P. (1992). The convergence of TD(λ) for general λ. *Machine Learning*, 8:341–362.

[Dietterich, 2000] Dietterich, T. (2000). Hierarchical reinforcement learning with the MAXQ value function decomposition. *Journal of Artificial Intelligence Research*, 13:227–303.

[Dorigo and Colombetti, 1998] Dorigo, M. and Colombetti, M. (1998). *Robot Shaping: An Experiment in Behavior Engineering.* MIT Press/Bradford Books.

[Fikes and Nilsson, 1971] Fikes, R. and Nilsson, N. J. (1971). STRIPS: A new approach to the application of theorem proving to problem solving. *Artificial Intelligence*, 2:189–208.

[Gachet et al., 1994] Gachet, D., Salichs, M., Moreno, L., and Pimental, J. (1994). Learning emergent tasks for an autonomous mobile robot. In *Proceedings of the International Conference on Intelligent Robots and Systems (IROS'94)*, pages 290–97, Munich, Germany.

[Garcia et al., 2001] Garcia, R., Batlle, J., Cufi, X., and Amat, J. (2001). Positioning an underwater vehicle through image mosaicking. In *IEEE International Conference on Robotics and Automation*, pages 2779–2784, Rep.of Korea.

[Garcia et al., 2002] Garcia, R., Puig, J., Ridao, P., and Cufi, X. (2002). Augmented state kalman filtering for AUV navigation. In *IEEE International Conference on Robotics and Automation*, pages 4010–4015, Washington.

[Gaskett, 2002] Gaskett, C. (2002). *Q_learning for Robot Control.* PhD thesis, Australian National University.

[Gat, 1991] Gat, E. (1991). *Reliable Goal-directed Reactive Control for Real-World Autonomous Mobile Robots.* PhD thesis, Virginia Polytechnic and State University, Blacksburg, Virginia.

[Gill et al., 1981] Gill, P., Murray, W., and Wright, M. (1981). The levenberg-marquardt method. In *Practical Optimization*, pages 136–137. London: Academic Press.

[Gonzalez and Woods, 1992] Gonzalez, R. and Woods, R. (1992). *Digital Image Processing.* Addison-Wesley, Reading, MA.

[Gordon, 1999] Gordon, G. (1999). *Approximate Solutions to Markov Decision Processes.* PhD thesis, Carnegie-Mellon University.

[Gracias and Santos-Victor, 2000] Gracias, N. and Santos-Victor, J. (2000). Underwater video mosaics as visual navigation maps. *Computer Vision and Image Understanding*, 79(1):66–91.

[Gross et al., 1998] Gross, H., Stephan, V., and Krabbes, M. (1998). A neural field approach to topological reinforcement learning in continuous action spaces. In *Proceedings of the IEEE World Congress on Computational Intelligence, WCCI'98 and International Joint Conference on Neural Networks, IJCNN'98*, Anchorage, Alaska.

[Hagen and Krose, 2000] Hagen, S. and Krose, B. (2000). Neural q_learning. Technical Report IAS-UVA-00-09, Computer Science Institute, University of Amsterdam, The Netherlands.

[Harvey et al., 1997] Harvey, I., Husbands, P., Cliff, D., Thomson, A., and Jakobi, A. (1997). Evolutionary robotics: the sussex approach. *Robotics and Autonomous systems*, 20(2-4):205–224.

[Haykin, 1999] Haykin, S. (1999). *Neural Networks, a comprehensive foundation.* Prentice Hall, 2nd ed. edition.

[Huang, 1996] Huang, H. M. (1996). An architecture and a methodology for intelligent control. *IEEE Expert: Intelligent Systems and their applications*, 11(2):46–55.

[Jaakkola et al., 1995] Jaakkola, T., Singh, S., and Jordan, M. (1995). *Reinforcement Learning algorithms for partially observable Markov decission problems*, volume 7, pages 345–352. Morgan Kaufman.

[Kaelbling, 1999] Kaelbling, L. P. (1999). Robotics and learning. In *The MIT encyclopedia of the cognitive sciences*. MIT Press.

[Kaelbling et al., 1996] Kaelbling, L. P., Littman, M. L., and Moore, A. W. (1996). Reinforcement learning: A survey. *Journal of Artificial Intelligence Research*, 4:237–285.

[Kalmar et al., 1997] Kalmar, Z., Szepesvari, C., and Lorincz, A. (1997). Module-Based Reinforcement Learning: Experiments with a Real Robot. In *Proceedings of the 6th European Workshop on Learning Robots*.

[Kawano and Ura, 2002] Kawano, H. and Ura, T. (2002). Fast reinforcement learning algorithm for motion planning of non-holonomic autonomous underwarter vehicle in disturbance. In *IEEE/RSJ International Conference on Intelligent Robots and Systems*, Lausanne, Switzerland.

[Khatib, 1985] Khatib, O. (1985). Real-time obstacle avoidance for manipulators and mobile robots. In *Proceedings of the IEEE International Conference on Robotics and Automation*, pages 500–505, St. Louis, MO.

[Kondo and Ito, 2002] Kondo, T. and Ito, K. (2002). A Reinforcement Learning with Adaptive State Space Recruitment Strategy for Real Autonomous Mobile Robots. In *IEEE/RSJ International Conference on Intelligent Robots and Systems*, Lausanne, Switzerland.

[Kretchmar and Anderson, 1997] Kretchmar, R. and Anderson, C. (1997). Comparison of cmacs and radial basis functions for local function approximators in reinforcement learning. In *Proceedings os the IEEE International Conference on Neural Networks*, pages 834–837, Houston, TX.

[Laird and Rosenbloom, 1990] Laird, J. E. and Rosenbloom, P. S. (1990). Integrating, execution, planning, and learning in Soar for external environments. In Dietterich, T. S. W., editor, *Proceedings of the 8th Annual Meeting of the American Association for Artificial Intelligence*, pages 1022–1029, Hynes Convention Centre. MIT Press.

[Lefebvre and Saridis, 1992] Lefebvre, D. and Saridis, G. (1992). A computer architecture for intelligent machines. In *Proceedings of the IEEE International Conference on Robotics and Automation*, pages 245–250, Nice, France.

[Lin, 1992] Lin, L. (1992). Self-improving reactive agents based on reinforcement learning, planning and teaching. *Machine Learning*, 8(3/4):293–321.

[Lin, 1993] Lin, L. (1993). *Reinforcement Learning for Robots Using Neural Networks*. PhD thesis, Carnegie-Mellon University.

[Lyons, 1992] Lyons, D. (1992). Planning, reactive. In *Encyclopedia of Artificial Intelligence*. John Wiley and Sons, New York.

[Maes, 1989] Maes, P. (1989). How to do the right thing. *Connection Science*, 1(3):291–323.

[Maes, 1990] Maes, P. (1990). Situated agents can have goals. *Robotics and Automation Systems*, 6:49–70.

[Maes, 1991] Maes, P. (1991). A bottom-up mechanism for behaviour selection in an artificial creature. In Meyer, J.-A. and Wilson, S. W., editors, *From animals to animats*, pages 238–246. First International Conference on Simulation of Adaptive Behavior.

[Maes and Brooks, 1990] Maes, P. and Brooks, R. (1990). Learning to coordinate behaviors. In *Proceedings of Eighth AAAI*, pages 796–802. Morgan Kaufmann.

[Mahadevan and Connell, 1992] Mahadevan, S. and Connell, J. (1992). Automatic programming of behavior-based robots using reinforcement learning. *Artificial Intelligence*, 55:311–365.

[Maire, 2000] Maire, F. (2000). Bicephal reinforcement learning. In *Proceedings of the 7th International Conference on Neural Information Processing*, Taejon, Korea.

[Martinson et al., 2002] Martinson, E., Stoytchev, A., and Arkin, R. (2002). Robot Behavioral Selection Using Q_learning. In *IEEE/RSJ International Conference on Intelligent Robots and Systems*, Lausanne, Switzerland.

[Mataric, 1999] Mataric, M. (1999). Behavior-based robotics. In *The MIT encyclopedia of the cognitive sciences*. MIT Press.

[McCallum, 1995] McCallum, R. (1995). Instance-based state identification for reinforcement learning. In *Advances in Neural Information Processing Systems (NIPS 7).*

[McFarland, 1991] McFarland, D. (1991). What it means for robot behaviour to be adaptive. In Meyer, J.-A. and Wilson, S. W., editors, *From animals to animats*, pages 22–28. First International Conference on Simulation of Adaptive Behavior.

[Millan et al., 2002] Millan, J., Posenato, D., and Dedieu, E. (2002). Continuous-action q_learning. *Machine Learning*, 49:247–265.

[Moore, 1991] Moore, A. (1991). Variable resolution dynamic programming: Efficiently learning action maps on multivariate real-value state-spaces. In *Proceedings of the Eighth International Conference on Machine Learning.*

[Moravec, 1988] Moravec, H. (1988). *Mind Children: the future of robot and the human interaction.* Harvard University Press, 1988, 214 pages.

[Munos and Moore, 2002] Munos, R. and Moore, A. (2002). Variable resolution discretization in optimal control. *Machine Learning*, 49:291–323.

[Negahdaripour et al., 1999] Negahdaripour, S., Xu, X., and Jin, L. (1999). Direct estimation of motion from sea floor images for automatic station-keeping of submersible platforms. *IEEE Trans. on Pattern Analysis and Machine Intelligence*, 24(3):370–382.

[Nilsson, 1984] Nilsson, N. J. (1984). Shakey the robot. Technical Report 323, SRI International, Menlo Park, California.

[Nolfi, 1998] Nolfi, S. (1998). Evolutionary robotics: Exploiting the full power of self-organization. *Connection Science*, 10(3-4):167–183.

[Ormoneit and Sen, 2002] Ormoneit, D. and Sen, S. (2002). Kernel-based reinforcement learning. *Machine Learning*, 49:161–178.

[Parr, 1998] Parr, R. (1998). *Hierarchical Control and Learning for Markov Decision Processes.* PhD thesis, University of California, Berkeley, CA.

[Peng, 1995] Peng, J. (1995). Efficient Memory-based Dynamic Programming. *International Conference on Machine Learning.*

[Peng and Williams, 1994] Peng, J. and Williams, R. (1994). Incremental multi-step Q_learning. In *Proceedings of the Eleventh International Conference on Machine Learning*, San Francisco, USA.

[Pfeifer and Scheier, 1999] Pfeifer, R. and Scheier, C. (1999). *Understanding Intelligence*. MIT Press.

[Poggio and Girosi, 1990] Poggio, T. and Girosi, F. (1990). Regularization algorithms for learning that are equivalent to multilayer networks. *Science*, 247:978–982.

[Powell, 1987] Powell, M. (1987). Radial basis functions for multivariate interpolation: A review. In *Algorithms for Approximation*, pages 143–167. Clarendon Press, Oxford.

[Precup et al., 2001] Precup, D., Sutton, R., and Dasgupta, S. (2001). Off-policy temporal-difference learning with function approximation. In *Proceedings of the 18th International Conference on Machine Learning*.

[Pyeatt and Howe, 1998] Pyeatt, L. and Howe, A. (1998). Decision tree function approximation in reinforcement learning. Technical Report TR CS-98-112, Colorado State University.

[Reynolds, 2002] Reynolds, S. (2002). *Reinforcement Learning with Exploration*. PhD thesis, University of Birmingham, United Kingdom.

[Ridao, 2001] Ridao, P. (2001). *A hybrid control architecture for an AUV*. PhD thesis, University of Girona.

[Rosenblatt and Payton, 1989] Rosenblatt, J. and Payton, D. (1989). A fine-grained alternative to the subsumption architecture for mobile robot control. In *Proceedings of the International Joint Conference on Neural Networks*, pages 317–323.

[Rosenschein and Kaelbling, 1986] Rosenschein and Kaelbling (1986). The synthesis of digital machines with provable epistemic properties. *TARK: Theoretical Aspects of Reasoning about Knowledge*, pages 83–98.

[Rosenstein and Barto, 2001] Rosenstein, M. and Barto, A. (2001). Robot weightlifting by direct policy search. In *Proceedings of the International Joint Conference on Artificial Intelligence*.

[Rumelhart et al., 1986] Rumelhart, D., Hinton, G., and Williams, R. (1986). Learning representations of back-propagation errors. *Nature*, 323:533–536.

[Ryan and Pendrith, 1998] Ryan, M. and Pendrith, M. (1998). RL-TOPs: An Architecture for Modularity and Re-Use in Reinforcement Learning. In

Fifteenth International Conference on Machine Learning, Madison, Wisconsin.

[Ryan and Reid, 2000] Ryan, M. and Reid, M. (2000). Learning to fly: An application of hierarchical reinforcement learning. In *Proceedings of the Seventeenth International Conference on Machine Learning*, pages 807–814, San Francisco, USA.

[Saffiotti et al., 1995] Saffiotti, A., Konolige, K., and Ruspini, E. H. (1995). A multivalued-logic approach to integrating planning and control. *Artificial Intelligence*, 76(1-2):481–526.

[Saito and Fukuda, 1994] Saito, F. and Fukuda, T. (1994). Learning architecture for real robot systems- extension of connectionist q_learning for continuous robot control domain. In *Proceedings of the International Conference on Robotics and Automation*, pages 27–32.

[Santamaria et al., 1998] Santamaria, J., Sutton, R., and Ram, A. (1998). Experiments with reinofrcement learning in problems with continuous state and action spaces. *Adaptive Behavior*, 6:163–218.

[Santos, 1999] Santos, J. (1999). *Contribution to the study and design of reinforcement functions*. PhD thesis, Universidad de Buenos Aires, Universite d'Aix-Marseille III.

[Savitzky and Golay, 1964] Savitzky, A. and Golay, M. (1964). *Analytical Chemistry*, volume 36, pages 1627–1639.

[Shackleton and Gini, 1997] Shackleton, J. and Gini, M. (1997). Measuring the Effectiveness of Reinforcement Learning for Behavior-based Robotics. *Adaptive Behavior*, 5 (3/4):365–390.

[Singh et al., 1994a] Singh, S., Jaakkola, T., and Jordan, M. (1994a). Learning without state-estimation in partially observable markovian decision processes. In *Proceedings of the Eleventh International Conference on Machine Learning*, New Jersey, USA.

[Singh et al., 1994b] Singh, S., Jaakkola, T., and Jordan, M. (1994b). Reinforcement learning with soft state aggregation. In *Proceedings of the 1994 Conference on Advances in Neural Information Processing Systems*.

[Singh and Sutton, 1996] Singh, S. and Sutton, R. (1996). Reinforcement learning with replacing eligibility traces. *Machine Learning*, 22:123–158.

[Smart, 2002] Smart, W. (2002). *Making Reinforcement Learning Work on Real Robots.* PhD thesis, Department of Computer Science at Brown University, Rhode Island.

[Steels, 1992] Steels, L. (1992). The PDL reference manual. Technical Report 92-5, VUB AI Lab, Brussels, Belgium.

[Steels, 1993] Steels, L. (1993). Building agents with autonomous behaviour systems. In *The artificial route to artificial intelligence. Building situated embodied agents.* Lawrence Erlbaum Associates, New Haven.

[Sutton, 1984] Sutton, R. (1984). *Temporal Credit Assignment in Reinforcement Learning.* PhD thesis, University of Massachusetts, Amherst.

[Sutton, 1988] Sutton, R. (1988). Learning to predict by the method of temporal differences. *Machine Learning*, 3:9–44.

[Sutton, 1996] Sutton, R. (1996). Generalization in reinforcement learning: Successful examples using sparce coarse coding. *Advances in Neural Information Processing Sustems*, 9:1038–1044.

[Sutton and Barto, 1998] Sutton, R. and Barto, A. (1998). *Reinforcement Learning, an introduction.* MIT Press.

[Sutton et al., 2000] Sutton, R., McAllester, D., Singh, S., and Mansour, Y. (2000). Policy gradient methods for reinforcement learning with function approximation. *Advances in Neural Information Processing Systems*, 12:1057–1063.

[Sutton et al., 1999] Sutton, R., Precup, D., and Singh, S. (1999). Between MDPs and Semi-MDPs: A framework for temporal abstraction in Reinforcement Learning. *Artificial Intelligence*, 112:181–211.

[Takahashi and Asada, 2000] Takahashi, Y. and Asada, M. (2000). Vision-guided behavior acquisition of a mobile robot by multi-layered reinforcement learning. In *IEEE/RSJ International Conference on Intelligent Robots and Systems.*

[Tesauro, 1992] Tesauro, G. (1992). Practical issues in temporal difference learning. *Machine Learning*, 8(3/4):257–277.

[Theocharous, 2002] Theocharous, G. (2002). *Hierarchical Learning and Planning in Partially Observable Markov Decision Processes.* PhD thesis, Michigan State University.

[Touzet, 1997] Touzet, C. (1997). Neural reinforcement learning for behavior synthesis. *Robotics and Autonomous Systems*, 22:251–281.

[Tsitsiklis and Roy, 1996] Tsitsiklis, J. and Roy, B. V. (1996). Feature-based methods for large scale dynamic programming. *Machine Learning*, 22:59–94.

[Tsitsiklis and Roy, 1997] Tsitsiklis, J. and Roy, B. V. (1997). Average cost temporal-difference learning. *IEEE Transactions on Automatic Control*, 42:674–690.

[Tyrell, 1993] Tyrell, T. (1993). *Computational mechanisms for action selection*. PhD thesis, University of Edinburgh, Scotland.

[Uther and Veloso, 1998] Uther, W. and Veloso, M. (1998). Tree based discretization for continuous state space reinforcement learning. In *Proceedings of the Fifteenth National Conference on Artificial Intelligence*.

[Vollbrecht, 1999] Vollbrecht, H. (1999). kd-Q_learning with hierarchic generalization in state space. Technical Report SFB 527, Department of Neural Information Processing, University of Ulm, Germany.

[Watkins, 1989] Watkins, C. (1989). *Learning from Delayed Rewards*. PhD thesis, Cambridge University.

[Watkins and Dayan, 1992] Watkins, C. and Dayan, P. (1992). Q-learning. *Machine Learning*, 8:279–292.

[Weaver et al., 1998] Weaver, S., Baird, L., and Polycarpou, M. (1998). An Analytical Framework for Local Feedforward Networks. *IEEE Transactions on Neural Networks*, 9(3).

[Whitehead and Lin, 1995] Whitehead, S. and Lin, L. (1995). Reinforcement learning in non-markov environments. *Artificial Intelligence*, 73(1-2):271–306.

[Williams, 1992] Williams, R. (1992). Simple statistical gradient-following algorithms for connectionist reinforcement learning. *Machine Learning*, 8:229–256.

[Witten, 1977] Witten, I. (1977). An adaptive optimal controller for discrete-time markov environments. *Information and Control*, 34:286–295.

[Zhang and Dietterich, 1995] Zhang, W. and Dietterich, T. (1995). A reinforcement learning approach to job-shop scheduling. In *IJCAI95*.

[Ziemke, 1998] Ziemke, T. (1998). Adaptive behavior in autonomous agents. *Presence*, 7(6):564–587.